ANKARA YILDIRIM BEYAZIT UNIVERSITY

GRADUATE SCHOOL OF NATURAL AND APPLIED SCIENCES

GROWTH OF ZnO AND Al DOPED ZnO FILMS BY HYDROTHERMAL METHOD

M.Sc. Thesis by

Ümmügülsüm VAROL

Department of Materails Engineering

June, 2017

ANKARA

GROWTH OF ZnO AND Al DOPED ZnO FILMS BY HYDROTHERMAL METHOD

A Thesis Submitted to

The Graduate School of Natural and Applied Sciences of

Ankara Yıldırım Beyazıt University

In Partial Fulfillment of the Requirements for the Degree of Master of Science

in Material Engineering, Department of Material Engineering

by

Ümmügülsüm VAROL

June, 2017

ANKARA

M.Sc. THESIS EXAMINATION RESULT FORM

We have read the thesis entitled **"Growth of ZnO and Al doped ZnO (AZO) Films by Hydrothermal Method"** completed by **Ümmügülsüm VAROL** under supervision of **Prof. Dr. Aytunç ATEŞ** and we certify that in our opinion it is fully adequate, in scope and in quality, as a thesis for the degree of Master of Science.

Prof. Dr. Aytunç ATEŞ

Supervisor

Prof. Dr.Selim ACAR

Jury member

Prof. Dr. Abdullah YILDIZ

Jury Member

Prof. Dr. FatihVehbi ÇELEBİ

Director

Graduate School of Natural and Applied Sciences

ETHICAL DECLARATION

I hereby declare that, in this thesis which has been prepared in accordance with the Thesis Writing Manual of Graduate School of Natural and Applied Sciences,

- All data, information and documents are obtained in the framework of academic and ethical rules,
- All information, documents and assessments are presented in accordance with scientific ethics and morals,
- All the materials that have been utilized are fully cited and referenced,
- No change has been made on the utilized materials,
- All the works presented are original,

and in any contrary case of above statements, I accept to renounce all my legal rights.

Date: 23.06.2017 **Signature:**

Name & Surname: Ümmügülsüm VAROL

ACKNOWLEDGEMENTS

I would like to express my deep gratitude to my advisor Prof. Dr. Aytunç ATEŞ for his guidance, motivation, encouragement and criticism during my whole master education. His experience always helped me at every steps of my thesis. I will be grateful to him to the end of my life.

Besides my advisor, I would like to thank to Doç. Dr. Memet Ali YILDIRIM for his helps and ideas during an experimental step of my study. I have learned many things from him.

I would like to thank my family stating with my precious mother and father. I am grateful to them for their endless support, patience, generosity, love and faith in me. I would not have accomplished anything without them by my side. I thank to my dear sisters for the joy and happiness they brought into my life.

Finally, my deepest gratitude goes to my dear husband Mesud Behlül VAROL, I cannot complete these works without his endless supports, helps, patience and love. No word is enough to express my thanks to him only I can say that without him everything would be meaningless.

I thank to TUBITAK (The Scientific and Technological Research council of Turkey) for the scholarship, with which they supported me financially during my studies.

This thesis was supported by Ankara Yıldırım Beyazıt University Projects Office (Project Nu.: 3336).

2017, May **Ümmügülsüm VAROL**

GROWTH OF ZnO AND Al DOPED ZnO (AZO) FILMS BY HYDROTHERMAL METHOD

ABSTRACT

Zinc oxide is extensively used as UV light filters, gas sensors and as conductive electrodes in solar cells. For this purpose, extensive research is being carried out to increase the properties of Zinc Oxide and doping. Therefore, in this study; undoped ZnO and AZO films with different Al (%1, %3, %5) content were prepared by hydrothermal method on glass substrates. The influence of Al doping on the structural, surface and optical properties of ZnO films was investigated. On the other hand, as a parameter of hydrothermal method; temperature, time and molarite effects on the properties of the ZnO and AZO film were investigated. After the coating process, for characterization; X-Ray Diffraction (XRD), Scanning Electron Microscopy (SEM), and absorption measurements were used. The XRD and SEM measurements showed that the films are covered well on the substrates and have hexagonal wurzite structure. With using the optical absorption measurements, the band gap values of the films were determined.

Keywords: ZnO, AZO, Hydrothermal method, XRD, SEM, UV/VIS spectrophotometer.

HİDROTERMAL YÖNTEMLE ZnO VE Al KATKILI ZnO (AZO) FİLMLERİNİN BÜYÜTÜLMESİ

ÖZ

Çinko oksit, UV ışık filtreleri, gaz sensörleri ve güneş pillerinde iletken elektrot olarak yaygın bir şekilde kullanılır. Bu amaçla, Çinko Oksit ve katkılamanın özelliklerini arttırmak için kapsamlı araştırmalar yapılmaktadır. Bu nedenle, bu çalışmada; katkısız ZnO ve farklı Al konsantrasyonlu (% 1,% 3,% 5) AZO filmleri, cam yüzeylerde hidrotermal yöntemle hazırlandı. Al katkılamanın, ZnO filmlerin yapısal, yüzeysel ve optik özelliklerine etkisi incelendi. Diğer taraftan, hidrotermal yöntem parametrelerinin; ZnO ve AZO filmi üzerindeki sıcaklık, zaman ve molarite etkileri araştırılmıştır. Karakterizasyon için kaplama işleminden sonra; X-Işını Kırınımı (XRD), Taramalı Elektron Mikroskopu (SEM) ve absorpsiyon ölçümleri alındı. XRD ve SEM ölçümleri, filmlerin alt tabaka üzerinde iyi kaplandığını ve hekzoganal wurzit yapıya sahip olduğunu gösterdi. Optik absorpsiyon ölçümleri kullanılarak filmlerin yasak enerji aralıkları belirlendi.

Anahtar kelimeler: ZnO, AZO, Hidrotermal Yöntem, XRD, SEM, UV/VIS Spektrofotometre.

CONTENTS

NOMENCLATURE

Subscripts

d	Distance Between the Layers
D	Grain Size
δ	Dislocation Density
ε	Strain

Acronyms

AZO	Aluminum Zinc Oxide
CL	Cathodoluminescence
DI	Deionized
DLE	Deep Level Emission
DRS	Diffuse Reflectance Spectroscopy
EDAX	Energy-Dispersive X-Ray
EDS	Energy Dispersive X-Ray Spectroscopy
EDXA	Energy Dispersive X-Ray Analysis
EDXMA	Energy Dispersive X-Ray Microanalysis
FESEM	Field-Emission Scanning Electron Microscope
FTO	Fluorine-Doped Tin Oxide
FWHM	Full Width at Half Maximum
HR-TEM	High-Resolution Transmission Electron Microscopy
ICP-AES	Inductively Coupled Plasma Atomic Emission Spectroscopy.
ITO	Indium Tin Oxide
MOCVD	Metal Organic Chemical Vapor Deposition
NBE	Near Band Emission
NIR	Near Infrared
NSSs	Nano-Superstructures
PL	Photoluminescence
SAED	Selected Area Electron Diffraction
SDS	Sodium Dodecyle Sulfate
SILAR	Successive Ionic Layer Adsorption and Reaction
SPB	Surface Plasmon Band

TC	Preferential Orientation Coefficient
TCO	Transparent Conductive Oxides
TEM	Transmission Electron Microscopy
UV	Ultraviolet
UV/ VIS	Ultraviolet-Visible Spectroscopy
XRD	X-Ray Difraction
ZnO	Zinc Oxide

LIST OF TABLES

LIST OF FIGURES

CHAPTER 1

INTRODUCTION

Currently, most of the energy demand in the world is met by fossil and nuclear power plants. A small part is drawn from renewable energy technologies such as wind, solar, fuel cell, biomass and geothermal energy. Wind energy, solar energy and fuel cells have experienced a remarkably rapid growth in the past ten years because they are pollution-free sources of power. Additionally, they generate power near the load centers, which eliminates the need to run high-voltage transmission lines through rural and urban landscapes [1].

The output power of solar cells fluctuates considerably depending on solar radiation, weather conditions and temperature [1]. Not all parts of the solar spectrum are absorbed equally well by a solar cell. The light that is absorbed weakly can be trapped inside the solar cell and there by travel a complicated optical path before being absorbed, reflected or transmitted. This makes solar cells complex optical devices [2].

One uses the solar energy in converting this energy into (a) heat, and (b) electricity. In the first case, it is used for directly heating homes or for water heating where the sun's rays are incident on a panel containing circulating water in tubes. In the second case, it is used for generating electricity using photovoltaic panels [3].

The cost of solar photovoltaic and fuel cell electricity is still high. Nevertheless, with on going research, development and utilization of these technologies around the world, the costs of solar cells and fuel cell energy are expected to fall in the next few years [1]. Solar energy provides us with an alternative where there is no pollution of the environment and its use decreases the rate of depletion of energy reserve [3].

Transparent conductive oxides (TCO) are necessary as front electrode for most film solar cells. The transparent conducting film should have low resistivity, high transmittance in the visible range and high stability against heat [4]. Zinc oxide and

doped zinc oxide films have received extensive attention in recent years due to their excellent optical and electrical properties.

TCO materials like ZnO has received a vast amount of attention in the last few years. These materials are transparent and conductive with a wide variety of applications in industry and research [5]. Particularly, ZnO has drawn attention because its large energy gap (3.36 eV at room temperature) and an exciton bond energy of 60 meV making it in a candidate material for ultraviolet and blue laser devices that works at room temperature [6,7,8]. For these reasons, the ZnO nano/micro-structures are attractive for high efficient short wavelength optoelectronics devices [7]. Plus, ZnO material is bio-safe and biocompatible so that it can be used also for medical applications without any coating [9]. Until now, have been successfully synthesized nano and micro-materials of ZnO with different morphologies and interesting structures, such as: nanowires, nanobelts, nanorings, nanobows, nano/microtubes, nano/microrods, flower-shaped, nanosaws [10], etc. These materials have been grown by different methods like metal organic chemical vapor deposition (MOCVD), dc magnetron sputtering, chemical spray, optical thermal evaporation, hydrothermal synthesis, Successive Ionic Layer Adsorption and Reaction (SILAR) [11] etc.

Andersson *et al.* had come up with a new microemulsion process combined with hydrothermal technique to overcome the difficulties involved in the general microemulsion process. In order to prevent grain growth of the nanoparticles, a new hydrothermal microemulsion process had been developed in their study. The former used tetra butyl titanate and the latter used titanium tetrachloride as the aqueous phase of the microemulsion [12].

N. Ueno *et al.* synthesized aligned ZnO nanorods by a simple hydrothermal method without calcination. A seed layer of zinc acetate ($ZnAc_2$) sodium dodecyle sulfate (SDS) nanocomposite was used for nucleation of ZnO nanorods. First, a $ZnAc_2$/SDS composite was deposited on a Si substrate by spin-coating. And then, ZnO nanorods were grown under hydrothermal conditions at 90°C. ZnO crystals were grown in the direction of c-axis perpendicular to the surface of the Si substrate. However, nucleation did not occur on the substrate of a $ZnAc_2$ seed layer without SDS,

indicating that the presence of the $ZnAc_2$/SDS seed enhanced the nucleation of ZnO crystals. These results show that high dispersion of $ZnAc_2$ in the nanocomposite effectively assists a nucleation of ZnO crystals [13].

D. Polsongkram *et al.* at this study ZnO nanorods with hexagonal structures were synthesized using hydrothermal method under different conditions. The effect of synthesis conditions on ZnO nanorod growth was systematically studied by SEM. All samples were characterized by XRD, Energy-Dispersive X-ray (EDAX) spectroscopy and micro-Raman spectroscopy. The results demonstrate that the morphology and ordering of ZnO nanorods are determined by the growth temperature, the overall concentration of the precursors and deposition time [14].

M. Yilmaz *et al.* are used low-temperature hydrothermal method to synthesize ZnO nanoparticles. The structural, morphological and optical characterizations of the nanoparticles were evaluated with regard to the zinc content by them. To achieve that, they changed the molar ratios of the precursors from 0.05 to 0.1 M. The structural and morphological analyses showed that all samples had a polycrystalline hexangonal wurtzite crystal structure and the shape of the ZnO nanoparticles changed with increasing zinc content. A possible growth mechanism of the ZnO nanoparticles is explained in terms of the zinc content [15].

S. Promnimit *et al.* synthesized hexagonal ZnO nanocrystals through a hydrothermal route under mild conditions. They used pre synthesized ZnO nanoparticles to serve as nucleation sites for the growth of the nanocrystals. They found the growth of ZnO nanorods were surface independently. The dimensions of the hexagonal ZnO nanocrystals were observed to be dependent on the concentration of the reactants used (sources of Zn^{2+} and OH^- ions), pH of the growth bath and also on the duration of crystal growth. The average diameter and height of the ZnO nanocrystals was found to be directly proportional to the concentration of the reactants as well as hydrolysis time. The orientation of the nanocrystals was found to be dependent upon the seeding method employed. Hexagonal single crystals of a wide range of dimensions and aspect ratios could be successfully synthesized through a control of growth parameters [16].

M. Søndergaard *et al*. they investigated the formation of ZnO nanoparticles using a fast continuous flow hydrothermal synthesis method. The synthesis conditions had varied with respect to temperature, pH, and concentration of the Zn $(NO_3)_2$ $4H_2O$ + NaOH aqueous precursor. The different conditions affected the size, morphology, and crystallinity of the produced ZnO nanoparticles. The nanoparticles were investigated by Rietveld refinement of powder X-ray diffraction data, Transmission Electron Microscopy (TEM), and SEM. The particle size and morphology were highly temperature dependent: Anisotropic particles of a maximum length of 1 μm were produced at a reactor temperature of 122 C, while isotropic particles of around 25 nm were produced at temperatures above 200 C. The crystallinity of the particles increased from 90 (1) % at 122-200 ^oC to 99 (1) % at 390 C. The variation of the pH of the precursor results in different morphologies: (1) acidic conditions produce large rods, (2) neutral conditions give isotropic particles, and (3) alkaline conditions result in large plates. Finally, it was found that the particle size increases with the precursor concentration [17].

P. M. Aneesh *et al* they synthesized stable OH free ZnO nanoparticles using hydrothermal method by varying the growth temperature and concentration of the precursors. The formation of ZnO nanoparticles were confirmed by XRD, TEM and Selected Area Electron Diffraction (SAED) studies. The average particle size had found to be about 7-24 nm and the compositional analysis had done with inductively Coupled Plasma Atomic Emission Spectroscopy (ICP-AES). Diffuse Reflectance Spectroscopy (DRS) results shows that the band gap of ZnO nanoparticles is blue shifted with decrease in particle size [18].

J. K. Tsai *et al* fabricated ZnO microrods were on a fluorine-doped tin oxide (FTO) glass by using a high-temperature hydrothermal method. The main goal was to investigate the correlation between synthesis temperature and characteristics of ZnO microrods. The morphology of ZnO microrods was investigated by Field-Emission Scanning Electron Microscope (FESEM), the optical properties were measured by photoluminescence (PL) and the crystallinity was characterized by XRD. SEM images showed that morphology of ZnO was rod-like. The growth mechanism explained by Oswald ripening process. The synthesis temperatures were associated

with pH values and the pH value was related to cation concentration in the solution. Thus Zn ion concentration plays an important role in controlling the morphology of microrods. In this study ZnO microrods grown at 90 °C have the best crystallinity and fewer defects with preferred optical properties than other samples is found [19].

S. Baruah *et al.* summarized the conditions leading to the growth of different ZnO nanostructures using hydrothermal technique. Doping of ZnO nanostructures through hydrothermal method were also highlighted. One-dimensional nanostructures exhibited interesting electronic and optical properties due to their low dimensionality leading to quantum confinement effects. ZnO had received lot of attention as a nanostructured material because of unique properties rendering it suitable for various applications. Amongst the different methods of synthesis of ZnO nanostructures, the hydrothermal method was attractive for its simplicity and environment friendly conditions [20].

L. Dangol *et al.* growth the ZnO films which has average thickness 364 nm were deposited on glass substrates via hydrothermal process using a mixture of 25 mM aqueous solutions of zinc nitrate and hexamethylenetetramine at a constant temperature of 75 ± 5^{o}C. The structure of ZnO film was analyzed by using XRD. Their result showed that ZnO film is of polycrystalline nature with preferential orientation along (002) perpendicular to the substrate. Average crystallite size of prepared ZnO film was found to be 18 nm. SEM image clearly showed the growth of nano-plate structure with an average thickness and breadth of 90 nm and 390 nm respectively. The band gap of ZnO was determined from transmittance spectrum captured in the visible wavelength. The calculated value of direct band gap was 3.24 eV [21].

A. Alkahlout *et al.* investigated the stable crystalline AZO nanopowders were synthesized using hydrothermal treatment processing. Three different aluminum precursors had been used. The Al precursors were found to affect the morphology of the obtained nanopowders. AZO nanoparticles based on zinc acetate and aluminum nitrate had been prepared with different Al/Zn molar ratios. XRD investigations was revealed that all the obtained powders had single phase zincite structure with purity of about 99%. The effect of aluminum doping ratio in AZO nanoparticles (based on

Al-nitrate precursor) on structure, phase composition, and particle size had been investigated. The incorporation of Al in ZnO was confirmed by UV-Vis spectroscopy revealing a blue shift due to Burstein-Moss effect [22].

M. Jiao *et al.* grew ZnO nanorods selectively on-chip with a two-step low-temperature hydrothermal method and their gas sensing properties were investigated. Small Zinc islands were deposited by sputtering on a glass substrate and used as nucleation sites for the ZnO nanorod growth. An equimolar aqueous solution of 0.005 m $Zn(NO_3)_2•6H_2O$ and $(CH_2)_6N_4$ at 85 °C was used in two steps. The first step was used for nucleation and growth of short ZnO nanorods for 4 hours, whereas the second step was used for elongation of the nanorods for 36 hours. Long porous nanorods from neighboring islands connected to each other and formed nanorod junctions. A gas sensor with such nanorods was evaluated towards NO_2, ethanol, hydrogen, and ammonia to characterize its sensing properties. It showed that the gas sensor has the highest sensitivity to NO_2, and a very high selectivity to this gas when measured at 450°C [23].

A. R. Reddy *et al* studied the ZnO nano crystals prepared using zinc nitrate hexahydrate ($Zn(NO_3)_26H_2O$) and sodium hydroxide (NaOH) as the starting precursors in the molar ratio's of 1:2 and 1:10 through the hydrothermal method. The effects of NaOH concentration on structural and optical properties of ZnO nano crystals were investigated. The ZnO nanoparticles were characterized with XRD, FE-SEM and UV-VIS absorption spectroscopy. The hexagonal wurtzite structure of ZnO nanocrystals was confirmed from XRD results. The Full Width at Half Maximum (FWHM) of XRD peaks increased with increase of NaOH concentration which indicates that the average crystallite size of ZnO nano crystals decreased with increase of NaOH concentration. FESEM pictures exhibited hexagonal shaped ZnO nanocrystals comprising of cylindrical pores of diameters ranging from 9 nm to 12 nm. The number of pores as well as their diameters enhanced with increasing concentration of NaOH. Absorption spectra of these ZnO nano crystals showed an absorption peak positioned at 350 nm. This was due to the excitonic absorption in the ZnO nano crystals. The prepared porous ZnO samples using hydro thermal method

might reduce the required reflection losses in the front surface which was one of the important desirable features in optoelectronic devices [24].

R. Savu ***et al.*** studied the ZnO nanorods in the form of powder or nanostructured films which synthesized by the hydrothermal method using aqueous solutions. Once the synthesis time was completed, the reaction vessel was naturally cooled submitted to a quenching process. XRD, SEM and TEM techniques were employed to characterize the crystallinity, morphology, and dimensions of the nanorods, as well as their growth direction. Suspensions of powder material were spin coated over oxidized silicon substrates in order to obtain nanostructured layers. Photodetectors based on in-situ grown and spin coated films were prepared in order to evaluate the influences of cooling rate and device configuration on the UV sensing characteristics. Spin coated layers showed an excellent performance, better than nanorods grown directly on the substrate during the hydrothermal process. For both configurations, the sensitive layers built from quenched samples exhibited enhanced UV photoresponses when compared to the naturally cooled ones [25].

X. Xu ***et al.*** ZnO nano-superstructures (NSSs) had attracted intense research interests due to their large surface areas and unique properties. At this work, they reported an original approach to synthesize ZnO NSSs in a one-step manner with a hydrothermal method. The crystalline structures and growth mechanism could be understood by surface energy calculations. The reaction kinetics was investigated for the control of the morphology of ZnO NSSs. The critical role of the morphology of Au catalysts in the synthesis of ZnO nanostructures had been demonstrated. Such ZnO NSSs could be fabricated on various rigid and flexible substrates for applications in electronics, solar cells and piezoelectric devices [26].

E.Chitanu ***et al.*** presented the results of synthesis of ZnO nanowires by hydrothermal method from 0.04 M of Zn(NO3)2 6H2O and C6H12N4, solutions using ZnO:Al thin film substrate. Temperature was kept constant at 90oC for 2 hours. Nanowires of ZnO were cleaned with DI water and drayed with nitrogen and structural and morphological characterized. XRD pattern of the ZnO nanowire growth on a Al:ZnO thin film substrate. A dominant diffraction peak for (002) indicated a high degree of orientation with the caxis vertical to the substrate surface.

SEM imagines showed that a dense array of hexagonal ZnO nanowires having a diameter of from 25nm to 90 nm and length between 100 and 170nm [27].

Akhiruddin *et al.* synthesized ZnO nanoparticles with hydrothermal method using ethylene glycol as a stabilizer and as well as a template. Their study was aimed to examine the influence of hydrothermal duration (3, 6 and 12 hours) on the structures and optical properties of ZnO nanoparticles. XRD results showed that all peaks appear in the diffraction pattern indicate the hexagonal wurtzite structure of ZnO. The lattice parameters found just slightly varied with addition of hydrothermal duration. It was found that the particles size decreased whereas the average crystals size increased with hydrothermal duration. The average crystal size found increase with addition of hydrothermal duration. On the other hand, the particle grains were spread evenly distributed with decreasing size with hydrothermal duration increase, as indicated in the SEM images. Optical properties were investigated based on the optical transmission of the ZnO films. It was known that the films strongly absorb the visible region, whereas the absorption edge in the UV region. Bandgap energy of the films found increase with hydrothermal duration, that were 3.18 eV, 3.21 eV and 3.24 eV for 3 hours, 6 hours and 12 hours, respectively [28].

H. F. Quintero *et al.* synthesized ZnO rods with hydrothermal method. Physical dimensions of the ZnO rods were changed systematically as a function of: precursor salt, deposition time, molarity, and temperature parameters. Nano and Microrods were obtained by using nitrate and acetate, respectively. The morphology was obtained by SEM. Zinc acetate resulted as the optimum precursor salt to study the synthesis process of the rods. Diffuse reflectance, photo and cathode luminescence, and XRD techniques were employed to characterize the rods as a function of hexamine molarity/zinc acetate molarity ratio (MHMT/MZn). Optical results made possible to propose an energy diagram that presents different optical radiative desexcitation mechanisms. All rods resulted with an average energy gap of 3.36 eV and several energy levels into it associated to structural defects. The increase of neutral interstitial zinc and/or neutral oxygen vacancy shallow donors with the incorporation of HMT into precursor solution contributed to have a red shift of the ultraviolet emission [29].

K. Gautam *et al.* The structural and optical properties of ZnO nanorods were investigated as a function of growth temperature of the seed layer. The seed layer comprising of ZnO nanocrystallites was grown on ITO substrates at five different temperatures (150-550 ^{o}C) and the nanorods were grown on the seed layer by the facile hydrothermal method. The seed layer grown at 350^{0}C was observed to be uniformly textured with c-axis orientation leading to the synthesis of vertically aligned nanorods with smaller diameter. The HR-TEM analysis and the intense peak along (002) direction in the XRD spectra of this sample implied that the nanorods possess c-axis orientation. An enhanced UV emission was also observed in the PL spectra of the sample. The diversity in the morphology and orientation of the seeds at different temperatures had explained by the growth kinetics of the ZnO nanocrystallites [30].

N. Kiomarsipour *et al.* successfully synthesized well-dispersed two new structures of scale-and spindle-like ZnO with using zinc nitrate hexahydrate as the starting material and also the low temperature hydrothermal process and any additional surfactant, organic solvents or catalytic agent. The ZnO structures were characterized by XRD, FESEM and TEM. Optical property of the ZnO structures was investigated by room temperature PL spectroscopy. The results revealed that ZnO powders have hexagonal (wurtzite-type) crystal structure and a large amount of well dispersed ZnO scale and spindle-like structures was formed. The thickness of scales was in the range 40–60 nm and the diameter of spindles was in the range 50–70 nm. Room temperature PL spectra from the ZnO structures showed aweak UV emission peak at ~382 nm and a very strong visible green emission at 530 nm, that was a scribed to the transition between V_oZn_i and valence band [31].

P. M. Aneesh *et al.* synthesized ZnO nanoparticles with using hydrothermal method by varying the growth temperature and concentration of the precursors. The formation of ZnO nanoparticles were confirmed by XRD, TEM and SAED studies. The average particle size had found to be about 7-24 nm and the compositional analysis was done with ICP-AES. DRS results showed that the band gap of ZnO nanoparticles was blue shifted with decrease in particle size. PL properties of ZnO nanoparticles at room temperature were studied and the green photoluminescent

emission from ZnO nanoparticles can originate from the oxygen vacancy/ZnO interstitial related defects [32].

S.N. Bai *et al.* growth one dimensional AZO nanowires on a silicon substrate with a ZnO seeding layer by using a low temperature hydrothermal method was demonstrated. The structural and optical characteristics of the solution-grown AZO nanowires were studied using FE-SEM, XRD, and cathodoluminescence (CL) measurements. The FE-SEM images showed that the ZnO nanowires were hexagonal column shaped and stood perpendicularly on the silicon substrate. The ZnO nanowires annealed at various temperatures are all wurtzite crystal structure and have (002) preferred orientation is founded in XRD patterns. As the annealing temperature changed, the intensity of (100) and (101) peaks reveals distinct change. The CL spectra show the as-grown ZnO nanowires display a weak and narrow UV emission centered at 376 nm. A strong and very broad green–yellow emission band with a center at 575 nm as well as a shoulder like orange–red emission band centering at 625 nm was also demonstrated. It was shown that the luminescence intensity centered at 376 nm increased, the shoulder like emission centered at 625 nm decreased but emission centered at 575 nm disappeared after thermal annealing treatment in oxygen atmosphere [33].

S. Yun *et al.* High-density, single-crystal, quasi-aligned, AZO nanorod arrays were grown on a silicon substrate using a low temperature hydrothermal process. Different Al atomic concentrations had successfully doped into the ZnO lattice using different Zn and Al precursors in the synthesis solution. The effects of Al doping on the microstructure characteristics, elemental composition and optical properties of the nanorod arrays were studied. It was shown that the morphology, density, and surface compositions of ZnO nanorod arrays had been sensitive to the concentration and variety of zinc and aluminum precursors. The ratio of ultraviolet to visible emission peak (IUV/IVis) increased as the aluminum nitrate concentration increases up to 5mM. The best optical property was obtained for AZO nanorods grown in a 0.04 M zincacetate dihydrate solution with 5mM of aluminum sulfate hydrate. The improved optical property in AZO nanorods could be attributed to the decrease in oxygen deficiency after Al doping [34].

E. Burunkaya *et al.* synthesized AZO nanometricparticles using hydrothermal method. Aluminumnitrate hydrate, aluminum sec-butoxide and zincnitrate hydrate were used as the starting materials, and n-propanol and 2-butanol were used as solvents. Ratio of Al_2O_3 in ZnO was kept at 10 wt%. Reaction was conducted in a teflon autoclave at 175–225 ^oC for 5 h. Ratios of alcohol, H_2O and HCl to zinc nitrate hydrate were altered and 6 different sets of parameters were investigated. Obtained products were subjected to powder-XRD, particlesize measurement, TEM examination and AAS analysis. Single phase AZO particles were obtained at alcohol to zinc nitrate ratio of 35, acid to zinc nitrate ratio of 0.2, at 225 ^oC. Particle size was determined as 3.2 ± 0.4 nm from TEM examinations and as 1–2 nm from dynamic light scattering. Synthesized particles had amphiphilic character, thus they could be dispersed in both polar and non-polar media. It was seen from the UV-diffuse reflectance spectra that the AZO powder had low reflectance in the UV region and high reflectance in the visible region. The obtained powder had the potential to be utilized in the form of thin films for optical and electronic purposes [35].

J.T. Chen *et al.* fabricated the undoped and AZO nanostructures on the ITO substrates pre-coated with ZnO seed layers using the hydrothermal method. The undoped well-aligned ZnO nanorods were synthesized. When introducing the Al dopant, ZnO shows various morphologies. The morphology of ZnO changes from aligned nanorods, tilted nanorods, nanotubes/nanorods to the nano sheets when the Al doping concentrations increase. The ZnO nano structures were characterized by XRD, FESEM, XPS, PL and Raman technology. The Al doping concentrations play an important role on the morphology and optical properties of ZnO nanostructures. The possible growth mechanism of the ZnO nanostructures was discussed [36].

T. Y. Hsieh *et al.* synthesized AZO nanostructures FEAs hydrothermally on AZO/glass substrate. The samples with Al-dosage of 3 at.% showed the morphology as nanowires vertically grown on the substrates and a structure of c-axis had elongated single-crystalline wurtzite. The good field-emission (i.e., the large anode current and low fluctuation of 15.9%) could be found by AZO nanostructure FEAs with well-designed Al-dosage (i.e., 3 at.%) because of the vertical nanowires with the less structural defects and superior crystallinity. Moreover, the FWHM of near

band-edge emission (NBE) decreased as the increase of annealing temperature, representing the compensated structural defects during oxygen ambient annealing. After the oxygen annealing at 500^0C, the hydrothermal AZO nanostructure FEAs revealed the excellent electrical characteristics (i.e., the larger anode current and uniform distribution of induced fluorescence) and enhanced field-emission stability (i.e., the lowest current fluctuation of 5.97%) [37].

B.V. Shrisha *et al.* prepared Pure and Al doped (0 - 5 at %) ZnO nanorods using two step hydrothermal method. In the first step, ZnO thin films were deposited on glass substrates by sol-gel spin coat method. In the next step, AZO nanorods were grown on the ZnO film coated glass substrates by hydrothermal method using the aqueous solution of [$Zn(NO_3)_2.6H_2O$] (0.1 M), [HMT;$C_6H_{12}N_4$] (0.1 M) and [$AlCl_3.6H_2O$] prepared using double distilled water. The growth was carried out by maintaining thetemperature of the autoclave at 90 °C for 6 h. The structural, morphology and optical properties of the grown ZnO nanostructures were characterized by XRD, FESEM, EDX, UV-Vis and PL spectroscopy. XRD spectra shows both ZnO and Al doped nanorod shave the hexagonal wurtzite structure with a strong (002) preferred orientation. As Al doping percentage increased, the XRD spectra showed dominance of (101) orientation. The surface morphology of the films were studied using SEM, shows that the both pure and AZO films have hexagonal shaped nanorods. The band gap of ZnO nanorods increased with Al doping concentration. The optical parameters such as refractive index, extinction coefficient and dielectric constants were determined using the absorbance and the reflectance data. The PL spectrum showed emission peaks in UV and visible region related to NBE and deep level emission (DLE), respectively. As Al doping increased NBE intensity decreased, this might be due to the doping related defects [38].

M. Mazilu *et al.* The study presents the optical properties of undoped and AZO nanostructures grown on glass substrates using the hydrothermal method. The obtained ZnO-based nanostructures showed optical transmittance over 75% and low reflectance in the visible domain. The increasing of optical transmittance of AZO nanostructures with increased doping concentrations was observed. The optical constants such as refraction index, extinction coefficient, dielectric constants and

optical conductivity were determined using the transmission and the reflection at normal incidence of light in the wavelength range of 200–1100 nm. The band gap broadens with increasing dopant concentration from 2% to 4%. The obtained nanostructured layers with size in the range of subwavelength of visible light can act as anti-reflective coating that reduces reflectance based on the Moth Eye principle [39].

S. Huang *et al.* The AZO rod-like whiskers were synthesized by a simple hydrothermal method in the study. The resistivity of whisker (AZOw) samples significantly decreased with the increase of Al^{3+} concentration and showed a minimum when Al^{3+} doping concentration was 2.0%. If Al^{3+} concentration continued to increase, namely more than 2.0%, the resistivity of AZO samples would increase. So, in this study the optimum Al doping concentrationwas 2.0%, and the lowest electric resistivity was obtained [40].

Z. Chen *et al.* synthesized for the first time AZO nanopowders using a novel sol–gel hydrothermal route. The results revealed that the morphology of the AZO nanopowders could be effectively controlled by varying the concentration of mineralizer. The obtained rod-like AZO nanopowders with an average diameter of about 40 nm showed a minimum electrical resistivity, which was lower than that of spheroidal and flake-like AZO. The formation mechanism of the AZO crystalline was also discussed [41].

CHAPTER 2

THEORETICAL BASES

2.1 Semiconductors

Semiconductors are materials with electronic properties intermediate between those of metals and insulators. Semiconductors are insulators at 0 Kelvin and that at this temperature the valence band is completely filled while the conduction band is empty [42].

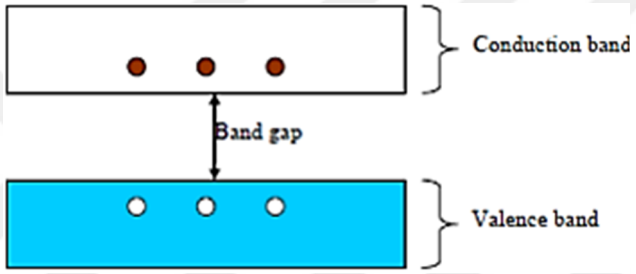

Figure 1.1 Schematic energy band representation of a semiconductor [42].

At room temperature, the energy band gap of the semiconductor is smaller, so also, the valence band is less populated and the conduction band is more populated with electrons than for the case of an insulator. A typical schematic diagram of the band structure of a semiconductor is shown in Figure 1.1. When an electron is raised into the conduction band, this leads to a missing electron or an empty state in the valence band. This empty state may be filled by neighbouring electrons in the valence band that in turn results in a shift in the location of the empty state. The empty state in the valence band is considered to be a quasiparticle called a hole. It carries a positive charge and moves in the opposite direction to the electron [42].

There is no doubt that semiconductors changed the world beyond anything that could have been imagined before them. Although people have probably always needed to communicate and process data, it is thanks to the semiconductors that these two important tasks have become easy and take up infinitely less time. Semiconductors

may be considered as the information carrier of our times. In the history of information, there were two revolutions (approximately 500 years apart). The first was that of Johan Gutenberg who made information available to many, the other is the invention of the transistor. Currently the global amount of information doubles every year. Many things we are taking for granted (such as, e.g., computers, Internet 11 and mobile phones) would not be possible without silicon microelectronics. Electronic circuits are also present in cars, home appliances, machinery, etc. Optoelectronic devices are equally important in everyday life, e.g., fiberoptic communications for data transfer, data storage (CD and DVD recorders), digital cameras, etc. [43]. Semiconductor devices such as diodes, transistors and integrated circuits can be found everywhere in our daily lives, in Walkman, televisions, automobiles, washing machines and computers. We have come to rely on them and increasingly have come to expect higher performance at lower cost [44].

2.1.1 Types of Semiconductors

Semiconductors are either elements or compounds. Si and Ge are most common elemental semiconductors. InSb, InAs, GaP, GaAs, SiC and GaN are compound semiconductors [45].

An intrinsic semiconductor conducts in its pure state. In this case, electron-hole pairs are equally thermally generated and the concentration of the electrons equals that of the holes [46]. According to, the generation of intrinsic carriers is determined by the thermal excitation and recombination of electron holes. Under steady state conditions, the generation rate of electron-hole pairs must be equal to the recombination rate of electrons and holes. In solid-state electronics, either pure silicon or germanium may be used as the intrinsic semiconductor that forms the starting point for fabrication. As shown in Figure 1.2, Silicon crystallizes in the same pattern as diamond, in a structure which Ashcroft and Mermin call "two interpenetrating face-centered cubic" primitive lattices. The lines between silicon atoms in the lattice illustration indicate nearest-neighbor bonds. The cube side for silicon is 0.543 nm. Germanium has the same diamond structure with a cell dimension of 0.566 nm. However, germanium will at a given temperature have more free electrons and a higher conductivity. Silicon is by far the more widely used

semiconductor for electronics, partly because it can be used at much higher temperatures than germanium [47].

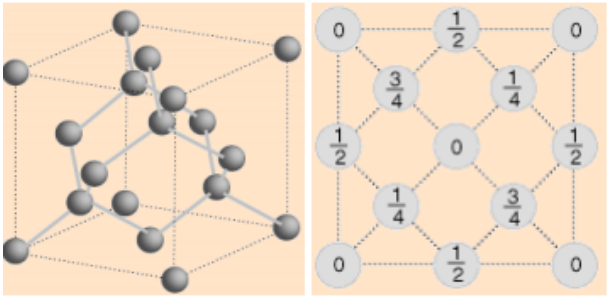

Figure 1.2 The diamond lattice of silicon and germanium [47].

An extrinsic semiconductor is formed when small quantity of foreign atoms known as dopant is introduced to the crystal of an intrinsic semiconductor in order to increase its electrical conductivity. Dopants introduce energy levels from which free carriers can move into the bands. Either extra electrons or holes can be introduced into the crystal by doping. The respective dopants are known as donors for semiconductors that have excess electrons (n-type) and acceptors for semiconductors that have excess holes (p-type) as carriers [42].

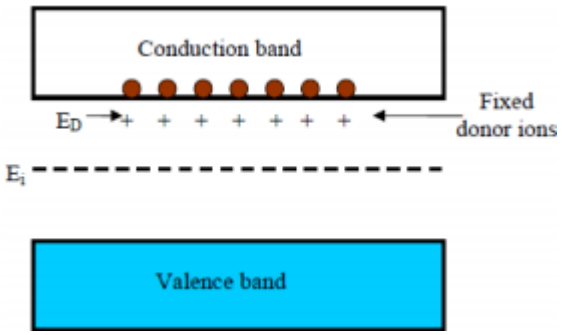

Figure 1.3 Schematic energy band representation of n-type extrinsic semiconductor [42].

The band diagrams of both n and p-type semiconductors are shown in Figure 1.3 and 1.4, respectively. The donor impurity level is normally situated near the conduction band and when the thermal energy exceeds the small ionisation energy of the donor atoms, electrons will be raised into the conduction band as shown in Figure 1.4, resulting in electrical conduction [42].

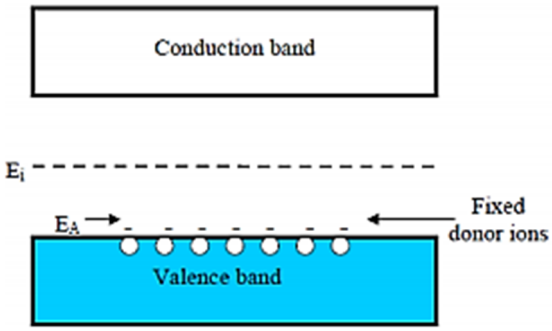

Figure 1.4 Schematic energy band representation of p-type extrinsic semiconductor [42].

In a similar manner to the donor levels, at sufficient thermal energy, electrons are raised from the valence band to the acceptor level leading to the formation of holes in the valence band as illustrated in Figure 1.4 [42].

As shown in Figure 1.5, the addition of pentavalent impurities such as antimony (Sb), arsenic (As) or phosphorous (P) contributes free electrons, greatly increasing the conductivity of the intrinsic semiconductor. (n-type Semiconductor) [47].

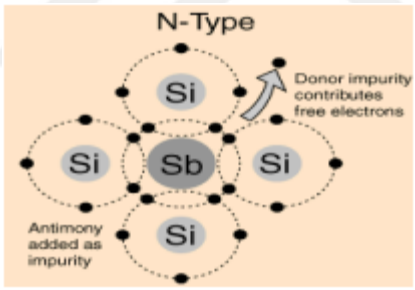

Figure 1.5 The lattice of n-type silicon [47].

As shown in Figure 1.6, the addition of trivalent impurities such as boron (B), aluminum (Al) or gallium (Ga) to an intrinsic semiconductor creates deficiencies of valence electrons, called "holes" [47].

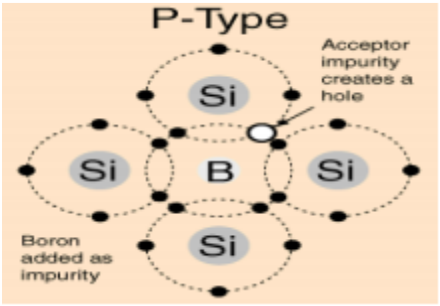

Figure 1.6 The lattice of p-type silicon [47]

2.2 ZnO Films

In last years, metal oxide semiconductor films have been widely studied and have drawn much attention due to their optical and electrical properties. Some of these oxide semiconductors are suitable candidates for TCO films [48].

2.2.1 Properties of ZnO Films

Among TCO materials, ZnO has raised as one of the most promising materials due to its optical and electrical properties [49], suitability to doping, non-toxicity [50], high resistivity control [51] high chemical, mechanical [49] and high thermal [52] stability together with its abundance in nature which makes it a lower cost material [49]. Due to these superior properties ZnO is a good choice for electronic or optoelectronic applications [53] such as antireflection coatings [54], transparent electrodes in solar cells [55], gas sensors [56], varistors [57], light emitting diodes [58], nanolasers [59] heterojunctions etc. On the other hand, pure ZnO thin films are sensitive to oxidation and O_2 absorption in the films cause a decrease in the electrical conductivity. The optical properties of ZnO are widely affected by surface morphology and optical energy band gaps [48]. ZnO crystallizes in the hexagonal wurtzite structure (c=5,205 and a=3,249) [60] and each Zn atom in the lattice is bonded tetrahedrally with four adjacent O atoms [54]. ZnO is an n-type [51] II-VI semiconductor which has a wide direct band gap of ~3.37 eV [61] and a huge exciton binding energy of ~60 meV at room temperature (300 K) [62]. Its n-type electrical conductivity is due to deviations from the stoichiometry resulting from oxygen vacancies and interstitial zinc, giving rise to a shallow donor level just below the conduction band [63]. ZnO has resistivity

control over the range 10^3 -10^5 Ω-cm [51], high transparency in the range of 0,4-2μm optical wavelength [64] and its transmittance is nearly 80-90% in the visible range [65].

2.2.2 ZnO Crystal Structure

Most of the group-II-VI binary compound semiconductors crystallize in either cubic zinc-blende or hexagonal wurtzite structure where each anion is surrounded by four cations at the corners of a tetrahedron, and vice versa. This tetrahedral coordination is typical of sp^3 covalent bonding, but these materials also have a substantial ionic character. ZnO is an II-VI compound semiconductor whose iconicity resides at the borderline between covalent and ionic semiconductor.

Zinc oxide crystallizes in three forms: hexagonal wurtzite, cubic zinc-blende, and the rarely observed cubic rock salt. The wurtzite structure is most stable and thus most common at ambient conditions. The zinc-blende form can be stabilized by growing ZnO on substrates with cubic lattice structure. In both cases, the zinc and oxide are tetrahedral. The rock salt NaCl type structure is only observed at relatively high pressures ~10 GPa. The hexagonal and zinc-blende ZnO lattices have no inversion symmetry (reflection of a crystal relatively any given point does not transform it into itself).

The lattice constants are a = 3.25 Å and c = 5.2 Å; their ratio c/a ~ 1.60 is close to the ideal value for hexagonal cell c/a = 1.633 [66].

The wurtzite and zinc-blende crystal structure of ZnO are schematically shown in Figure 1.7. As in most II-VI materials, the bonding in ZnO is largely ionic, which explains its strong piezoelectricity. Due to this ionicity, zinc and oxygen planes bear electric charge (positive and negative, respectively). Therefore, to maintain electrical neutrality, those planes reconstruct at atomic level in most relative materials, but not in ZnO its surfaces are atomically flat, stable and exhibit no reconstruction. This anomaly of ZnO is not fully explained yet [67].

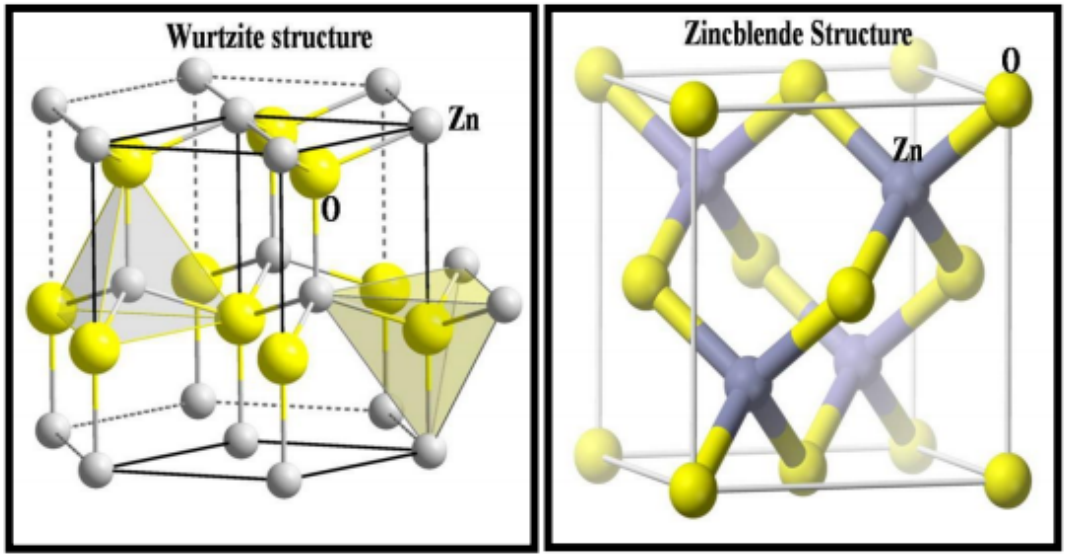

Figure 1.7 Crystal structure of ZnO

2.3 AZO Films

ZnO has wide conductivity range changing with respect to different oxidation conditions. Doping with group II, group III and group VII elements such as Indium (In), Aluminum (Al), Gallium (Ga), Copper (Cu), Cadmium (Cd), Fluorine (F) etc. increases the stability, conductivity and transparency of ZnO films [68,69]. "The ZnO doping for n-type conductivity could be achieved by replacing Zn atoms with atoms of higher valance elements such as Aluminum (Al), Indium (In) and Gallium (Ga)." The electrical characteristic of semiconductor materials can be positively altered by adding controlled amount of particular impurity atoms. The technique of adding impurity atoms to semiconductor materials in order to change its conductivity is celled doping. Dopant atoms may be change charge carriers. Aluminum doping is particularly suitable for those purposes. Among group III element much of the work has been done by using Al as a dopant because the ionic radius of Al is smaller than that of In and Ga and also free energy of formation of Al_2O_3 is lower than that of ZnO [70]. "Al doping is preferable due to its easy incorporation in ZnO structure thus decreasing resistivity of the materials without impairing the optical transmission of thin film."

Moreover, “Al is a cheap, abundant and non-toxic material which could produce AZO thin film with low resistivity and high optical transmittance in visible and near infrared region [71].” Ionization energy calculated of 120 meV and low formation energy, referenced to the elemental Al phase.

Al is introduced as a dopant in terms of donor behavior increase in the conductivity of ZnO because the Zn^{2+} ion is greater than the Al^{3+} ion and could easily be accommodated in either hole and Al has one valence electron more than Zn. Substitution of Al for the Zn atom or Al occupation of the interstitial sites increases the concentration of charge carriers present in the material [72].

There are some supported studies about this concept by introducing extrinsic dopant Al, the defect environment is changed, whether the Al atom substitutes the zinc atom or it occupies the interstitial site. Al doping in ZnO has been reported to be able to change the electrical and optical properties of ZnO thin films [73].

CHAPTER 3

MATERIAL PRECEDURE

In this work, it was decided to use hydrothermal method to grow ZnO and AZO films because of simple equipment, no catalyst growth, low cost, wide area uniform production, environment friendly, less dangerous.

3.1 Hydrothermal Method

3.1.1. History and Development of Hydrothermal Method

The term “hydrothermal” was first used by Sir Roderick Murchison in the mid 19th century. The first paper on hydrothermal research was on the synthesis of tiny quartz crystals and published in 1845 by K.F.E. Schafthaul. Then, many scientists especially the ones from Europe, started to fabricate other minerals using hydrothermal method. In the beginning, interest in hydrothermal method was only in the fabrication of specific minerals or compounds similar to natural minerals instead of investigating the phase relations or geochemistry of earth’ s interior. It was later on realized that using hydrothermal conditions, it is possible to imitate the natural processes that cause the formation of rocks and minerals. Through the World War II, hydrothermal research facilities became larger and the interest in hydrothermal technology moved to Europe. Today, hydrothermal method is widely used for various purposes by different branches of science including organic chemistry, materials science and biotechnology, and so on [74]. In this thesis, hydrothermal method is used for the growth of ZnO and AZO nanowires.

The hydrothermal method provides an excellent possibility for processing of advanced materials whether it is fine particles, or nanoparticles.

3.1.2 Definitions

In literature many different definitions have been used for hydrothermal synthesis. Rabenau in 1985 defined hydrothermal synthesis as the heterogeneous reactions in aqueous media above 100°C and 1 bar [75]. Lobachev defined it as a group of

methods in which crystallization is carried out from superheated aqueous solutions at high pressures [76]. According to Roy hydrothermal synthesis involves water as a catalyst and occasionally as a component of solid phases in the synthesis at elevated temperature (>100°C) and pressure (greater than a few atmospheres) [77]. Byrappa in 1992 defines hydrothermal synthesis as any heterogenous reaction in an aqueous media carried out above room temperature and at pressure greater than 1 atm [78]. Yoshimura in ref [79] defined it as "…reactions occurring under the conditions of high-temperature–high-pressure (>100°C, >1 atm) in aqueous solutions in a closed system". With the vast number of publications under mild hydrothermal conditions in recent years, K. Byrappa in 2001 propose to define hydrothermal reaction as "any heterogenous chemical reaction in the presence of a solvent (whether aqueous or nonaqueous) above room temperature and at pressure greater than 1 atm in a closed system."[74].

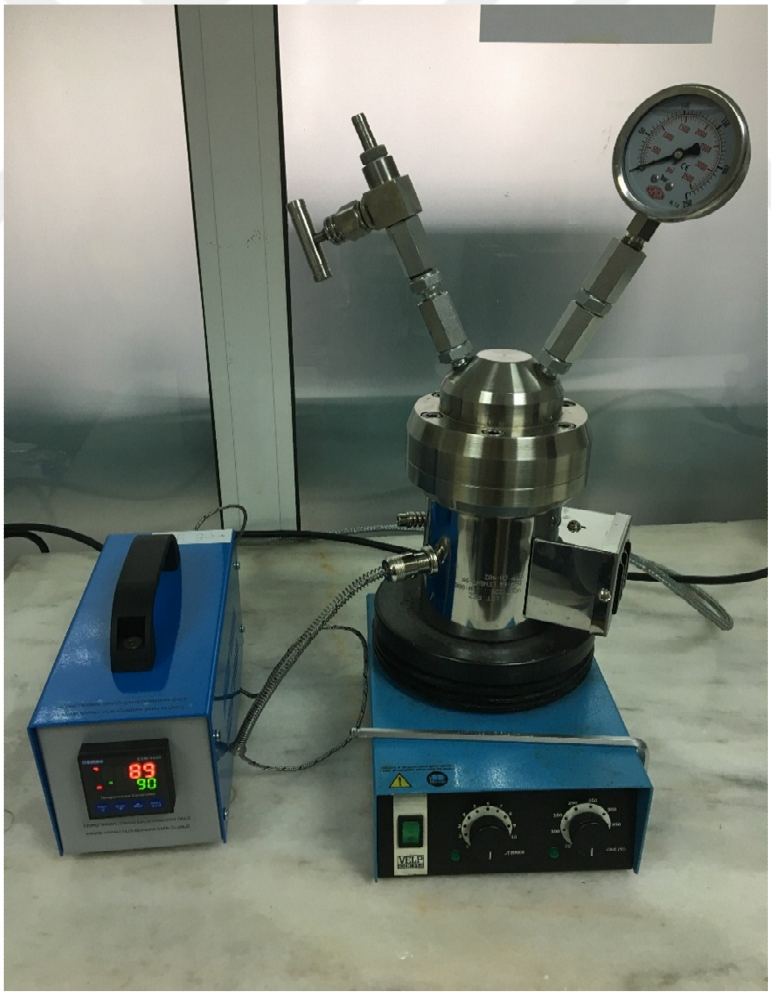

Figure 3.1 Hydrothermal system

3.1.3 Advantages of Hydrothermal Synthesis

Hydrothermal synthesis offers many advantages over conventional and non conventional synthesis methods. Unlike many advanced methods that can prepare a large variety of forms, the respective costs for instrumentation, energy and precursors are far less for hydrothermal methods. From the environmental perspective, hydrothermal methods are more environmentally benign than many other methods. This method is beneficial to different industries which rely on powder (e.g. materials, pigments, pharmaceuticals, medical diagnostics) will benefit from having an access to powders with controlled size and morphology for a wide range of reasons. Materials synthesized under hydrothermal conditions often exhibit differences in point defects when compared to materials prepared by high temperature synthesis methods. e.g. Tungstates of Ca, Ba, and Sr synthesized at room temperature by a hydrothermal method do not contain Schottky defects usually present in similarmaterials prepared at high temperatures [80] which results in improved luminescent properties.

A major advantage of hydrothermal synthesis is that this method can be hybridized with other processes like microwave, electrochemistry, ultrasound, mechano-chemistry, optical radiation and hot-pressing to gain advantages such as enhancement of reaction kinetics and increase ability to make new materials. A great amount of work has been done to enhance hydrothermal synthesis by hybridizing this method with many other processes. This facile method does not need any seed, catalyst, harmful and expensive surfactant or template thus it is promising for largescale and low-cost production with high-quality crystals.

3.1.4 Autoclave

Crystal growth under hydrothermal conditions requires a reaction vessel called an autoclave. In hydrothermal method highly corrosive salt are used to synthesis inorganic materials for longer reaction time. The Autoclave must be capable of sustaining highly corrosive solvent at high temperature and pressure for a longer duration of time. For selecting a suitable autoclave, the first and foremost parameter is the experimental temperature and pressure conditions and the corrosion resistance

in that pressure-temperature range in a given solvent or hydrothermal fluid. In our case as the reaction is taking place directly in the vessel, the corrosion resistance is a prime factor in the choice of the autoclave material. The most successful corrosion resistant materials high-strength alloys, such as 316 series (austenitic) stainless steel, iron, nickel, cobalt-based super alloys, and titanium and its alloys. To avoid corrosion of autoclave material it should coated with non reactive material called Teflon from inside. Due to the larger coefficient of thermal expansion of Teflon (the liner) versus metal (the material in which the liner is enclosed), the Teflon will expand and contract much more upon heating and cooling cycles than its enclosure material.

An ideal hydrothermal autoclave should have the following characteristics:

(i) Inert to acids, bases and oxidizing agents.
(ii) It should be easily assemble and dissemble.
(iii) It should have sufficient length to obtain a desired temperature gradient.
(iv) It should be leak-proof at desired temperature and pressure.
(v) It should bear high pressure and temperature for long duration of time.

3.2 XRD

XRD which is a vigorous method can be used for investigation of crystal structure of a solid with lattice constants and geometry. On the other hand, it can be also used for orientation of single crystals, orientation of defects in crystal structure and identification of unknown solids [81]. X-ray region is identified with a wavelength of approximately 0.5-2.5Å in electromagnetic spectrum. XRD with typical instrumentation can be seen in Figure 3.2. Under the high voltage system, high speed electron with a metal target collided to produce X-rays in Xray tube. Beam of X-rays fall on a specimen as it generated, the crystalline phases in the specimen are diffracted according to the Bragg's law:

$$n\lambda = 2d \sin\theta \tag{3.1}$$

where n is the order of reflection, λ is the wavelegth of incident X-rays, d is the interplanar spacing between planes of a crystal and θ is the angle between incident beam and specimen surface [82].

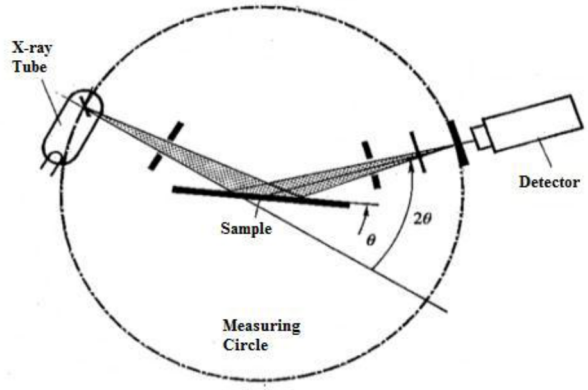

Figure 3.2 The X-ray Spectrometer

Diffracted X-ray intensity is measured kind of function of the diffraction angle, 2θ and the specimen's orientation. This diffraction pattern is used to obtain information of the structural properties and to define the specimen's crystalline phases. It is a group of lines or peaks that has discrete intensity and position. These intensities are charactrestic feature of a material.

Preferential orientation coefficient (TC) represents the texture of a particular plane, deviation of which from unity implies the preferred growth. Quantitative information concerning the preferential crystallite orientation was obtained from different preferential orientation coefficient TC(hkl) defined by well known relation [83],

$$TC(hkl) = \frac{I(hkl)/I_0(hkl)}{N^{-1}\sum_n I(hkl)/I_0(hkl)} \tag{3.2}$$

where $I_{(h\ k\ l)}$ is the measured relative intensity of a plane (h k l), $I_{o(h\ k\ l)}$is the standard intensity of the plane (h k l) taken from the ICDD PDF Card No. 01-089-7102 data, N is the reflection number and n is the number of diffraction peaks. A sample with randomly oriented crystallite presents TC(hkl)=1, while the larger this value, the larger abundance of crystallites oriented at the (h k l) direction.

The structural parameters such as grain size (D), dislocation density (δ), FWHM (β), strain (ε) for all films were evaluated by XRD patterns. The grain size of the thin films was calculated by XRD patterns using Debye Scherrer's formula,

$$D = \frac{0{,}9\lambda}{\beta Cos\theta} \tag{3.3}$$

where D is the grain size, λ is the used X-Ray wavelength, β is the angular line width at half-maximum intensity in radians and θ is Bragg's angle. The grain size, dislocation density and strain of the films were calculated using the FWHM for peaks. Additionally, to have more information on the amount of defects in the films, the dislocation density (δ) was calculated by using the formula below [84,85],

$$\delta = \frac{1}{D^2} \tag{3.4}$$

The strain values were calculated from the following relation [86],

$$\varepsilon = \frac{\beta \mathrm{Cos}\theta}{4} \tag{3.5}$$

3.3 SEM

SEM is a powerful technique in the examination of materials that provides detailed high resolution images of the sample by rastering a focussed electron beam across the surface and detecting secondary or backscattered electron signal. The primary electron beam interacts with the sample in a number of key ways as shown Figure 4.3 [87], this procedure can be considered of three main parts;

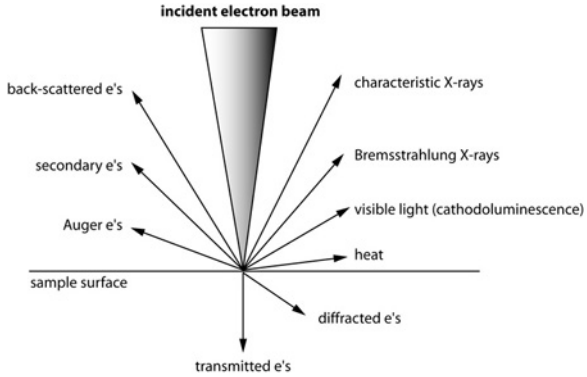

Figure 3.3 Electron beam interacts with the sample

(vi) When electron beam is striking the surface of the specimen and interacting with the sample at or near its surface, secondary electrons are emitted from the specimen surface. Topography of the surface can be observed by two-dimensional scanning of the electron probe over the surface and acquisition of an image from the detected secondary electrons.

(vii) "Primary electrons can be backscattered which produces images with a high degree of atomic number (Z) contrast."

(viii) "Ionized atoms can relax by electron shell-to-shell transitions, which lead to either X-ray Emission or Auger Electron ejection. The X-rays emitted are characteristic of the elements in the top few μm of the sample and are measured by the EDAX detector [88]."

"The SEM is an instrument that produces a largely magnified image by using electrons instead of light to form an image. A beam of electrons is produced by an electron gun at the top of the microscope. The electron beam follows a vertical path through the microscope, which is held within a vacuum. The beam travels through electromagnetic fields and lenses, which focus the beam down toward the sample. Once the beam hits the sample, electrons and X-rays are ejected from the sample. Detectors collect these X-rays, backscattered electrons, and secondary electrons and convert them into a signal that is sent to a screen similar to a television screen. This produces the final image. The schematic view of this process is shown in Figure 4.4 [89]."

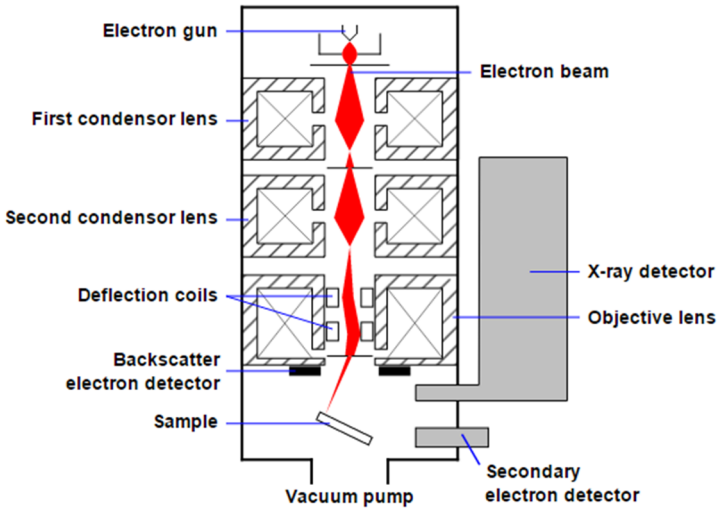

Figure 3.4 Schematic diagram of an SEM [81].

Some unique properties that mentioned below make the SEM one of the most useful instruments in research today. These are;

(i) Excellent depth of field, which allows more of a specimen to be n focus at one time.

(ii) Rapid, high resolution imaging of surface topography with identification of elements present.

(iii) Characterization of particulates and defects.

(iv) Examination of grain structure.

(v) Much more control in the degree of magnification.

Energy Dispersive X-ray Spectroscopy (EDS), sometimes called Energy Dispersive X-ray Analysis (EDXA) or Energy Dispersive X-ray Microanalysis (EDXMA), is an analytical technique used for the elemental analysis of a sample therefore It is help to provide elemental identification and quantitative compositional information.

3.4 UV-VIS Spectroscopy

When a light wave hits an interface between two mediums with different refractive indices, So the all of or some part of wave will be reflected, leaving the surface and some part of will be transmitted into the second medium. When passing through the medium, a fraction of light is absorbed in the material. The optical interface is characterized by the behavior of the light associated with the reflectance, absorbance, and the transmittance.

Ultraviolet-visible spectroscopy (UV/ VIS) involves the spectroscopy of photons in the UV-visible region. It uses light in the visible and adjacent near ultraviolet (UV) and near infrared (NIR) ranges. The wavelength range for light source used is from 200 nm to 1000 nm (from UV to IR range) [90].

Absorption spectra and transmittance spectra are usually registered by instruments called as spectrophotometers Figure 4.5 (a) shows a schematic diagram with the main

elements of the simplest spectrophotometer (a single-beam spectrophotometer) and Figure 4.5 (b) shows a double-beam spectrophotometer.

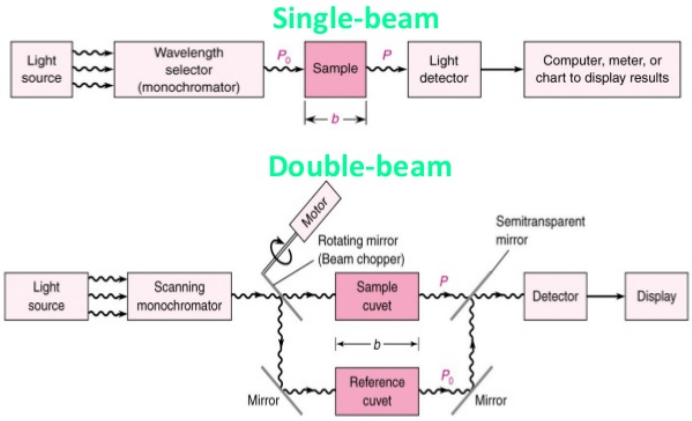

Figure 3.5 Schematic diagrams of (a) A single-beam spectrophotometer and (b) A double-beam spectrophotometer.

Basically, "it consists of the following elements: a light source (usually a deuterium lamp for the UV spectral range and a tungsten lamp for the VIS and IR spectral ranges) that is focused on the entrance to a monochromator, which is used to select a single frequency (wavelength) from all of those provided by the lamp source and to scan over a desired frequency range; a sample holder, followed by a light detector (usually a photomultiplier for the UV–VIS range and a SPB (surface Plasmon band) cell for the IR range) to measure the intensity of each monochromatic beam after traversing the sample; and finally a computer, to display and record the absorption spectrum."

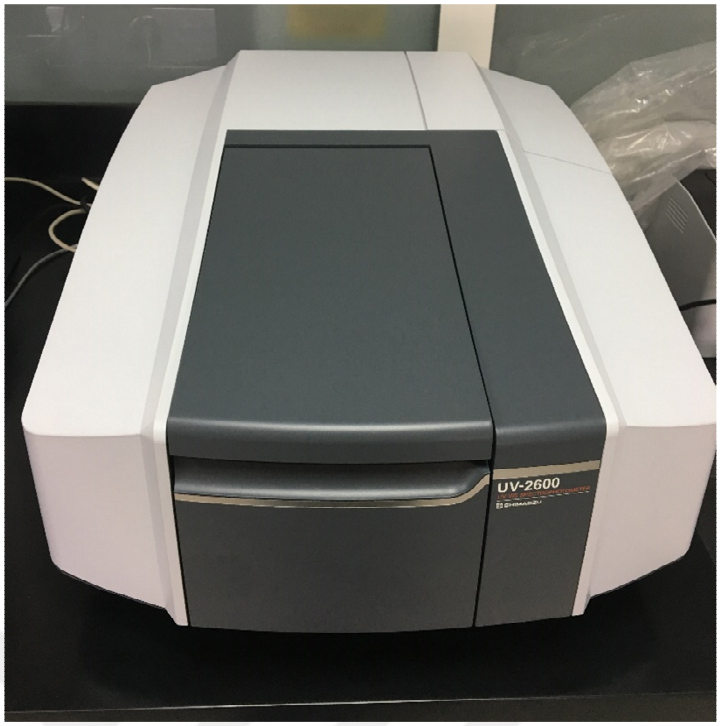

Figure 3.6 The picture of UV-VIS spectrophotometer

The refractive index of the films was calculated using Moss relation [91,92] which is directly related to the fundamental energy bandgap (Eg),

$$Egn^4 = k \tag{3.6}$$

where k is a constant with a value of 108 eV. This relation is preferred to other relations because it is found to give better agreement with the known data for n in II–VI semiconductors. A different relation between the refractive index and bangap energy is presented by Herve and Vandamme in the following for [93,94],

$$\mathrm{n} = \sqrt{1 + \left(\frac{\mathrm{A}}{\mathrm{Eg+B}}\right)^2} \tag{3.7}$$

where A and B are numerical constants with values of 13.6 and 3.4 eV, respectively.

The dielectric behavior of solids is important for several electrondevice properties. Both static and high frequency dielectric constants were evaluated for all the films. The high frequency dielectric constant (ε_∞) was calculated from the following relation [95],

$$\varepsilon_{\infty} = n^2 \tag{3.8}$$

where n is refractive index. The static dielectric constant ($\varepsilon_{\circ}$) of the films was calculated using a relation expressing the energy band gap dependence of 3o for semiconductors compounds in the following form [96,97],

$$\varepsilon_{\circ} = 18.52 - 3.08Eg \tag{3.9}$$

Similarly to the static dielectric constant, a relation expressing the energy bandgap dependence of the electron effective mass for the semiconductor compounds in the following form [98],

$$\frac{m_e^*}{m_0} = 5.17004 - 7.46699\text{Eg} + 3.63286\text{Eg}^2 - 0.57525\text{Eg}^3 \tag{3.10}$$

3.5 Cleaning of Substrate

For growth the film the glass substartes are used. The cleanning procedure steps of glass are given below;

(i) Glass base materials were ultrasonically cleaned in deionized water for 10 minutes,

(ii) It was cleaned in acetone for 2 minutes,

(iii) It was cleaned in a (1: 1) ethanol water mixture for 2 minutes,

(iv) Then it was cleaned in a deionized water for 1minutes.

3.6 Growth of ZnO Films

The nanorod arrays were prepared from solutions of zinc nitrate tetrahydrate and hexamethylene tetramine on glass substrates. 0.03 M -0.05 M Zinc nitrate tetrehydrate [$Zn(NO_3)_2$ $4H_2O$] and with 0.03 M -0.05 M Hexamethylenetetramine (HMT) ($C_6H_{12}N_4$) was prepared in 30 ml deionized water and they were mixed solution slowly stirring (180 rpm) until complete dissolution. An equimolar solution zinc nitrate tetrehydrate and hexamethylenetetramine was prepared in the deionized water and the substrates were fixed in a Teflon liner. The growth solution was kept in

a stainless steel autoclaves for three to twelve hours at 90 ºC and 100 ºC. It was then allowed to cool naturally to room temperature. After the reaction was complete, the samples dried at room temperature.

The chemical reactions by hydrothermal method to grow ZnO microrods in this study can be given as follows:

$$Zn(NO_3)_2\ 4\ H_2O + 2OH^- \rightarrow 4Zn(OH)_2 + NO^{2-}_3 + H_2O$$

$$Zn(OH)_2 \rightarrow Zn^{2+} + 2OH^-$$

$$C_6H_{12}N_4 + 6H_2O \rightarrow 6HCHO + 4NH_3$$

$$NH_3 + H_2O \rightarrow NH_4^+ + OH^-$$

$$Zn^{2+} + 2OH^- \rightarrow ZnO + H_2O$$

3.7 Growth of AZO Films

Then appropriate amounts of aluminum doping were achieved by adding Aluminum chloride ($AlCl_3$) to the precursor solution. In order to study an effect of the Al doped concentration on microstructural and optical properties of the AZO thin films, Al is added to the starting solition (Al/Zn=5, 3, 1 at %, respectively). Then these solutions were mixed to yield clear and homogeneous solutions. As a result, AZO thin films were deposited on common glass substrate. For this aim, the growth solution was kept in a stainless steel autoclaves for twelve hours at 90 ºC and 100 ºC.

3.8 Calculating of Film Thicknesses

The thicknesses of ZnO and AZO films obtained on glass base materials were determined by Gravimetric method. This process was performed with an electronic scale with a sensitivity of 0,0001 grams. This process were carried out in two stages. Glass materials were weighed before the shytesiss. Than the same materials were

weighed after the film growth again. The difference between the two scales gives the film mass formed on the base materials. The film thicknesses is calculated by,

$$d = \frac{\Delta m}{S\rho} \tag{3.11}$$

Here; ρ is the film density, Δm is the film mass diffrencess, S is the film surface area, d is the film thickness. The density of the ZnO compound (ρ) is 5.61 g / cm^3.

CHAPTER 4

EXPERIMENTAL PRECEDURE

4.1 Structural characterization

4.1.1 XRD Measurements of Films

In order to investigate the structural properties of the films grown by the hydrothermal method, XRD patterns of the films were taken at 2θ = 20-90 °C using Rigaku MiniFlex 600 X-ray diffractometer (using Cu-Kα λ = 1.5405 Å radiation).

With the aid of these patterns, the crystallization levels of the films were investigated and structural properties of the films were analyzed by calculating some structural parameters. For this purpose, structural parameters such as distance between the layers (d), grain size (D), dislocation density (δ) and the strain (ε) values of the films were calculated using the diffraction angle (2θ) and full width at half maximum (FWHM) values obtained from the XRD patterns. In the XRD patterns of ZnO and AZO films, the Miller indices of the corresponding planes within the parentheses were indicated.

If the intensities of the peaks in the diffraction patterns are large and their widths are narrow, it means that the crystallization in the films is good. Films with large peak width and low peak intensity are thought to be close to the amorphous structure.

4.1.1.1 ZnO Films

The XRD patterns of ZnO films grown on glass substrates by hydrothermal method at different synthesis temperature, different growth time, and different solution molarity values are given in Figure 4.1-3.

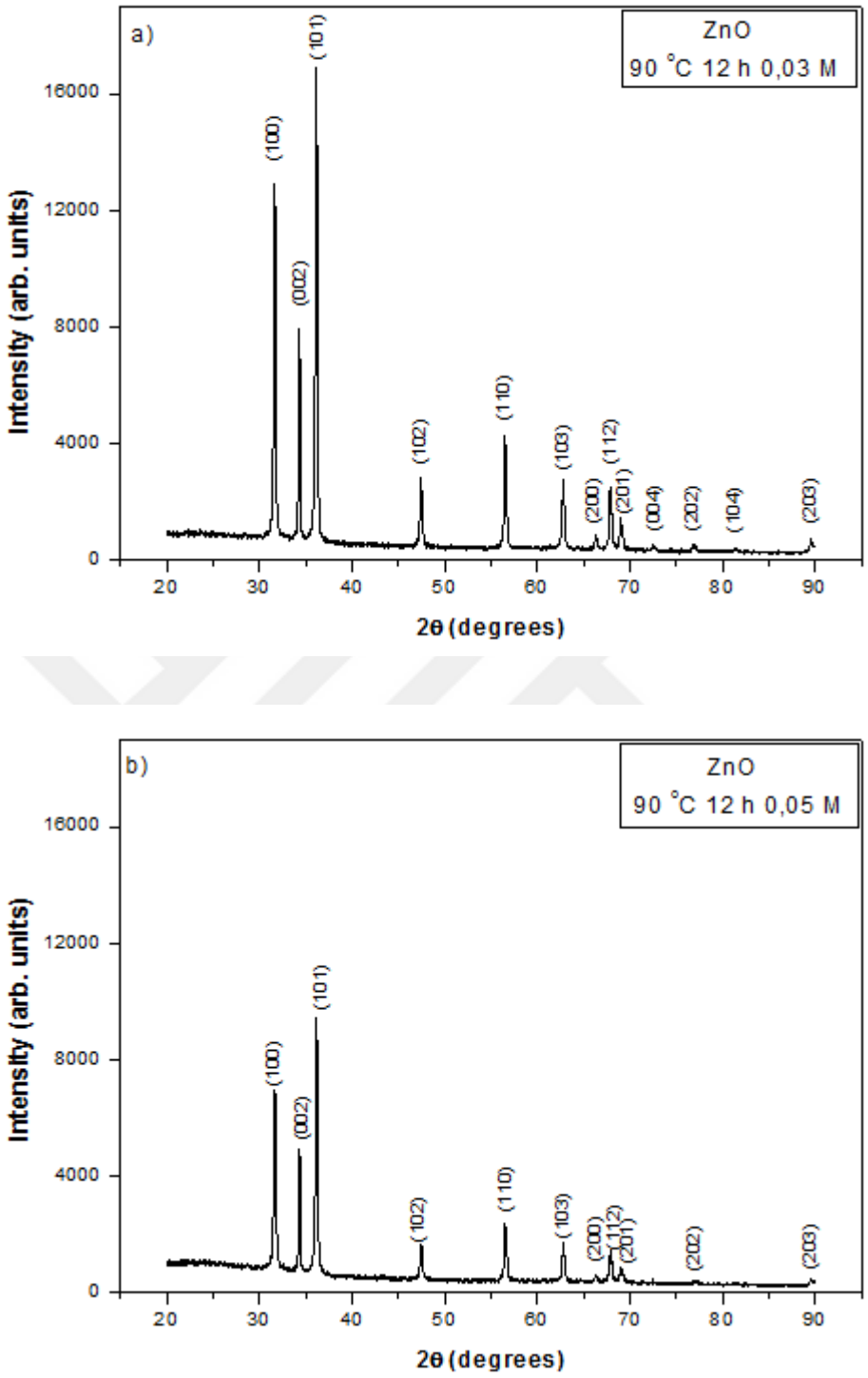

Figure 4.1 The XRD patterns of 90 °C, 12 h ZnO films [a) 0.03 M, b) 0.05 M].

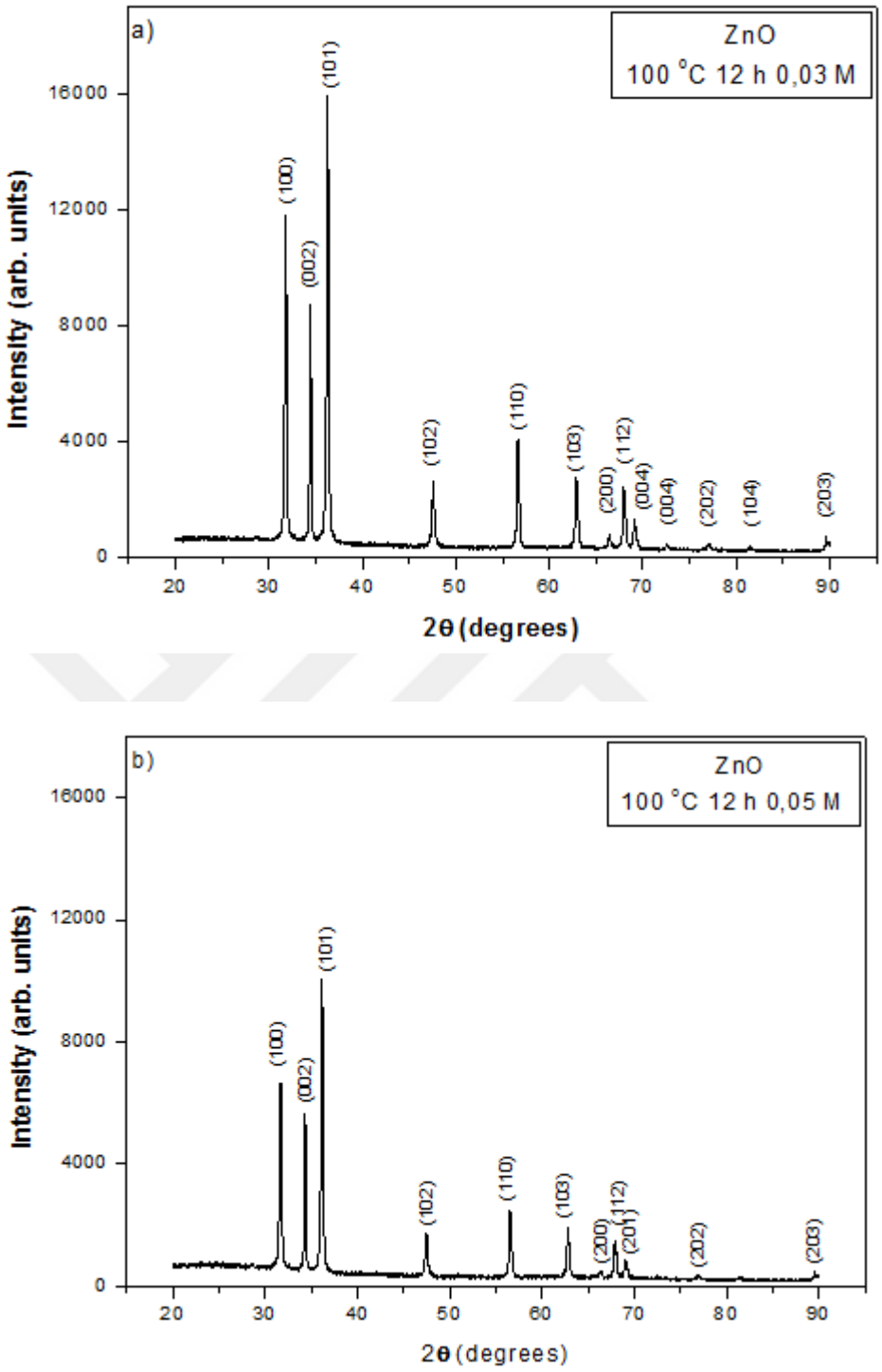

Figure 4.2 The XRD patterns of 100 ºC, 12 h ZnO films [a) 0.03 M, b) 0.05 M].

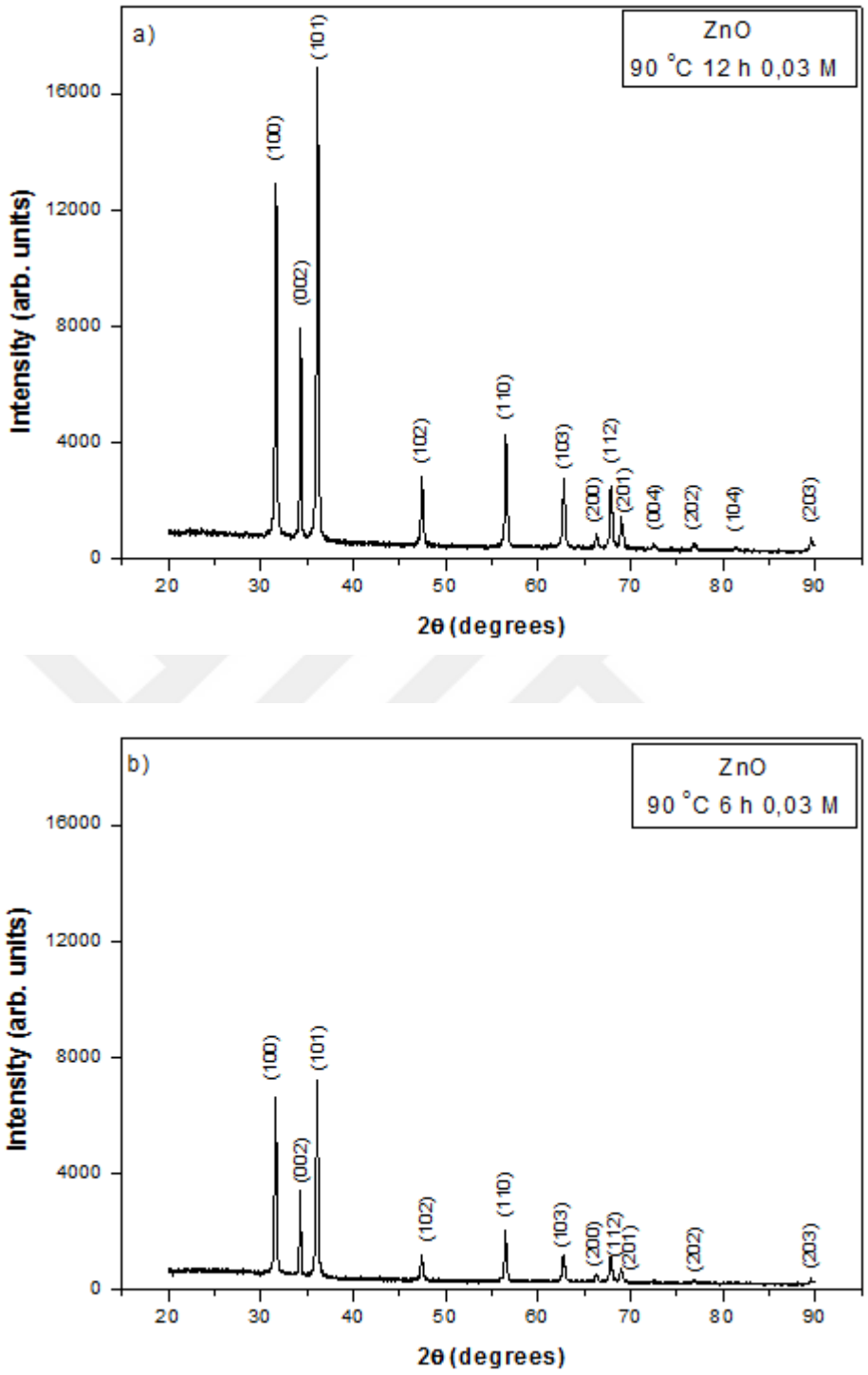

Figure 4.3 The XRD patterns of 90 ºC, 0.03 M ZnO films [a) 12 h, b) 6 h].

4.1.1.2 AZO Films

The XRD patterns of AZO films grown glass substrates by hydrothermal method at different synthesis temperature, different amount of doping and different solution molarity values are given in Figure 4.4-7.

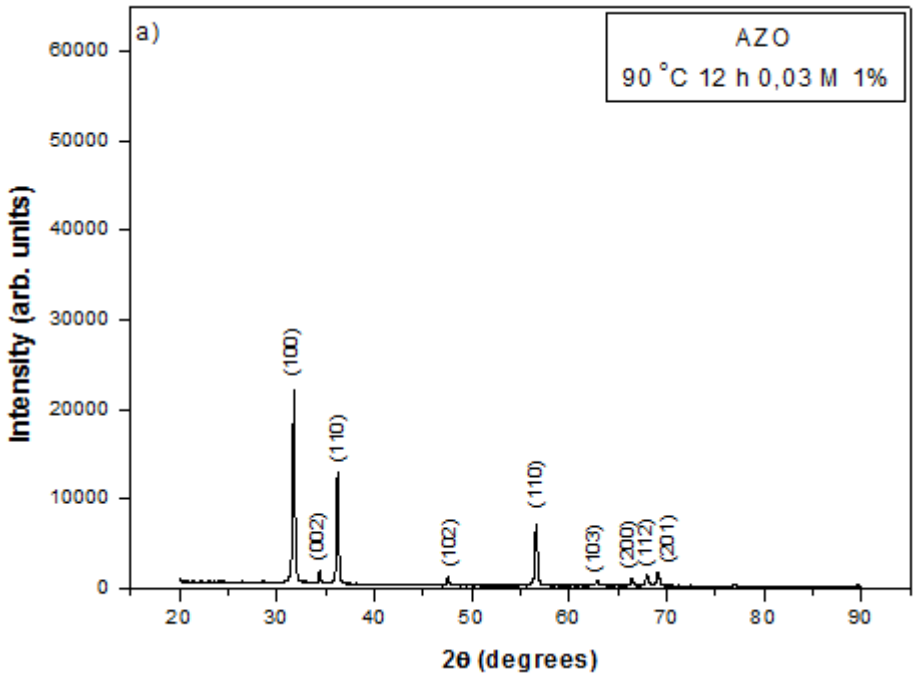

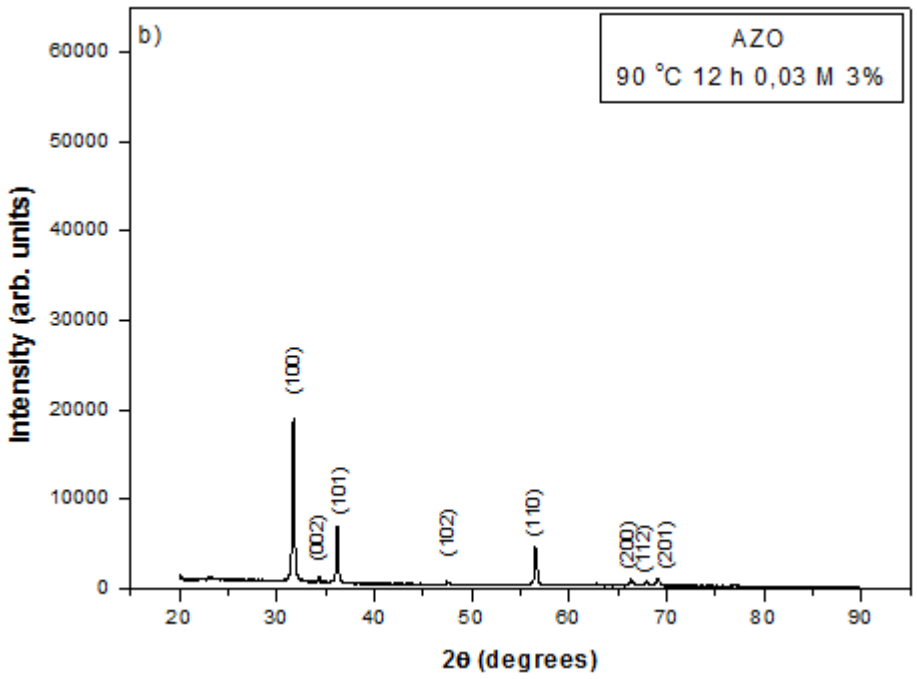

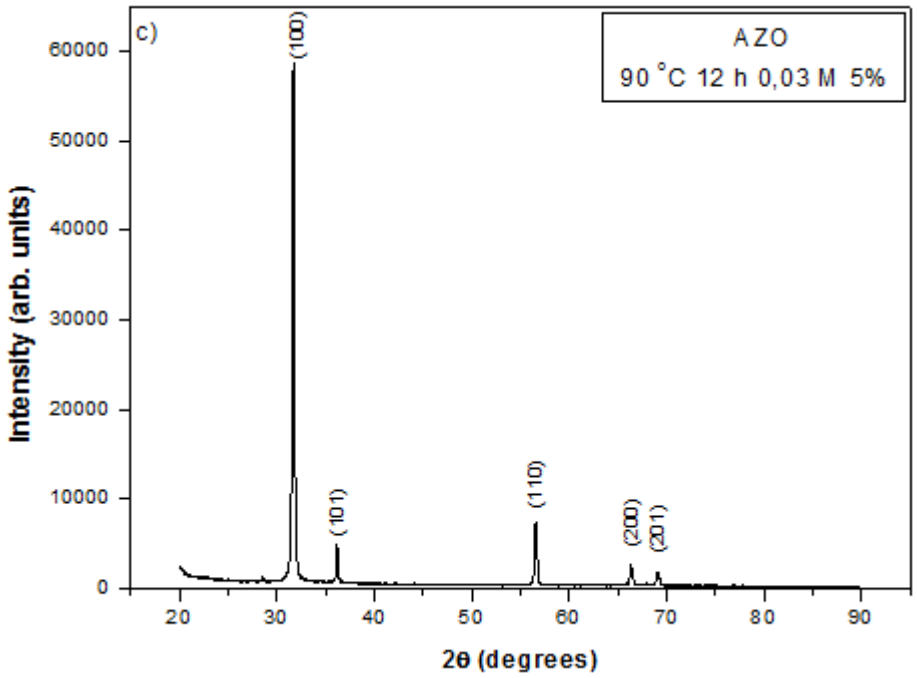

Figure 4.4 The XRD patterns of 90 ºC, 12 h, 0.03 M AZO films [a) 1%, b) 3%, c) 5%].

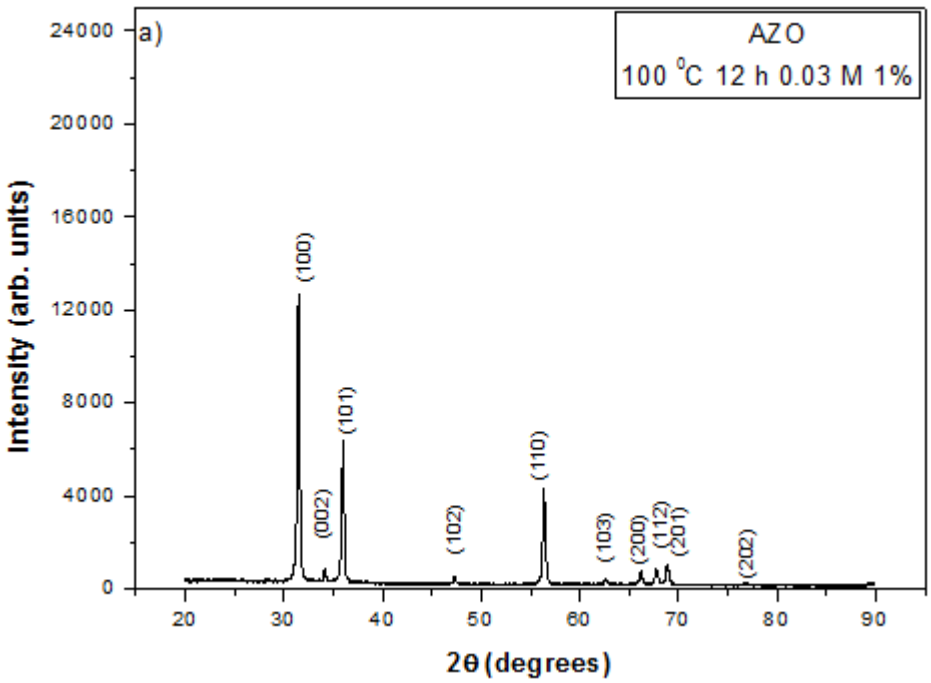

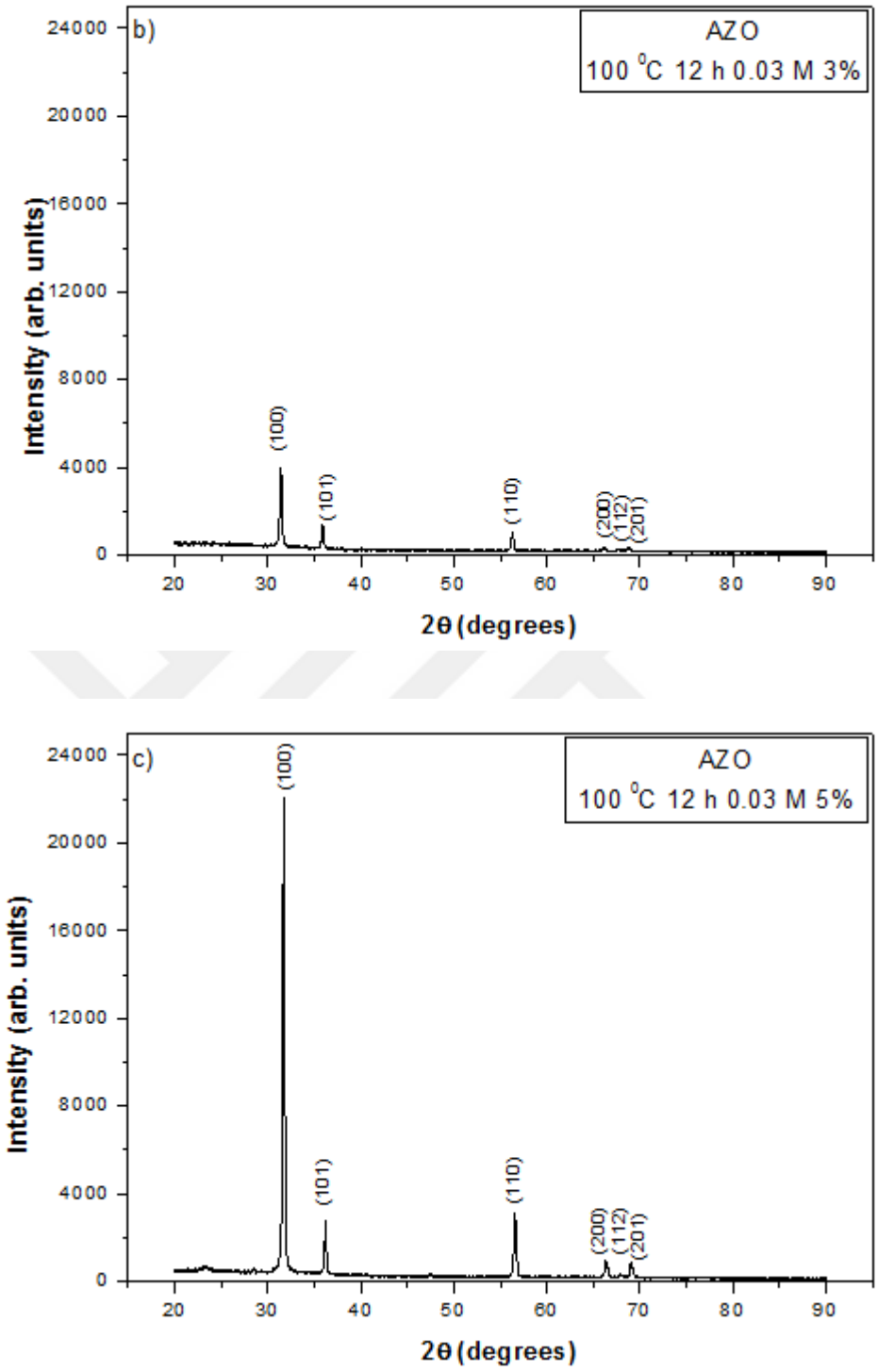

Figure 4.5 The XRD patterns of 100 ºC, 12 h, 0.03 M AZO films [a) 1%, b) 3%, c) 5%]

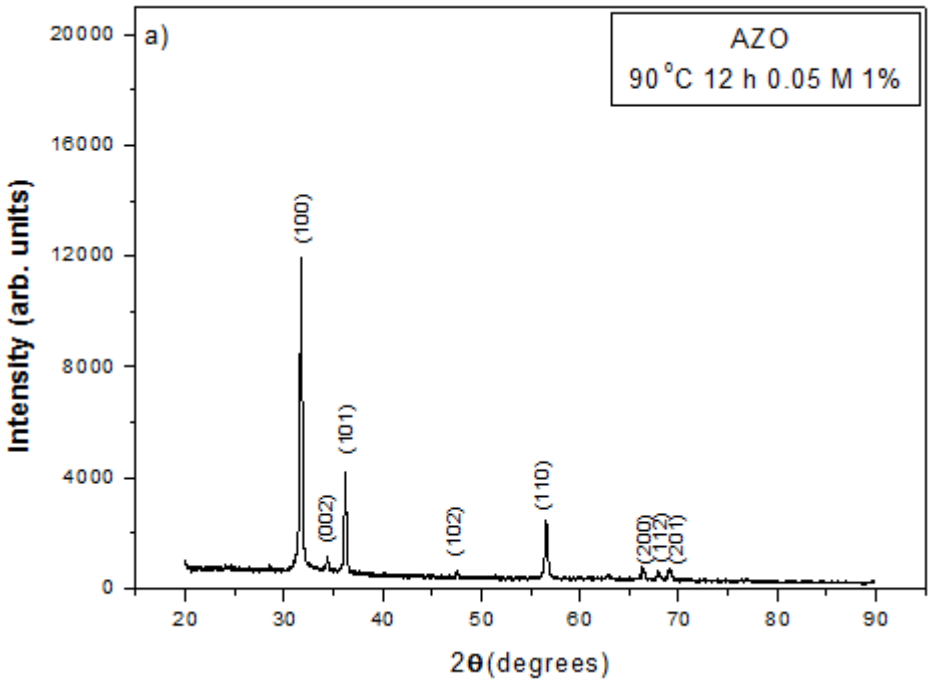
a)
AZO
90 °C 12 h 0.05 M 1%
Intensity (arb. units)
2θ(degrees)
(100)
(002)
(101)
(102)
(110)
(200)
(112)
(201)

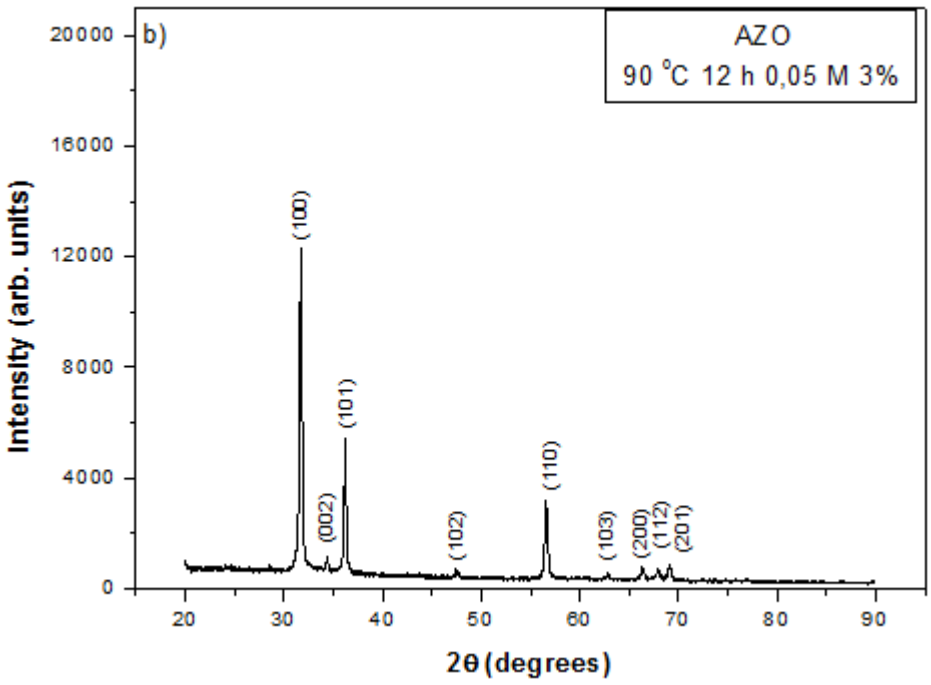
b)
AZO
90 °C 12 h 0,05 M 3%
Intensity (arb. units)
2θ (degrees)
(100)
(002)
(101)
(102)
(110)
(103)
(200)
(112)
(201)

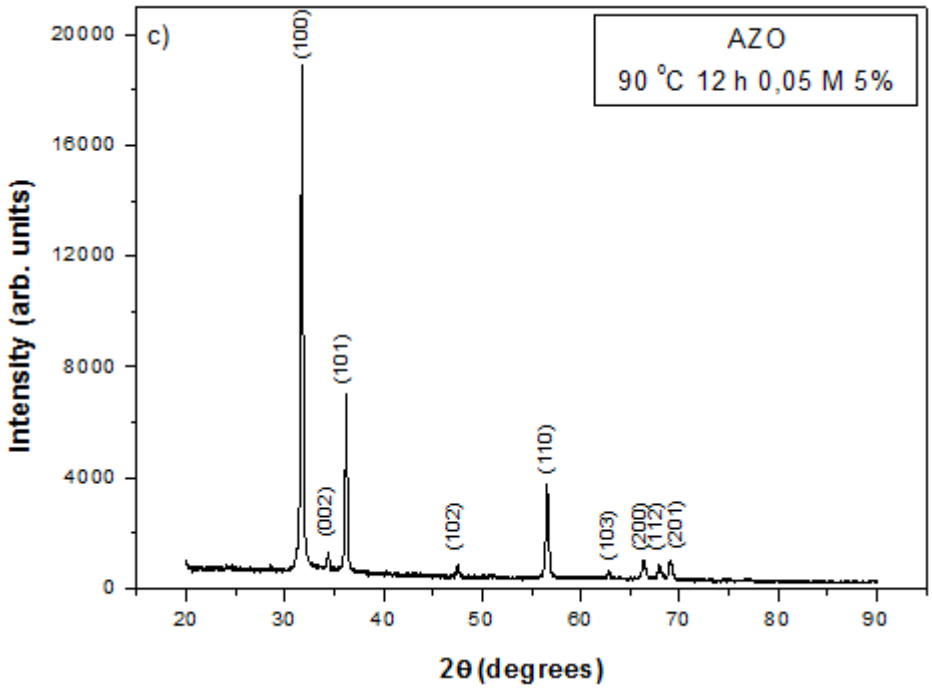

Figure 4.6 The XRD patterns of 90 ºC, 12 h, 0.05 M AZO films [a) 1%, b) 3%, c) 5%].

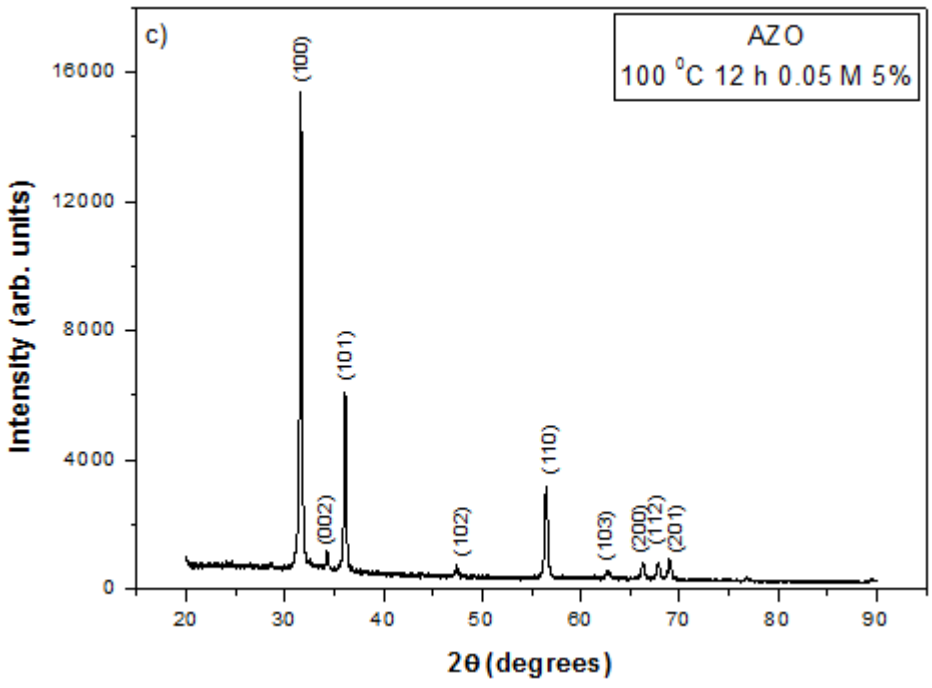

Figure 4.7 The XRD patterns of 100 ºC, 12 h, 0.05 M AZO films [5%].

4.1.2 Surface Images of Films

Surface characteristics of a material which is obtained as the semiconductor film significantly affect both electrical and optical properties. This is also an important factor that will affect the efficiency of the materials in optoelectronic devices. For example, the increase in surface roughness of the films will result in a reduction in the yield of photovoltaic solar cells. Therefore, the surface morphological properties of the films should be analyzed in detail. One of the most common techniques used for this is the Scanning Electron Microscope (SEM). As a result of the SEM examination, the information about the film roughness, well-adhered to the substrate of film, homogeneity of film and surface defects can be obtained. Surface images of ZnO and AZO films were taken using FEI Quanta FEG 450 model Scanning Electron Microscope (SEM).

SEM images of ZnO and AZO films were taken for investigation of effects of synthesis temperature, growth time and solution molarity on surface morphology of the films.

4.1.2.1 ZnO Films

SEM images of ZnO films grown glass substrates by hydrothermal method at different synthesis temperature, different growth time and different solution molarity values are given in Figure 4.8-10.

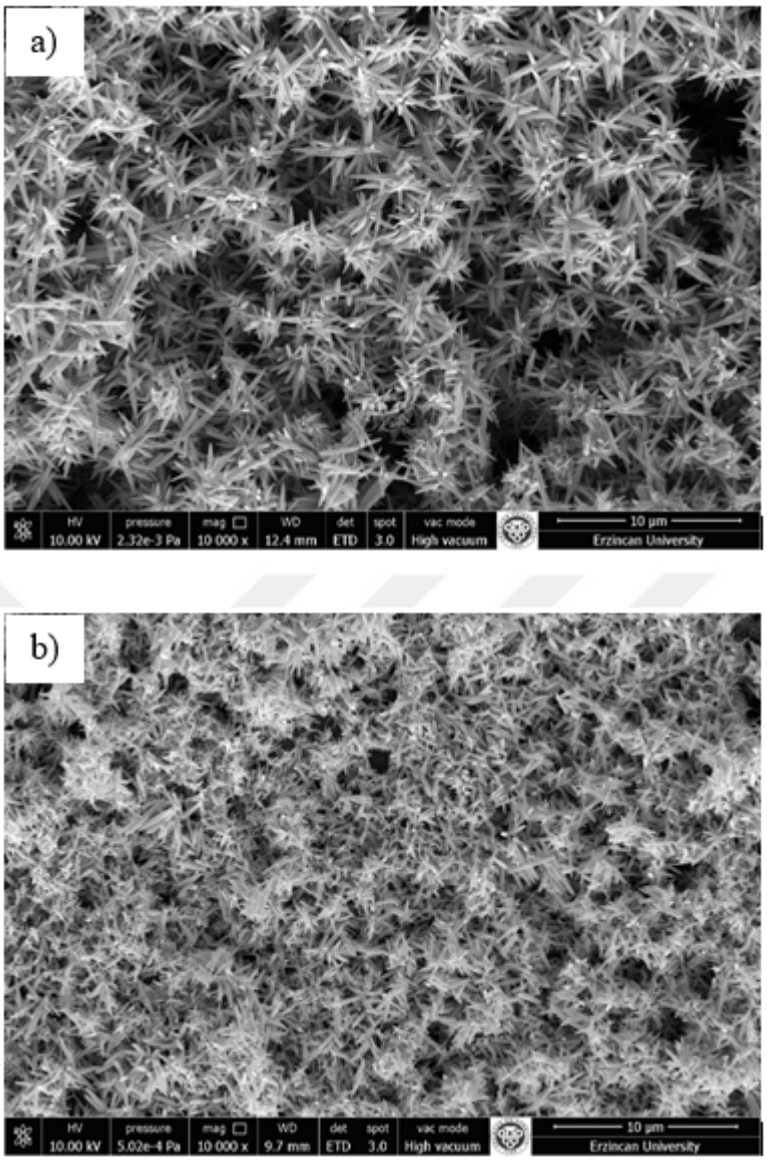

Figure 4.8 SEM images of 90 ºC, 12 h ZnO films [a) 0.03 M, b) 0.05 M] at 10000× magnification.

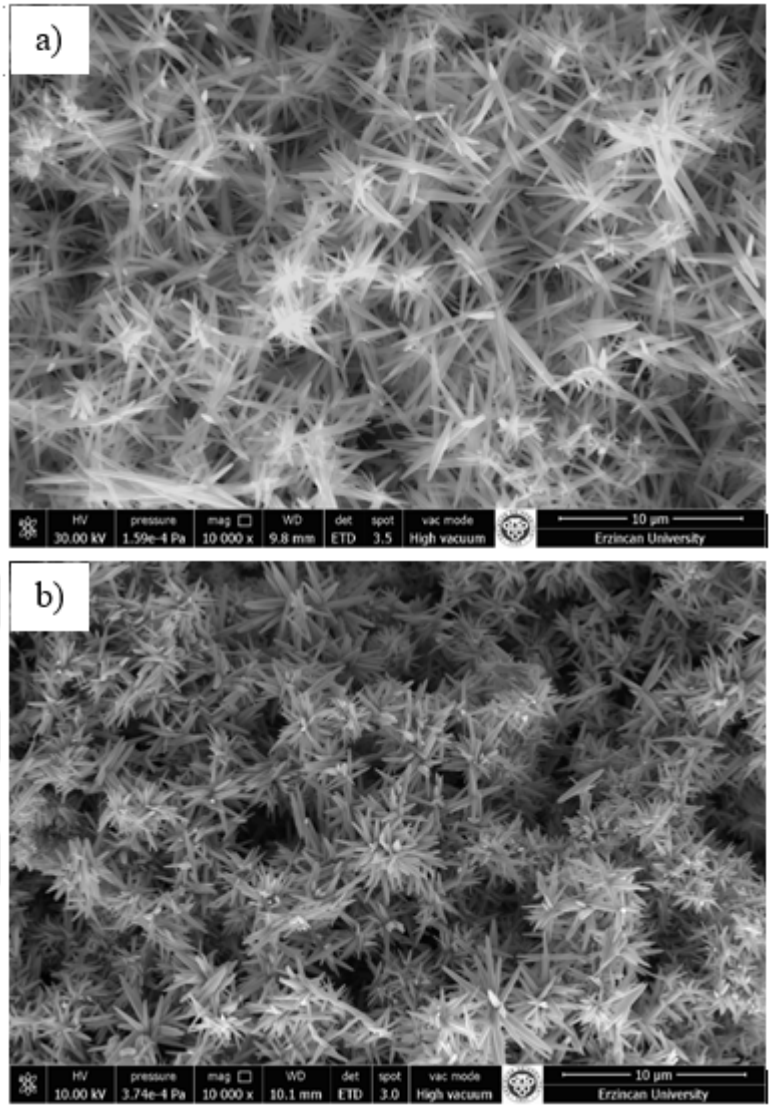

Figure 4.9 SEM images of 100 ºC,12 h ZnO films [a) 0.03 M, b) 0.05 M] at 10000× magnification.

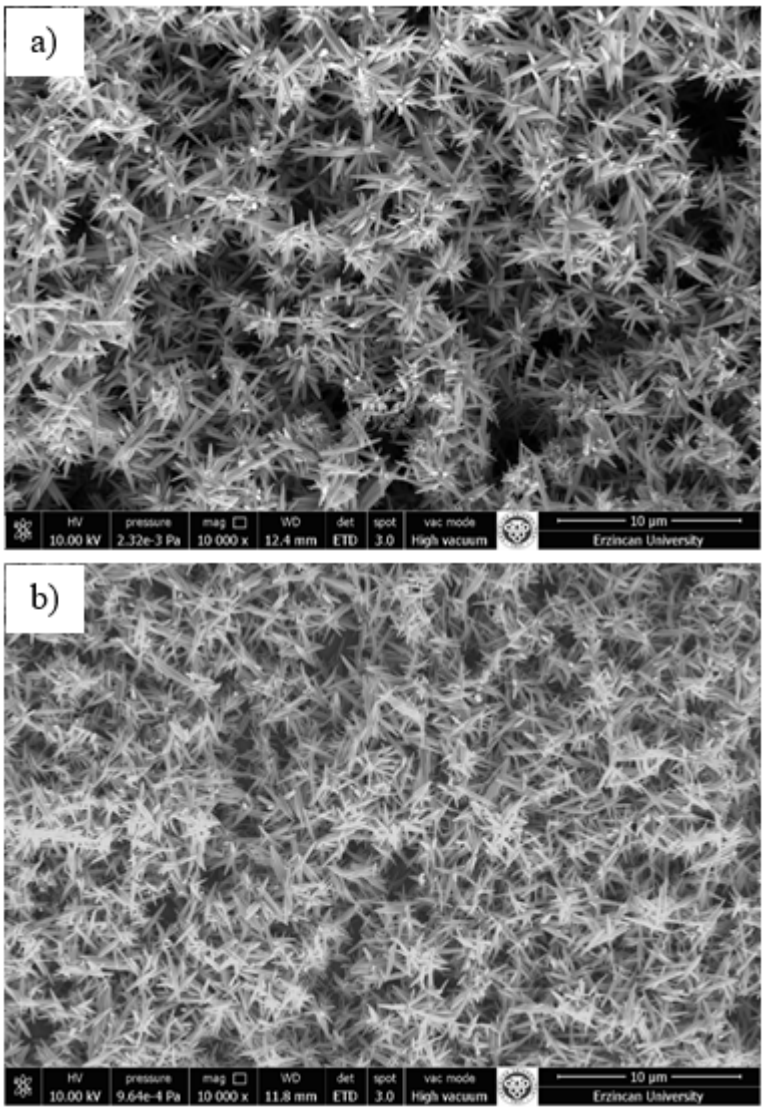

Figure 4.10 SEM images of 0,03M 90 ºC ZnO films [a) 12 h, b) 6 h,] at 10000× magnification.

4.1.2.2 AZO Films

SEM images of AZO films grown glass substrates by hydrothermal method at different synthesis temperature, different amount of doping and different solution molarity values are given in Figure 4.11-14.

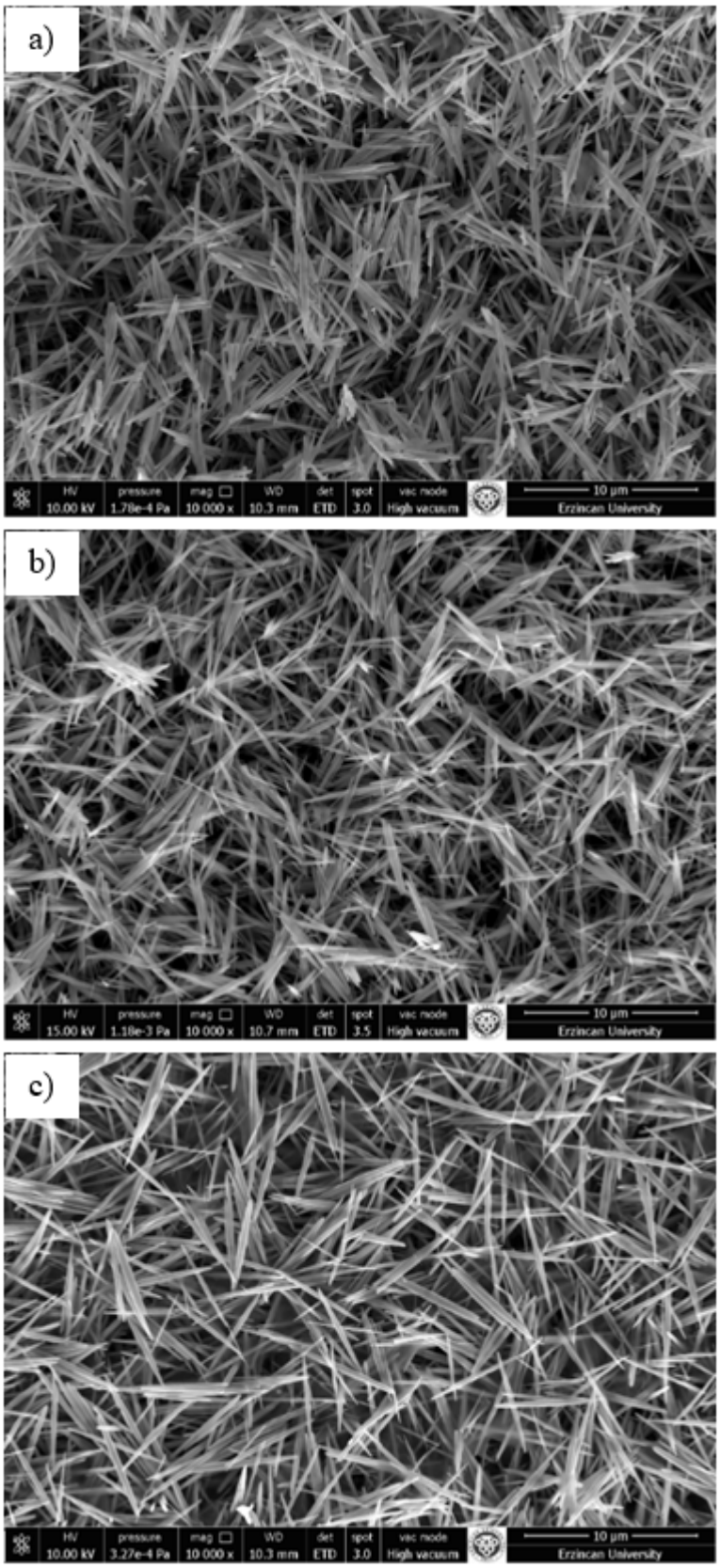

Figure 4.11 SEM images of 90 ºC, 12 h, 0.03 M AZO films [a) 1%, b) 3%, c) 5%] at 10000× magnification.

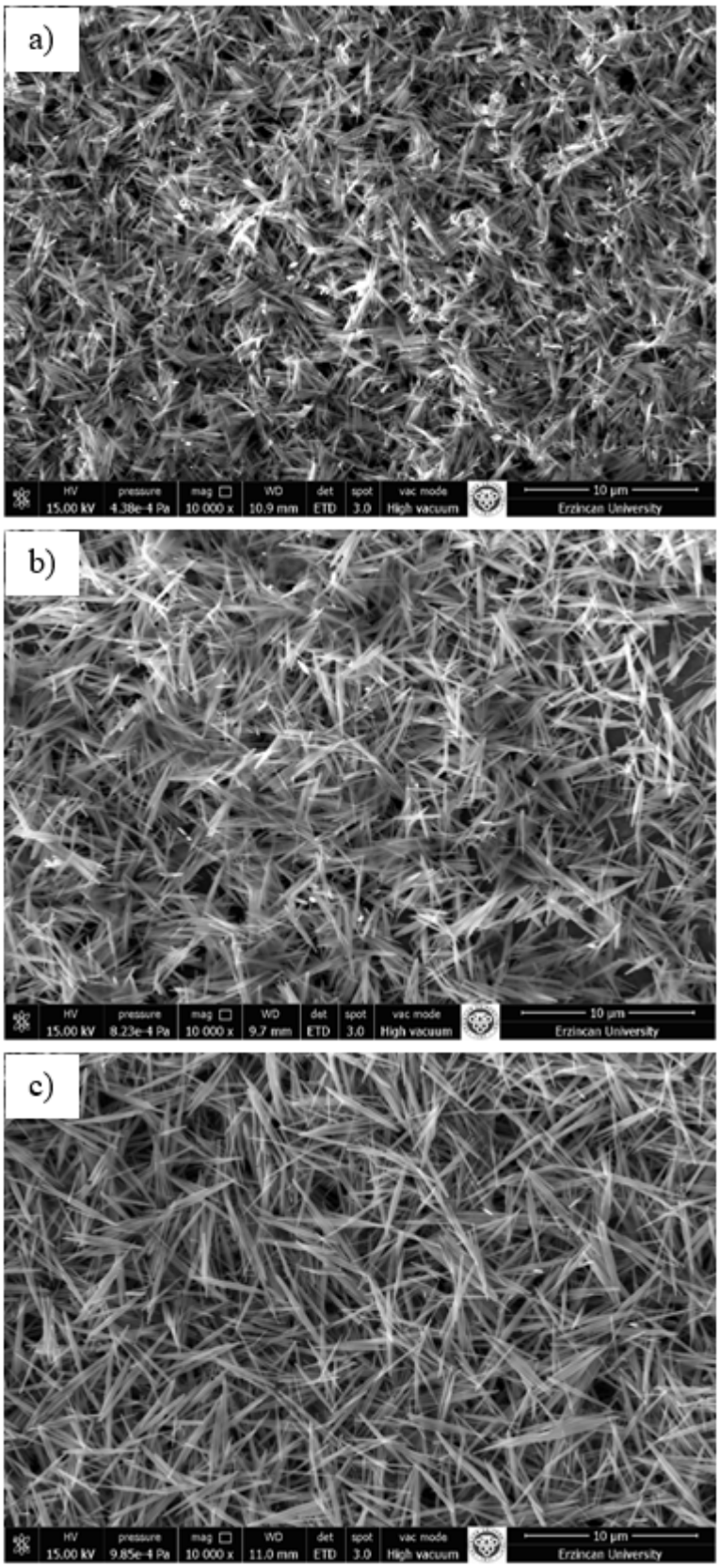

Figure 4.12 SEM images of 100 ºC, 12 h, 0.03 M AZO films [a) 1%, b) 3%, c) 5%] at 10000× magnification.

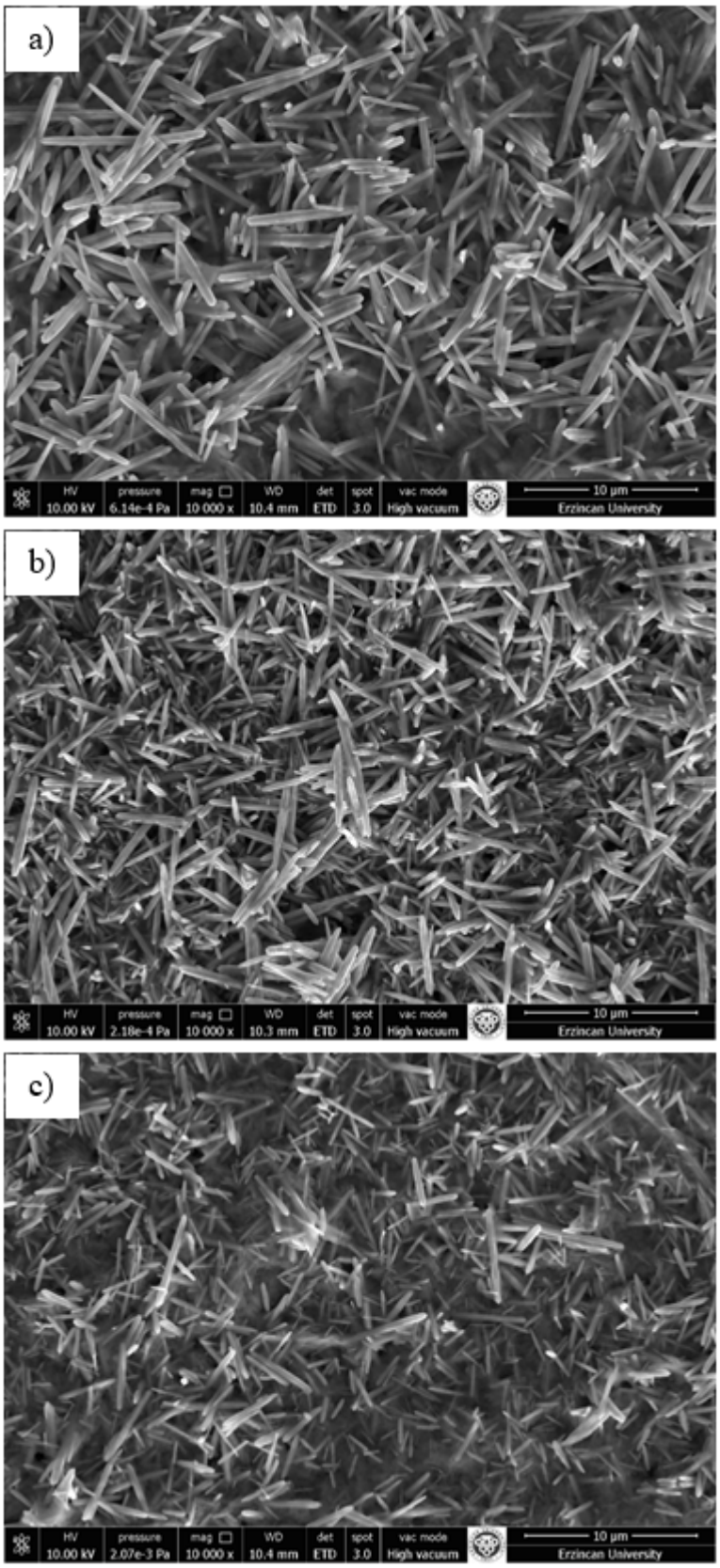

Figure 4.13 SEM images of 90 ºC, 12 h, 0.05 M AZO films [a) 1%, b) 3%, c)5%] at 10000× magnification.

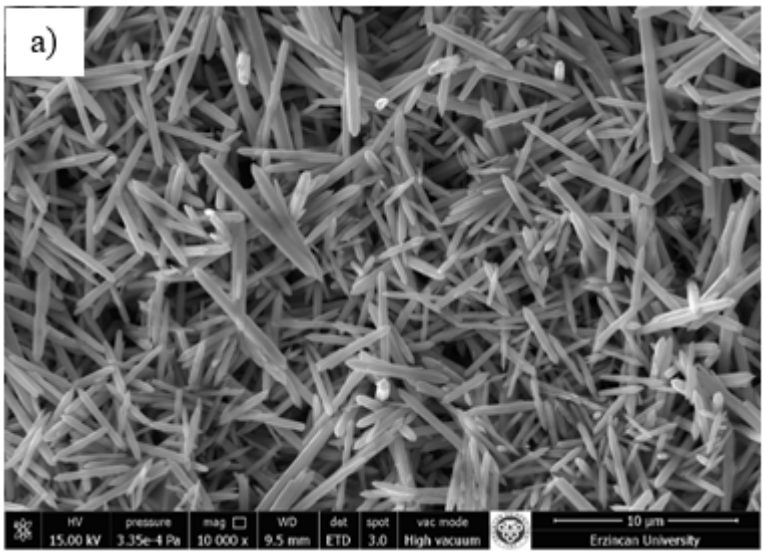

Figure 4.14 SEM images of 100 ºC,12 h, 0.05 M AZO films [a) 5%] at 10000× magnificüation.

4.2 Optical Characterization

4.2.1 Optic Absorption Measurement of Films

The optical properties of films were investigated by using Shimadzu UV-VIS 2600 Spectrophotometer. The effects of the synthesis temperature, different growth time and different solution molarity on the optical properties such as optical bandgap and refractive index (n) of ZnO and AZO films were investigated. To determine the bandgap values, we plotted $(\alpha h\nu)^2$ versus $(h\nu)$. The absorption coefficient (α) for the allowed direct transition can be determined as a function of photon energy $(h\nu)$ using below relation [99,100],

$$\alpha = \frac{A}{h\nu}(h\nu - Eg)^{1/2} \tag{4.1}$$

where A is a constant relative to the material and Eg is the optical bandgap. The bandgap energies of the films were determined by the extrapolation of the linear regions on the energy axis $(h\nu)$.

4.2.1.1 ZnO Films

The optical absorption spectra and the curves of $(\alpha h\nu)^2$ versus of ZnO films for different synthesis temperature, different amount of doping, different growth time and different solution molarity values are given in Figure 4.15-19.

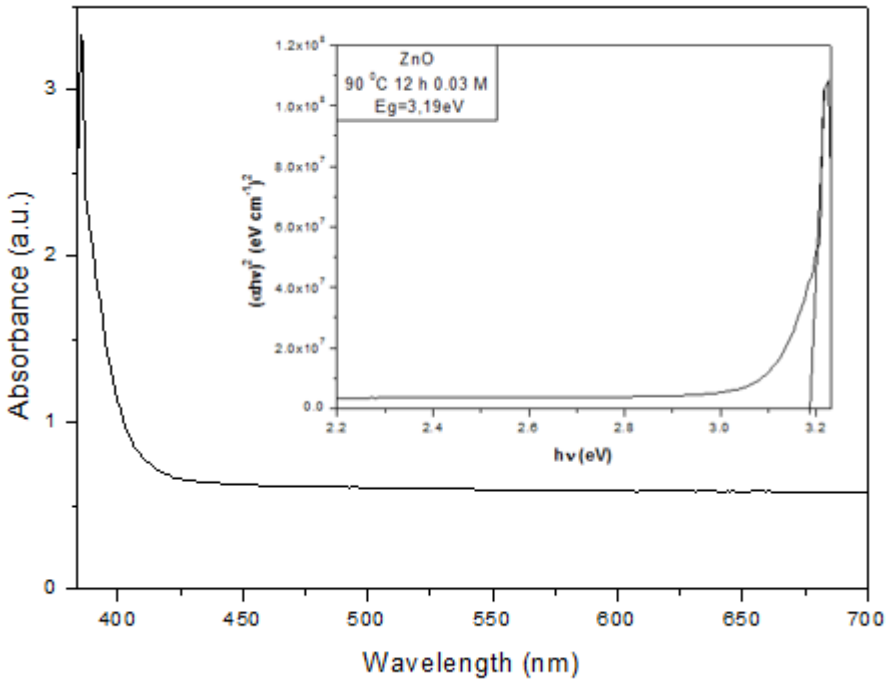

Figure 4.15 Plot of the absorbance with wavelength and $(\alpha h\nu)^2$versus $h\nu$ for 90 °C, 12 h, 0.03 M ZnO film.

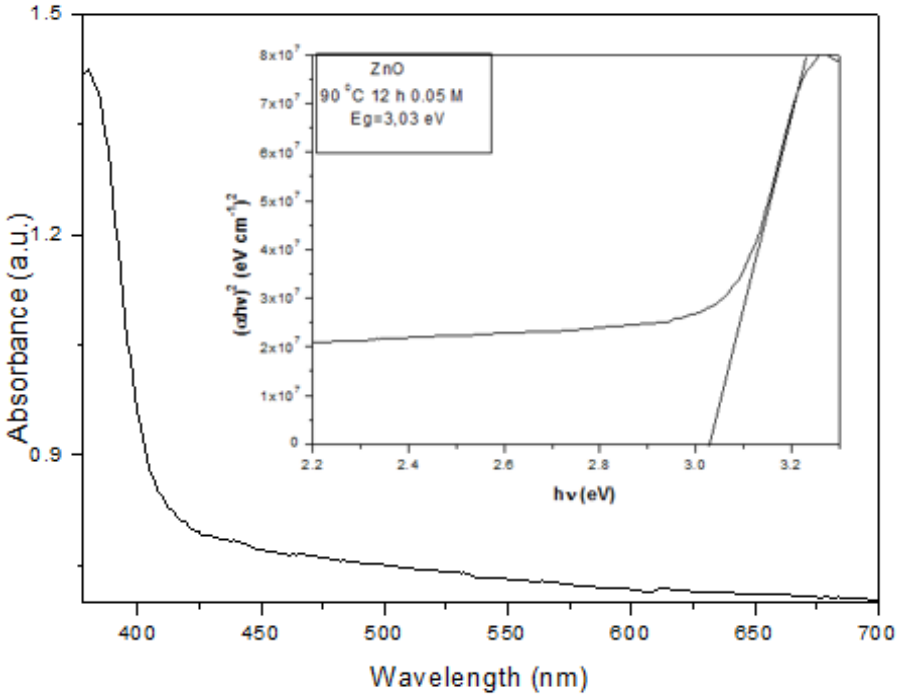

Figure 4.16 Plot of the absorbance with wavelength and $(\alpha h\nu)^2$versus hν for 90 ºC, 12 h, 0.05 M ZnO film.

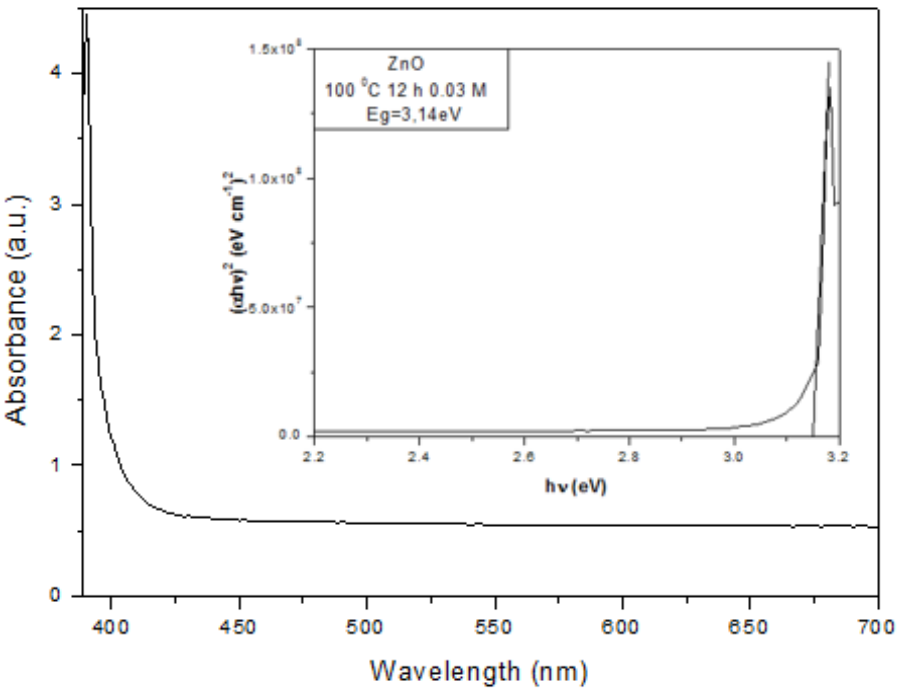

Figure 4.17 Plot of the absorbance with wavelength and $(\alpha h\nu)^2$ versus hν for 100 ºC, 12 h, 0.03 M ZnO film.

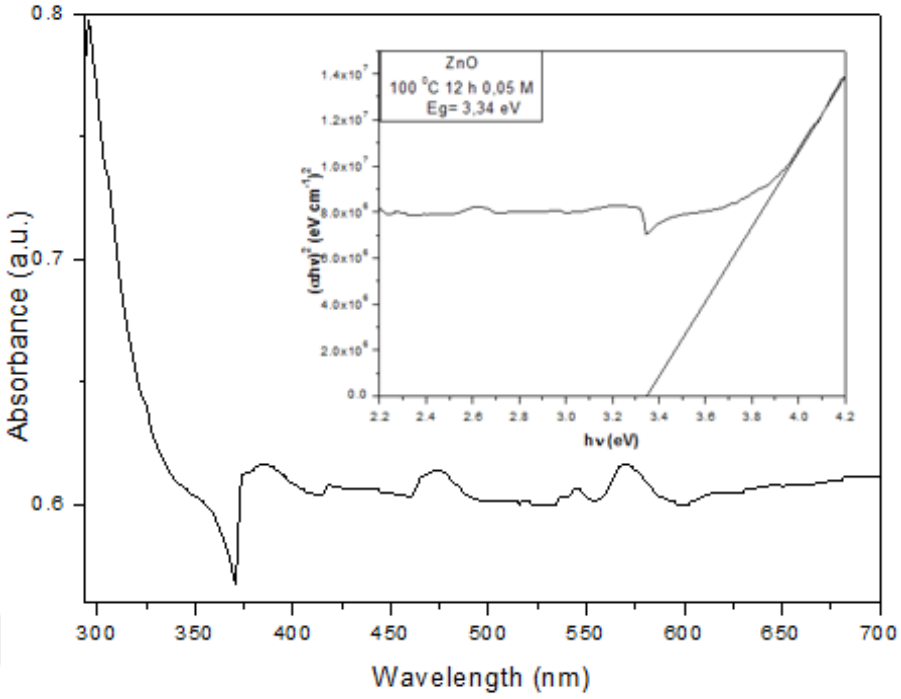

Figure 4.18 Plot of the absorbance with wavelength and $(\alpha h\nu)^2$ versus hν for 100 °C, 12 h, 0.05 M ZnO film.

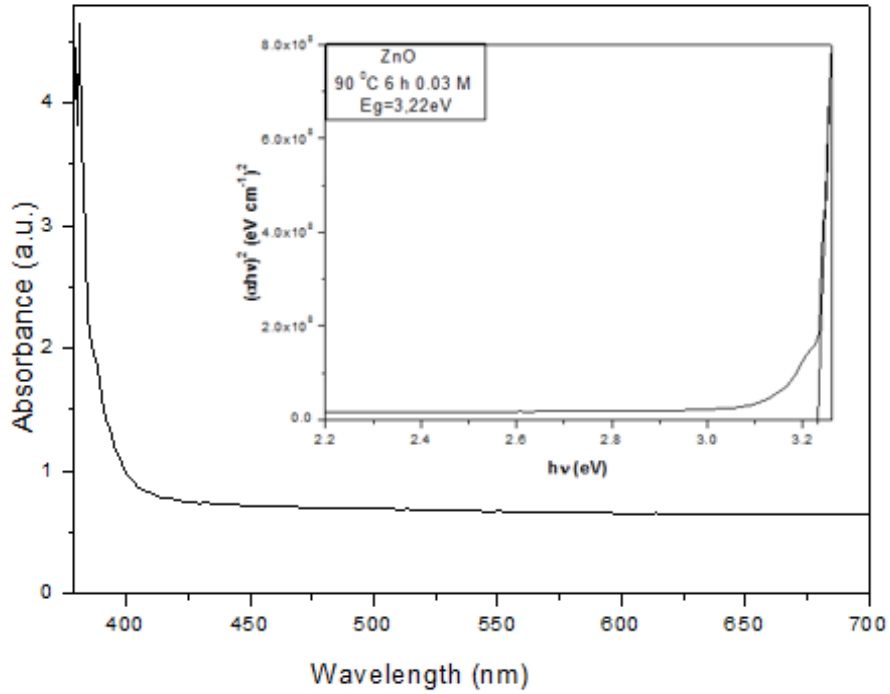

Figure 4.19 Plot of the absorbance with wavelength and $(\alpha h\nu)^2$ versus hν for 90 °C, 6 h, 0.03 M ZnO film.

4.2.1.2 AZO Films

The optical absorption spectra and the curves of $(\alpha h\nu)^2$ versus of AZO films for different synthesis temperature, different amount of doping and different solution molarity values are given in Figure 4.20-28.

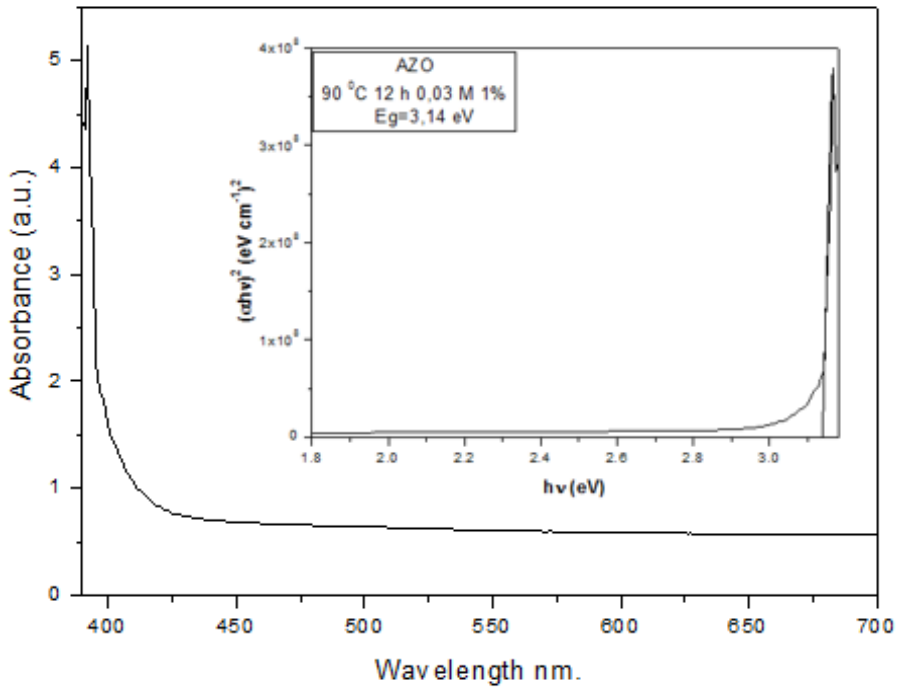

Figure 4.20 Plot of the absorbance with wavelength and $(\alpha h\nu)^2$ versus hν for 90 °C, 12 h, 0.03 M 1% AZO film.

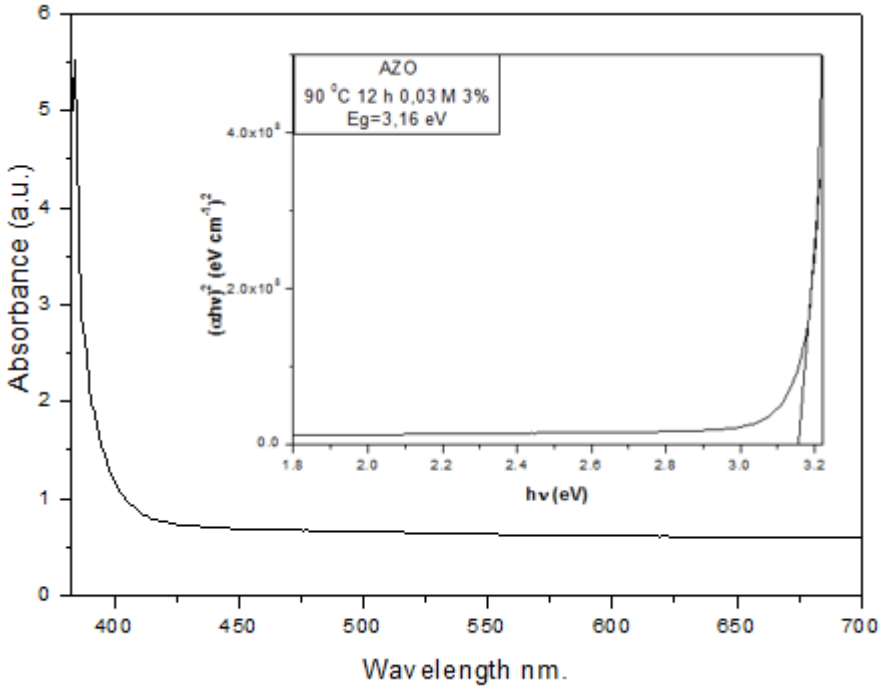

Figure 4.21 Plot of the absorbance with wavelength and $(\alpha h\nu)^2$ versus hν for 90 ºC,12 h, 0.03 M 3% AZO film.

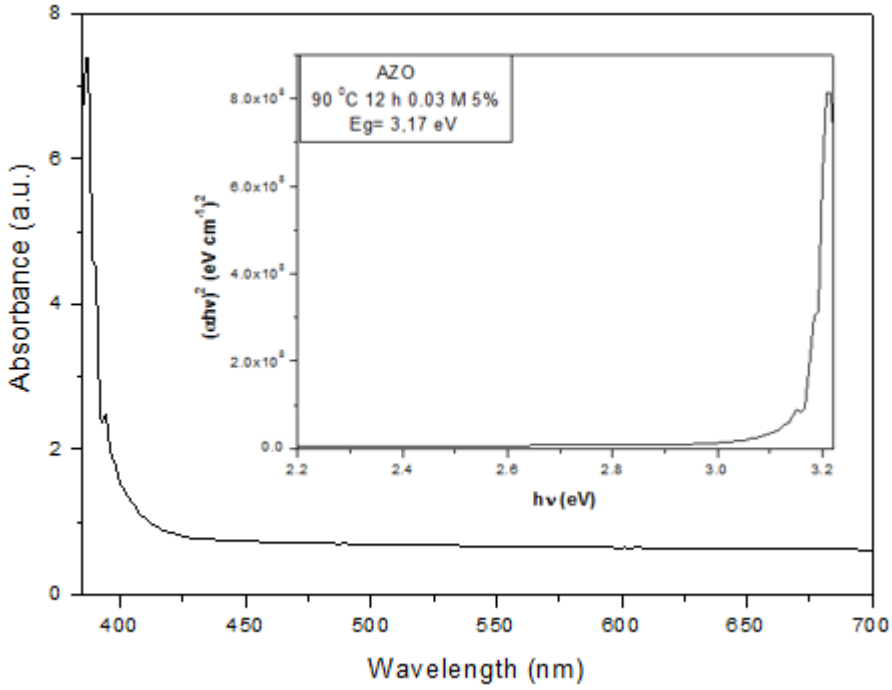

Figure 4.22 Plot of the absorbance with wavelength and $(\alpha h\nu)^2$ versus hν for 90 ºC,12 h, 0.03 M 5% AZO film.

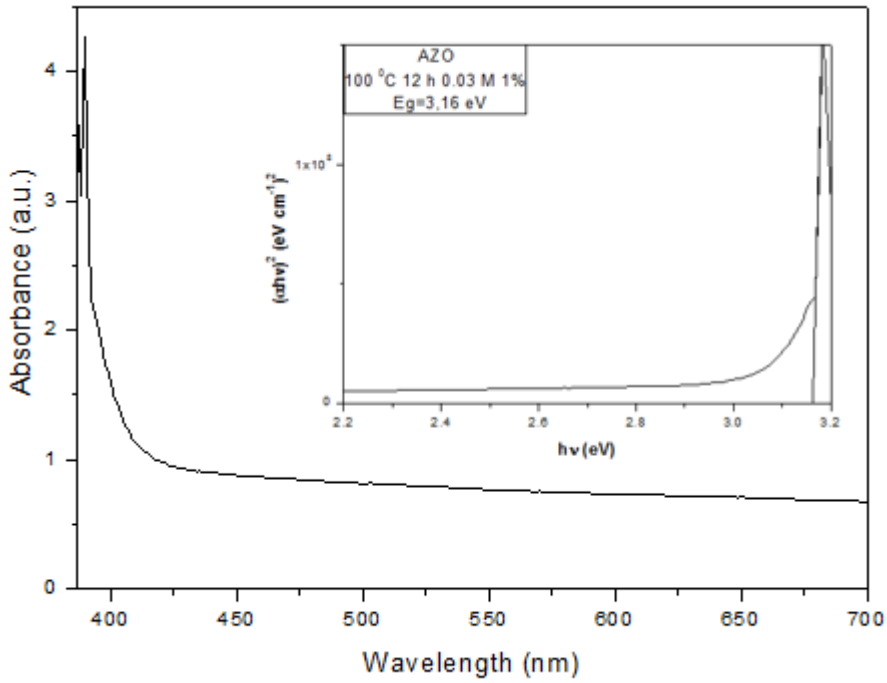

Figure 4.23 Plot of the absorbance with wavelength and $(\alpha h\nu)^2$ versus hν for 100 ºC,12 h, 0.03 M 1% AZO film.

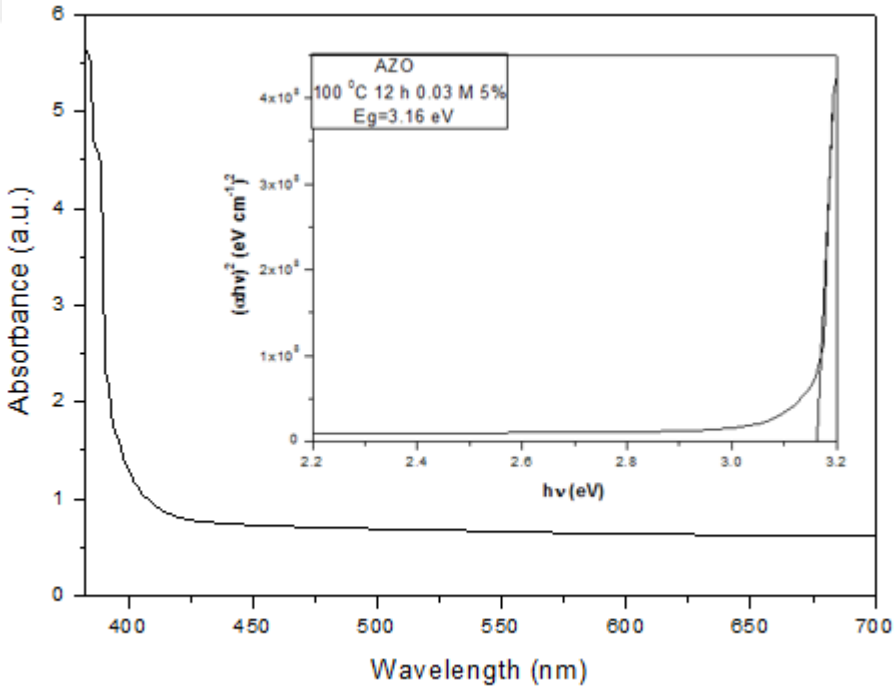

Figure 4.24 Plot of the absorbance with wavelength and $(\alpha h\nu)^2$ versus hν for 100 ºC,12 h, 0.03 M 5% AZO film.

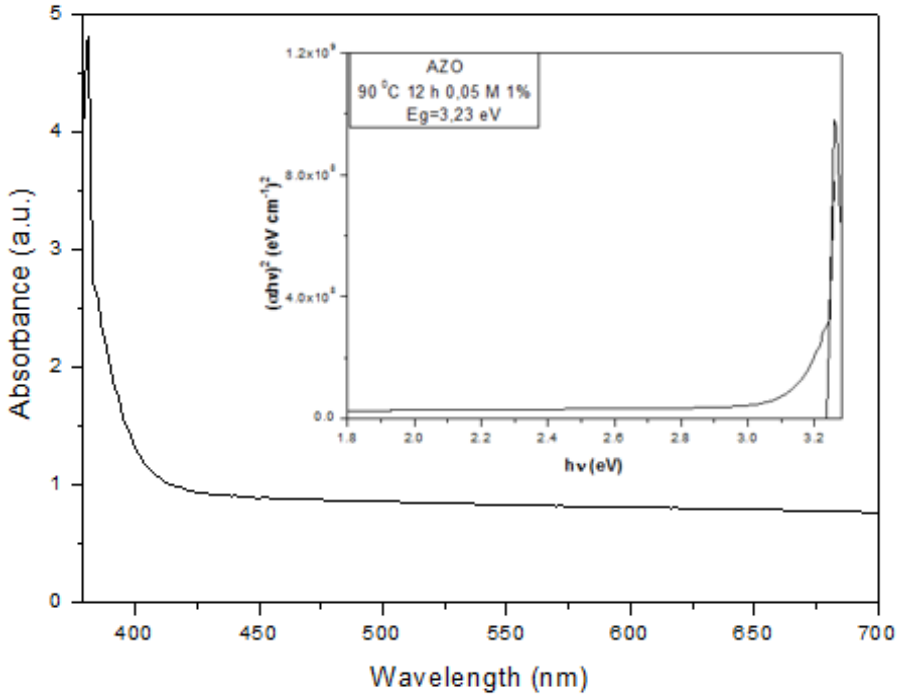

Figure 4.25 Plot of the absorbance with wavelength and (αhν)2 versus hν for 90 oC,12 h, 0.05 M 1% AZO film.

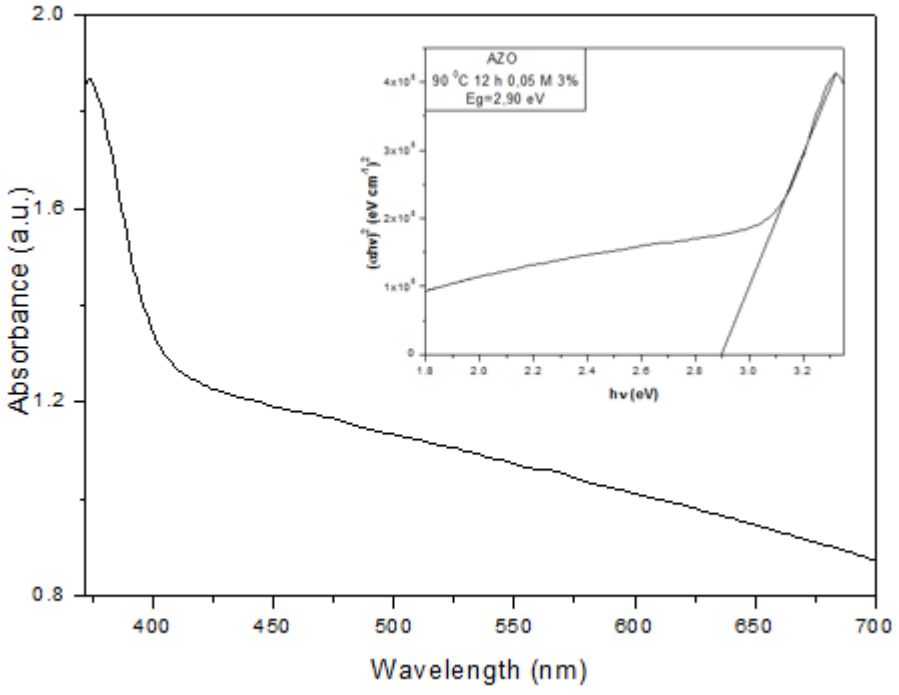

Figure 4.26 Plot of the absorbance with wavelength and $(\alpha h\nu)^2$ versus hν for 90 °C, 12 h, 0.05 M 3% AZO film.

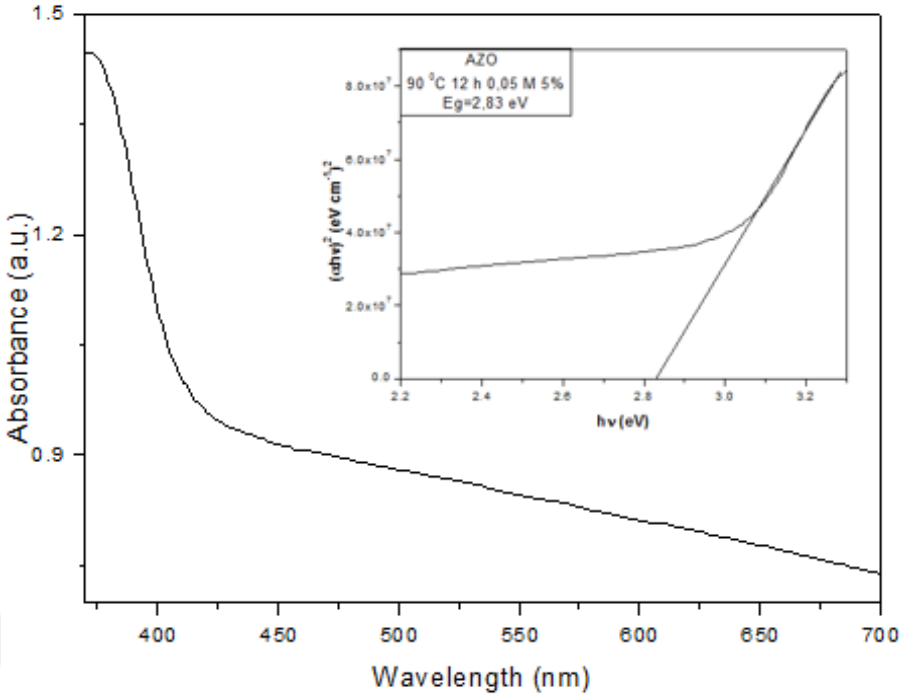

Figure 4.27 Plot of the absorbance with wavelength and $(\alpha h\nu)^2$ versus hν for 90 ºC, 12 h, 0.05 M 5% AZO film.

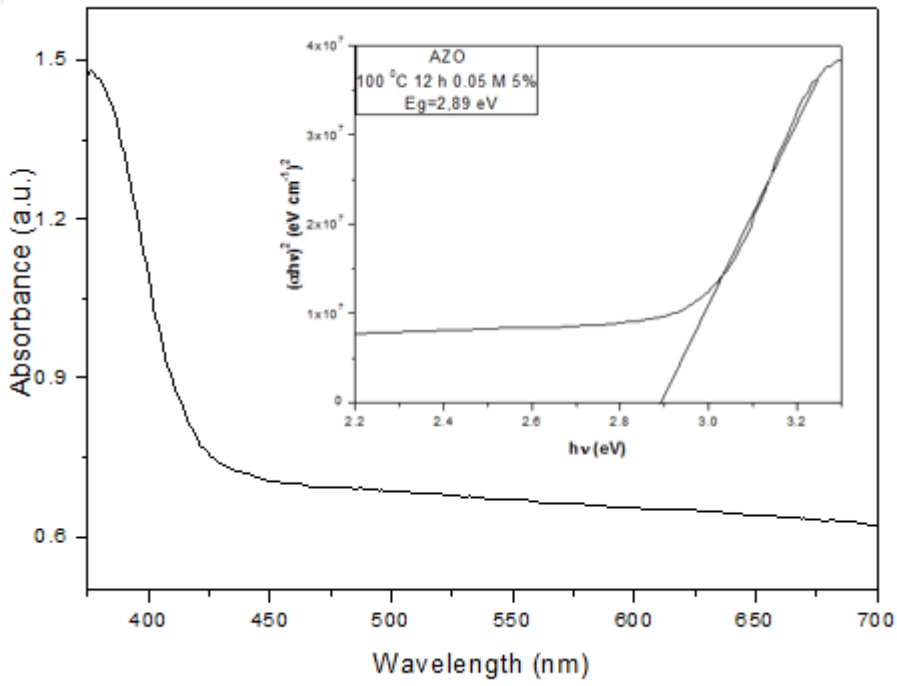

Figure 4.28 Plot of the absorbance with wavelength and $(\alpha h\nu)^2$ versus hν for 100 ºC, 12 h, 0.05 M 5% AZO film.

4.3 Elemental Analysis Mesurement for ZnO and AZO

Today, as an analysis method adopted EDAX is an indispensable method for quantitative elemental analysis of the sample. As a result of the non-elastic interference between the electron beam with the sample atoms, it occurs at the characteristic X-rays and continuous irradiation in the sample. Characteristic X-rays are transformed into signals, which are transformed into X-ray energy spectra of peaks having specific intensities.

EDAX measurements of the films were taken for investigation of effects of synthesis temperature, growth time, amount of doping and solution molarity on elemental analysis of ZnO and AZO films.

4.3.1 ZnO Films

EDAX analyses of ZnO films for different synthesis temperature, different amount of doping, diffrent growth time and different solution molarity values are given in Figure 4.29-33.

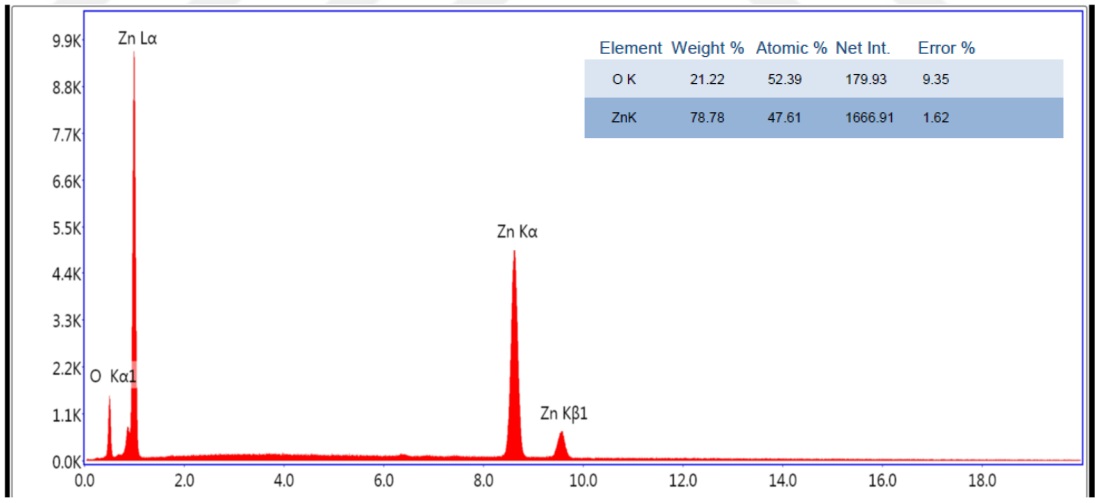

Figure 4.29 EDAX analysis for 90 °C, 12 h, 0.03 M ZnO film.

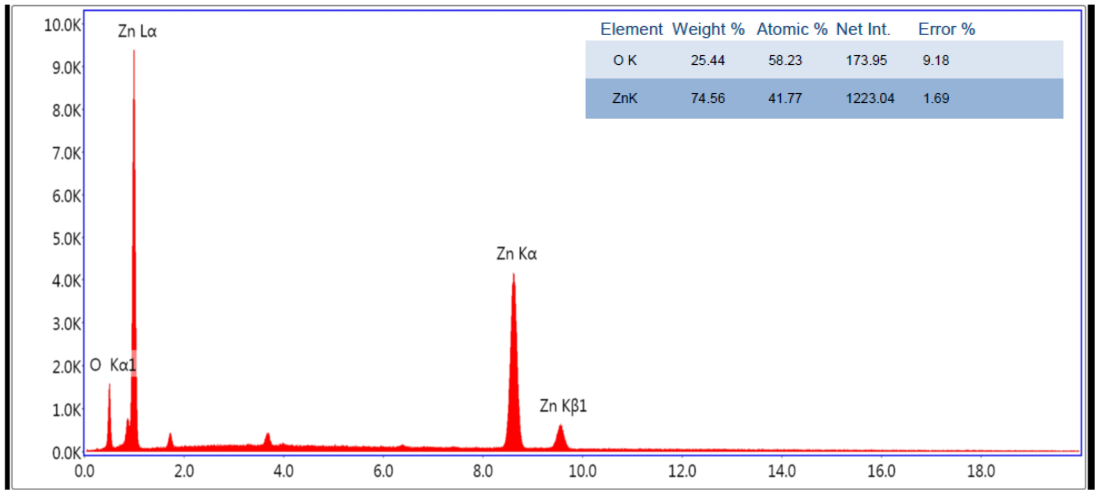

Figure 4.30 EDAX analysis for 90 ºC, 12 h, 0.05 M ZnO film

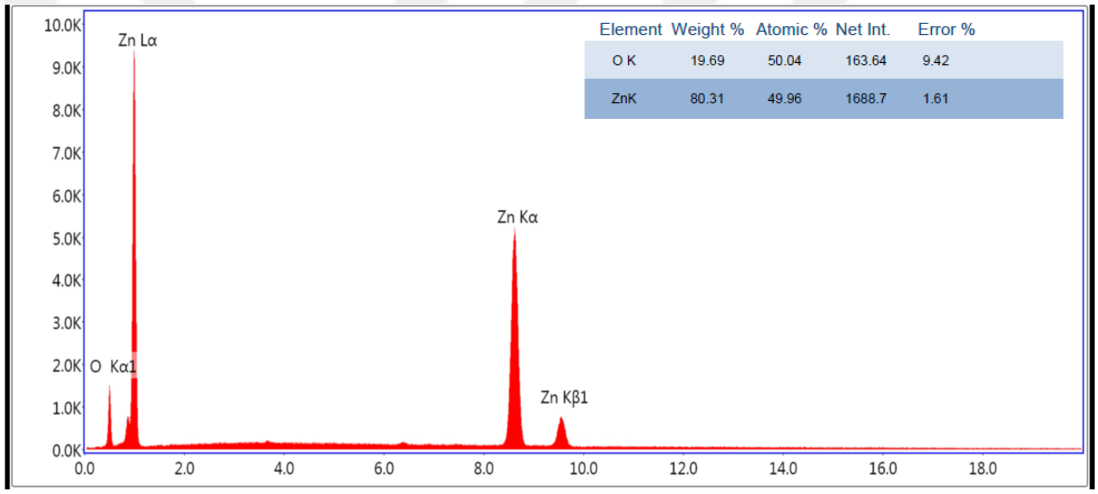

Figure 4.31 EDAX analysis for 100 ºC, 12 h, 0.03 M ZnO film.

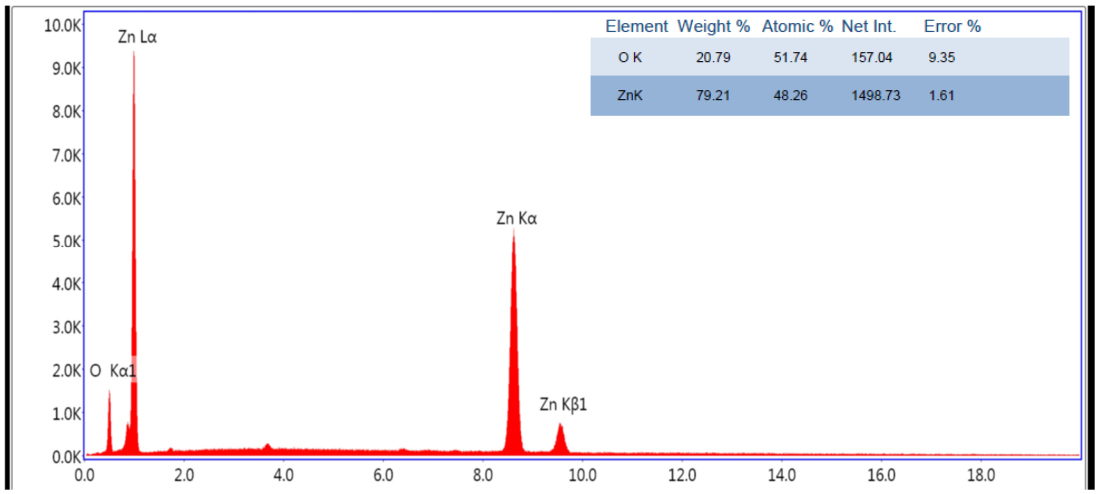

Figure 4.32 EDAX analysis for 100 ºC, 12 h, 0.05 M ZnO film

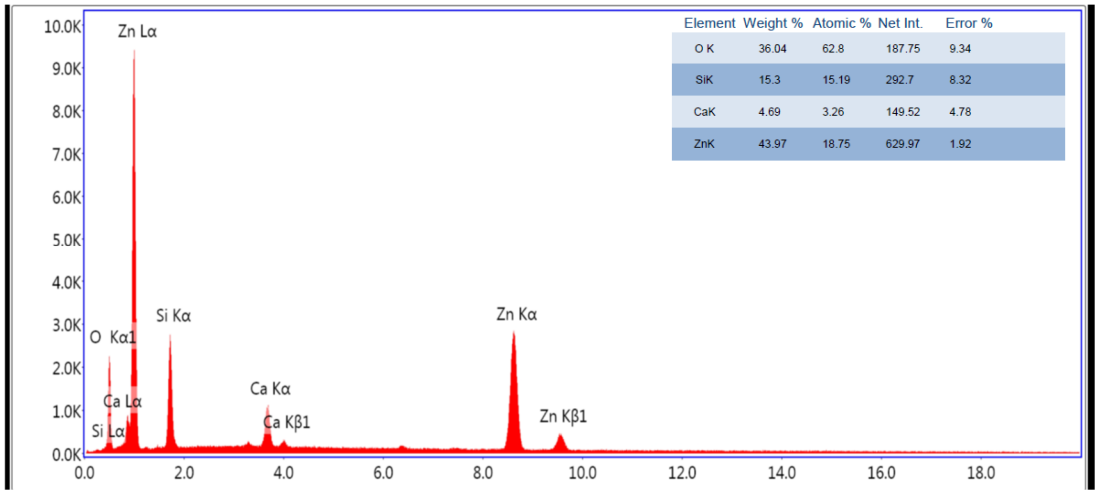

Figure 4.33 EDAX analysis for 90 ºC, 6 h, 0.03 M ZnO film.

4.3.2 AZO Films

EDAX analyses of AZO films for different synthesis temperature, different amount of doping, diffrent growth time and different solution molarity values are given in Figure 4.34-43.

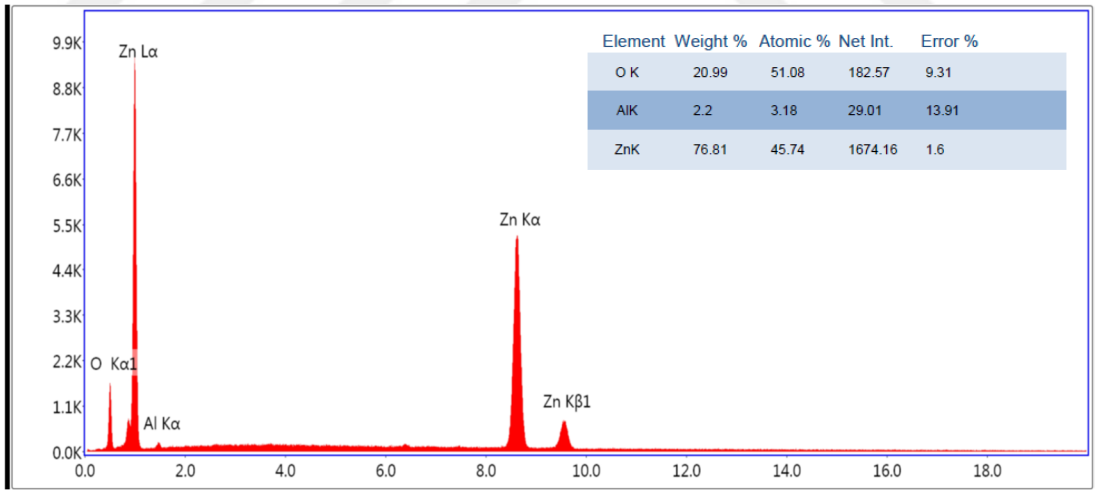

Figure 4.34 EDAX analysis for 90 ºC, 12 h, 0.03 M 5% AZO film.

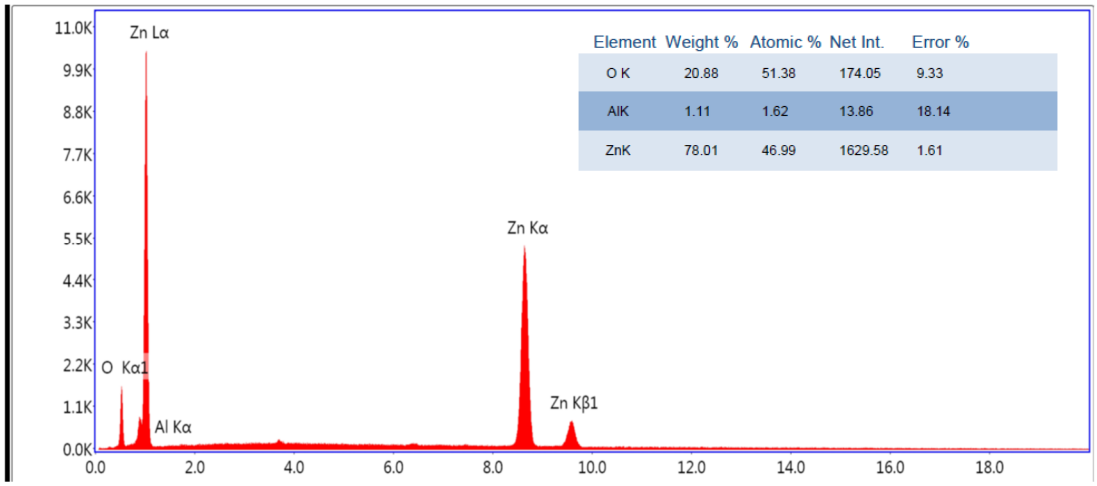

Figure 4.35 EDAX analysis for 90 ºC, 12 h, 0.03 M 3% AZO film.

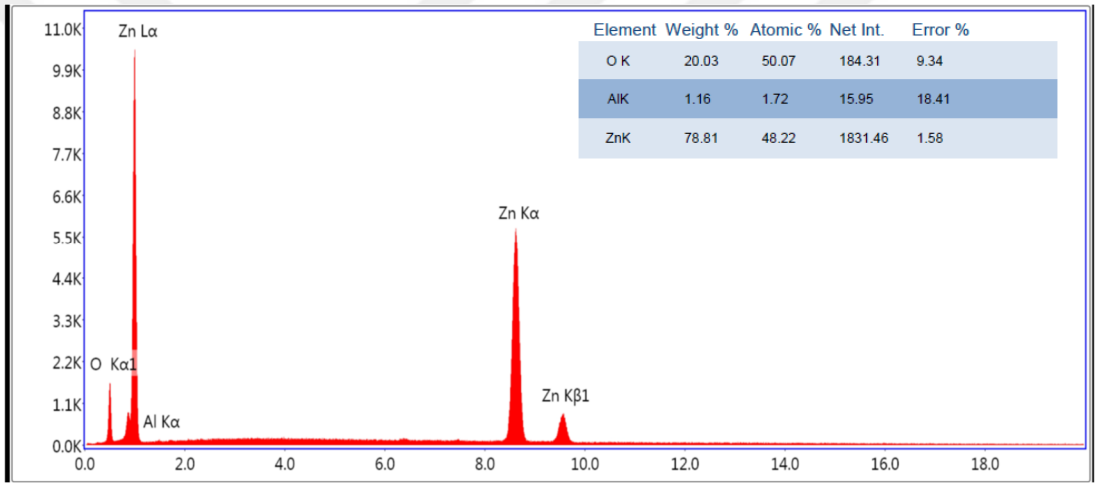

Figure 4.36 EDAX analysis for 90 ºC, 12 h, 0.03 M 1% AZO film

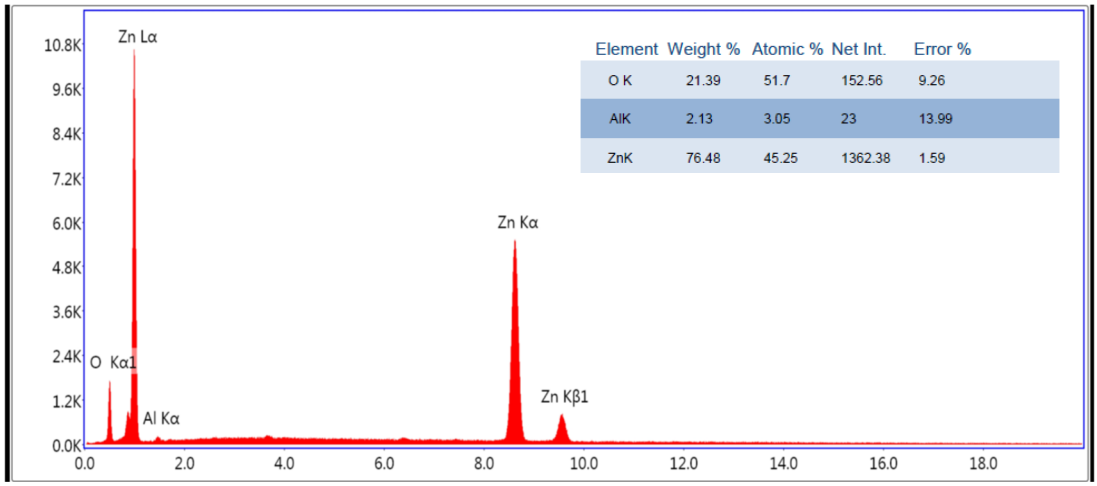

Figure 4.37 EDAX analysis for 100 ºC, 12 h, 0.03 M 5% AZO film.

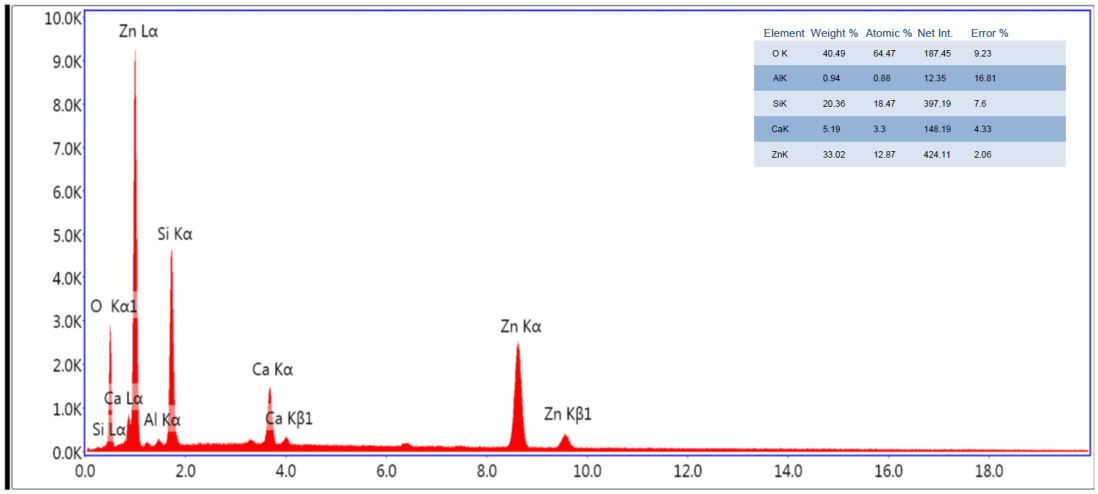

Figure 4.38 EDAX analysis for 100 ºC, 12 h, 0.03 M 3% AZO film.

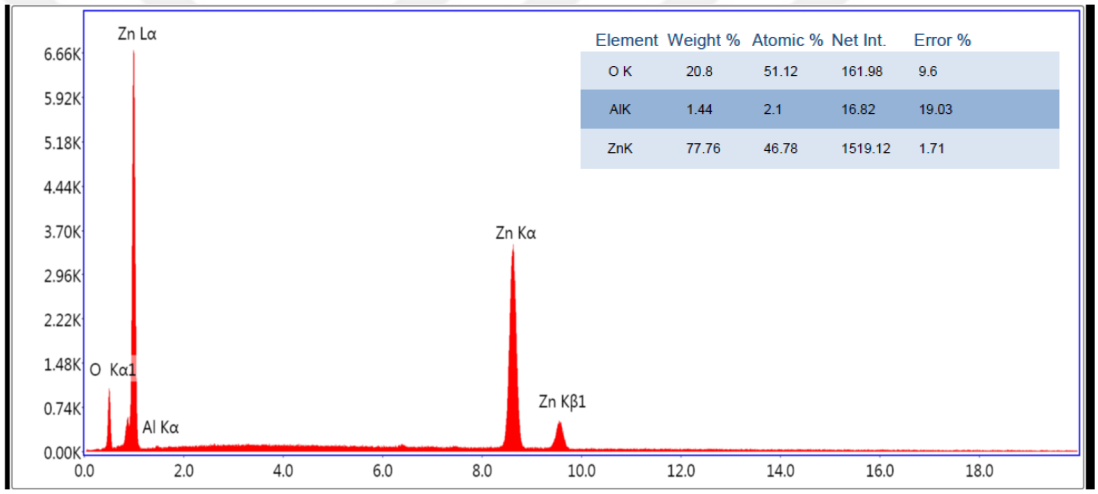

Figure 4.39 EDAX analysis for 100 ºC, 12 h, 0.03 M 1% AZO film.

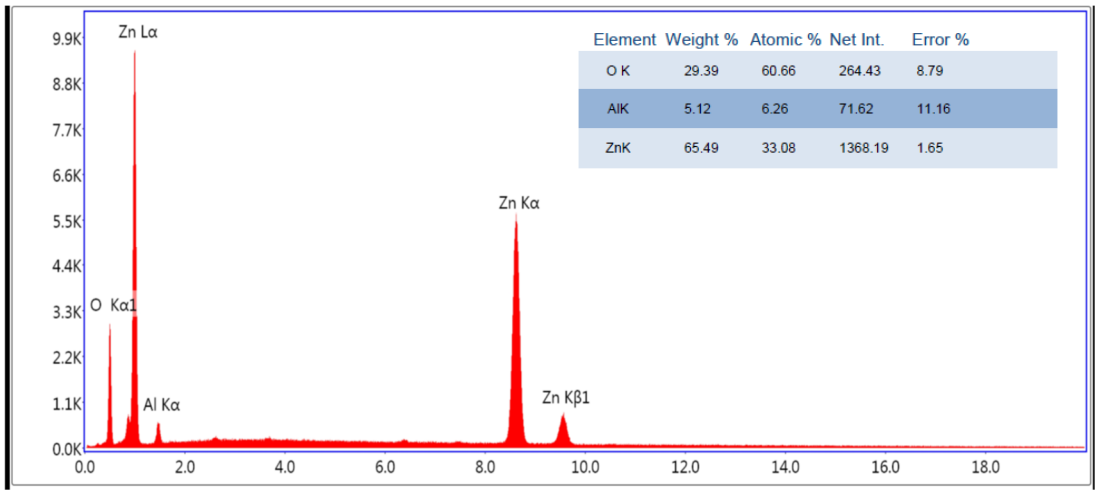

Figure 4.40 EDAX analysis for 90 ºC, 12 h, 0.05 M 5% AZO film.

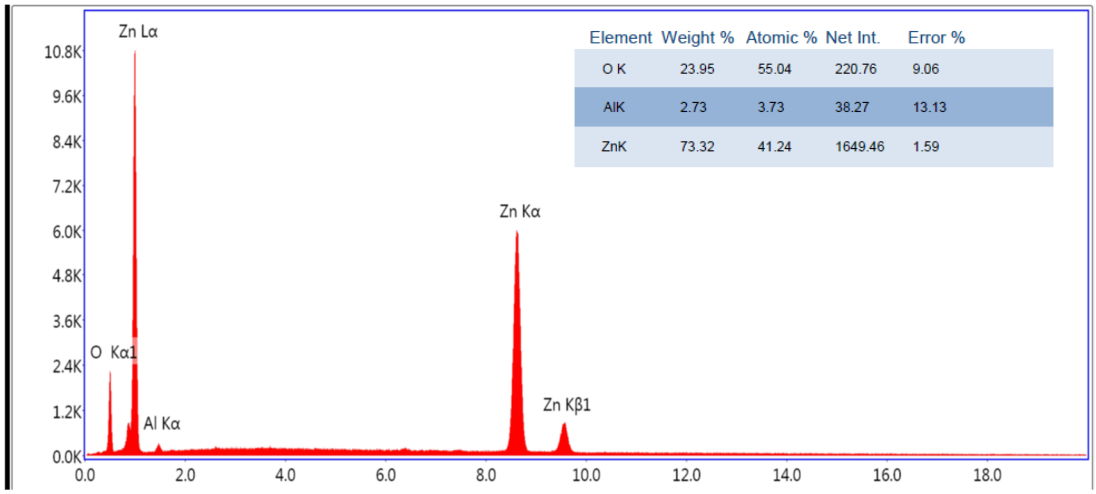

Figure 4.41 EDAX analysis for 90 ºC, 12 h, 0.05 M 3% AZO film.

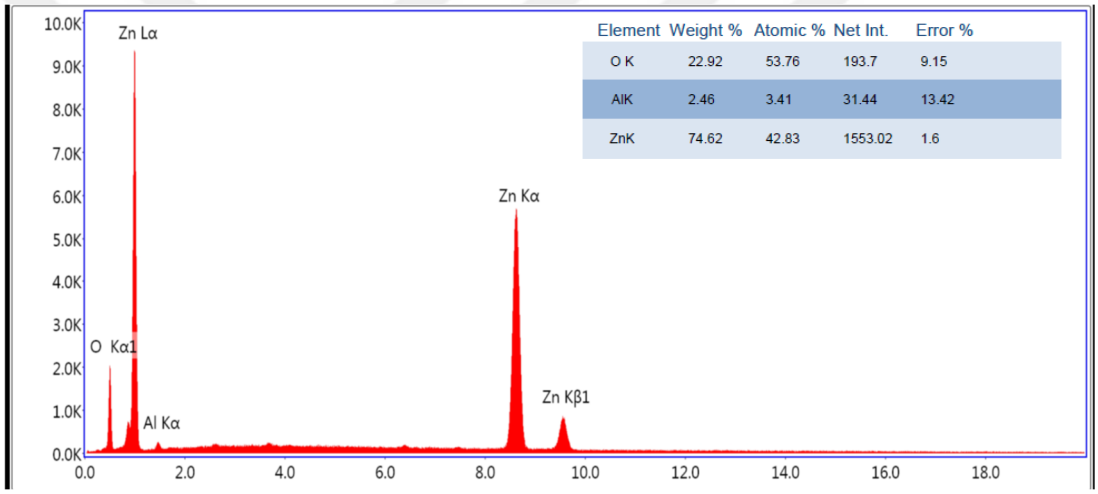

Figure 4.42 EDAX analysis for 90 ºC, 12 h, 0.05 M 1% AZO film.

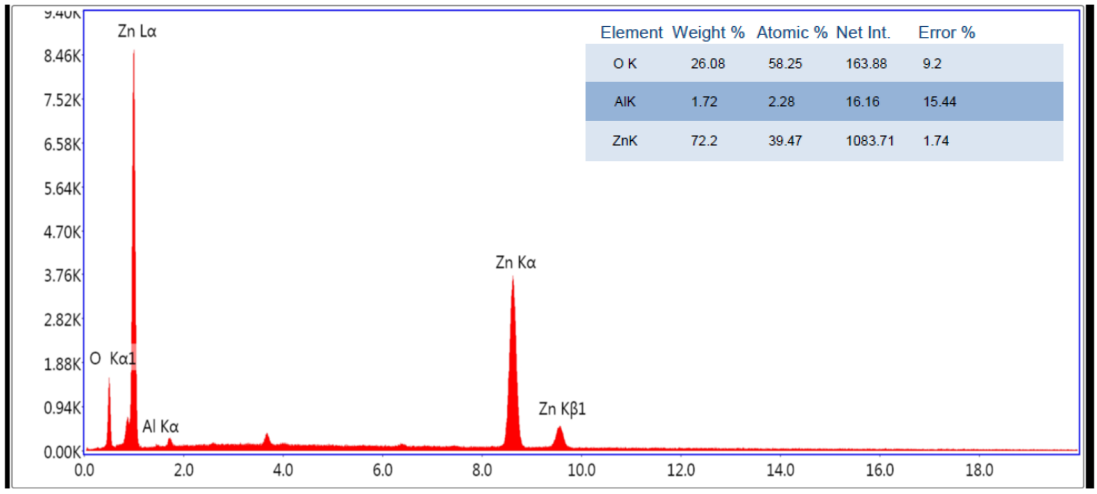

Figure 4.43 EDAX analysis for 100 ºC, 12 h, 0.05 M 5% AZO film.

CHAPTER 5

RESULTS AND DISCUSSIONS

5.1 XRD Results

5.1.1 ZnO Films

Figure 4.1-3 show the XRD patterns of ZnO films grown on glass substrate by hydrothermal method at 90 ºC and 100 ºC synthesis temperature, 6 h and 12 h growth time and 0.03 M and 0.05 M solution molarity. As seen in Figure 4.1-3, all the difraction peaks can be indexed as the hexagonal wurtzite structure ZnO with lattice constants of a=b=3.25 Å and c=5.20 Å (the data match with ICDD PDF Card No. 01-089-7102). No impurity phases are observed and the deposited films are polycrystalline. The results indicate that ZnO films grown on glass substrate have high crystallinity without any pre-deposited seed layer. The highest intensity peak locates at $2\theta=36.26^{o}$ which corresponded to (101) planes. Although the intensities and FWHM values of the peaks change with synthesis temperature, growth time and solution molarity, the (101) peak is dominant peak in all ZnO films. These results are in agreement with relevant literature [101, 102, 103]. The narrow and high intensity peaks show that ZnO films have good crystalline. The intensites of the peaks decreased with increasing solution molarity for all of the synthesis temperature. For 90 ºC synthesis temperature, the growth time effect on the properties of ZnO films has been investigated. It has seen that the intensities of the peaks decreased with decreasing growth time from 12 h to 6 h. These results showed that 12 h growth time results are better than 6 h growth time. These results are in agreement with relevant literature [28, 104].

The structural parameters such as grain size (D), dislocation density (δ), FWHM (β), strain (ε) values for all the films have been calculated by using XRD patterns and presented in Table 5.1-3. These values are calculated for (101) dominant peaks in all the films with using the Debye Scherrer's method. Additionally, to have more information abaut on the amount of defects in the films, the dislocation density has

been calculated by using the formula (3.4). The strain values have been calculated by using the formula (3.5).

Table 5.1 Structural parameters of the ZnO films which synthesized at 90 ºC, 12h and different solution molarity.

90 °C-12 h	**2θ (101)**	**d (Aº) (101)**	**FWHM (101)**	**D (nm)**	**δ (nm)$^{-2}$**	**ε (line^{-2} m^{-4})**
0.03 M	36.16	2.48	0.19	44.05	0.00052	0.04508
0.05 M	36.27	2.47	0.20	42.45	0.00055	0.04678

Table 5.2 Structural parameters of the ZnO films which synthesized at 100 ºC, 12 h and different solution molarity

100 °C-12 h	**2θ (101)**	**d (Aº) (101)**	**FWHM (101)**	**D (nm)**	**δ (nm)$^{-2}$**	**ε (line^{-2} m^{-4})**
0.03 M	36.25	2.48	0.20	41.92	0.00057	0.04738
0.05 M	36.16	2.48	0.19	43.32	0.00053	0.04584

Table 5.3 Structural parameters of the ZnO films which synthesized at 90 ºC, 0.03 M and different growth time

90 °C-0.03 M	**2θ (101)**	**d (Aº) (101)**	**FWHM (101)**	**D (nm)**	**δ (nm)$^{-2}$**	**ε (line^{-2} m^{-4})**
12 h	36.16	2.48	0.19	44.05	0.00052	0.04508
6 h	36.11	2.49	0.21	40.70	0.00060	0.04880

As seen in Table 5.1 (90 ºC, 12 h), the grain size has decreased, whereas FWHM, dislocation density and strain have increased with increasing solution molarity. The larger grain size, the smaller dislocation density and FWHM values indicate better crystallization of the films [106]. As seen in Table 5.2 (100 ºC, 12 h), the grain size has increased, whereas FWHM, dislocation density and strain values have decreased with increasing solution molarity [107, 108]. Dislocation densities exhibit a decreasing with increasing molar concentration, which indicates that the high molar concentration reduced the crystal lattice imperfections [108]. As seen in Table 5.3 (90 ºC, 0.03 M), the grain size has increased, whereas FWHM, dislocation density and strain values have decreased with increasing growth time from 6 h to 12 h [104].

5.1.2 AZO Films

Figure 4.4-7 show XRD patterns of AZO films at 90 ºC and 100 ºC synthesis temperature, 12 h growth time, 0.03 M and 0.05 M solution molarity and 1-3-5% Al doping concentrations. As seen in Figure 4.4-7, all the films have polycrystalline structure with hexagonal wurtzite phase of ZnO (the data match with ICDD PDF Card No. 01-089-7102). The results indicate that AZO films grown on glass substrate have high crystallinity without any pre-deposited seed layer. There are no impurity phases in all the patterns of the films and it has been believed that the impurification with Al occurs through substitution of Zn^{2+} ions by Al^{+3} ions in the synthesis process. The highest intensity peak locates at $2\theta=31.77^{o}$ which corresponded to (100) planes. Although the intensities and FWHM values of the peaks change with synthesis temperature, Al doping concentartion and solution molarity, the (100) peak is dominant peak in all AZO films. These results are in agreement with relevant literature [35]

The calculated diffraction angle (2θ), d, FWHM, grain size, dislocation density, strain values are given in Table 5.4-7 for different synthesis temperature, different doping concentration and different solution molarity values.

Table 5.4 Structural parameters of the AZO films which synthesized at 90 ºC, 12 h, 0.03 M and different doping concentrations.

90 °C-0.03 M	2θ (100)	d (Aº) (100)	FWHM (100)	D (nm)	δ $(nm)^{-2}$	ε $(line^{-2}\ m^{-4})$
1%	31.75	2.82	0.19	42.73	0.00055	0.04648
3%	31.71	2.82	0.19	43.19	0.00054	0.04598
5%	31.70	2.82	0.19	42.41	0.00056	0.04682

Table 5.5 Structural parameters of the AZO films which synthesized at 100 ºC, 12 h, 0.03 M and different doping concentrations.

100 °C-0.03 M	2θ (100)	d (Aº) (100)	FWHM (100)	D (nm)	δ $(nm)^{-2}$	ε $(line^{-2}\ m^{-4})$
1%	31.46	2.84	0.23	35.64	0.00079	0.05573
3%	31.39	2.85	0.23	36.03	0.00077	0.05511
5%	31.69	2.82	0.19	44.49	0.00051	0.04464

Table 5.6 Structural parameters of the AZO films which synthesized at 90 °C, 12 h, 0.05 M and different doping concentrations.

90 °C-0.05 M	2θ (100)	d (A°) (100)	FWHM (100)	D (nm)	δ $(nm)^{-2}$	ε $(line^{-2}\ m^{-4})$
1%	31.72	2.82	0.21	40.09	0.00062	0.04954
3%	31.69	2.82	0.23	36.51	0.00075	0.05440
5%	31.71	2.82	0.21	40.28	0.00062	0.04930

Table 5.7 Structural parameters of the AZO films which synthesized at 100 °C, 12 h, 0.05 M and different doping concentrations.

100 °C-0.05 M	2θ (100)	d (A°) (100)	FWHM (100)	D (nm)	δ $(nm)^{-2}$	ε $(line^{-2}\ m^{-4})$
5%	31.60	2.83	0.21	39.18	0.00065	0.05068

As seen in Table 5.4 (90 °C, 0.03 M), the grain size, d, FWHM, dislocation density and strain values have not been much changed with increasing Al doping concentrations. As seen in Table 5.5 (100 °C, 0.03 M), the grain size value increased, whereas d, FWHM, dislocation density and strain values decreased with increasing Al concentration. As seen in Table 5.6 (90 °C, 0.05 M), the d values have not been changed with increasing Al concentrations. FWHM, grain size, dislocation density and strain values have been changed with Al concentrations. The AZO films are grown for 0.05 M and different Al concentrations at 100 °C but it has not get good results for 0.05 M and %1, %3 Al concentration.

5.2 SEM Results

The morphology-controlled synthesis of ZnO and AZO films is of great interest for future ZnO nanodevice applications. By adjusting the solution molarity, synthesis temperature, growth time and doping concentration, different sizes of ZnO and AZO films have been synthesized via a hydrothermal method.

5.2.1 ZnO Films

Figure 4.8a and 4.8b show the SEM images of ZnO films grown at 0.03 M and 0.05 M solution molarities for 12 h growth time and 90 °C synthesis temperature, respectively. It is evident that the film mainly consists of ZnO nanorods and most of them assembly into branched morphologies (Fig. 4.8a). Figure 4.8b shows the

morphology of nanorods grown at 0.05 M under the same conditions. When the synthesis process has been carried out at lower molarity (0.03 M), thick ZnO nanorods and thick branched rods have been obtained. With increasing molarity, the homogenity increased.

Figure 4.9a and 4.9b show the SEM images of ZnO films grown at 0.03 M and 0.05 M solution molarities for 12 h growth time and 100 ^{o}C synthesis temperature, respectively. As seen in Figure 4.9a-b, ZnO films are composed of nanorod structures. The uniformity, density, smoothness and adhesion to the substrates of the films decreased with increasing solution molarity. SEM image of the film is composed of a dense packing of grains, indicating good quality (Fig. 4.9a).

Figure 4.10a and 4.10b show the SEM images of ZnO films synthesized at 90 ^{o}C synthesis temperature for two different growth times: 12 and 6 hours, respectively. The uniformity, dense, smooth and well adhered to the substrates of the films increased with increasing growth time from 6 h to 12 h. The grain size value of films increased with decreasing growth time. Consequently, the surface properties of the ZnO films appear to have changed significantly with growth time [28].

5.2.2 AZO Films

Figure 4.11 and Figure 4.12 show the SEM images for AZO films grown at 90 ^{o}C and 100 ^{o}C synthesis temperature with 0.03 M solution molarity and different Al concentrations, respectively. As seen in Figure 4.11-12, AZO films are composed of nanorod structures. The nanorods have grown at random angles and the films have homogeneous surface morphology. The size of the nanorods increased with increasing Al concentration from 1% to 5%. It is seen that the nanrods are separated more and more by the increase Al the concentrations.

Figure 4.13 shows the SEM images for AZO films grown at 90 ^{o}C synthesis temperature with 0.05 M solution molarity and different Al concentrations, respectively. As seen in Figure 4.13, AZO films are composed of nanorod structures. The nanorods have grown at random angles and the films has homogeneous surface

morphology. The size of the nanorods don't more change with increasing Al concentration from 1% to 5%.

For 100 ^{o}C synthesis temperature and 0.05 M solution molarity, AZO films have been grown for only 5% doping concentration. The AZO films are grown at different Al concentrations for 0.05 M at 100 ^{o}C, but it has not given better results for 0.05 M and %1, %3 Al concentration.

5.3 Absorption Results

5.3.1 ZnO Films

Figure 4.15-19 show the optical absorption spectras and the curves of $(\alpha h\nu)^2$ versus $(h\nu)$ of ZnO films for different synthesis temperature (90 ^{o}C and 100 ^{o}C), different growth time (6-12 hour) and different solution molarity (0.03 M and0.05 M). The synthesis temperature, solution molarity and growth time effects on the optical absorption measurements have been investigated.

The refractive index (n) and dielectric constant (ε) of semiconducting materials is very important in determining the optical and electrical properties of the crystals. Knowledge of n is essential in the design of heterostructure lasers in optoelectronic devices as well as in solar cell applications. The refractive index values of the ZnO films have been calculated using equation (3.6) and (3.7) .The changing of refractive index (n) with synthesis temperature, solution molarity and growth time has been given in Table 5.8-10 for these two models.

Table 5.8 The bandgap (Eg), refractive index (n), optical static dielectric constant (ε_0) and optical high frequency dielectric constant (ε_∞) values at 90 ^{o}C, 12 h ZnO films and different solution molarity.

			Herve and Vandamme		**Moss relation**	
90 °C-12 h	**Eg (eV)**	**ε_0**	**n**	**ε_∞**	**n**	**ε_∞**
0.03 M	3.19	8.69	2.29	5.26	2.41	5.82
0.05 M	3.03	9.19	2.34	5.47	2.44	5.97

Table 5.9 The bandgap (Eg), refractive index (n), optical static dielectric constant (ε_0) and optical high frequency dielectric constant (ε_∞) values at 100 ºC, 12h ZnO films and different solution molarity.

			Herve and Vandamme		Moss relation	
100 °C-12 h	**Eg (eV)**	**ε_0**	**n**	**ε_∞**	**n**	**ε_∞**
0.03 M	3.14	8.85	2.31	5.32	2.42	5.86
0.05 M	3.34	8.23	2.25	5.07	2.38	5.69

Table 5.10 The bandgap (Eg), refractive index (n), optical static dielectric constant (ε_0) and optical high frequency dielectric constant (ε_∞) values at 90 ºC, 0.03 M ZnO films and different growth time.

			Herve and Vandamme		Moss relation	
90 °C-0.03 M	**Eg (eV)**	**ε_0**	**n**	**ε_∞**	**n**	**ε_∞**
12 h	3.19	8.69	2.29	5.26	2.41	5.82
6 h	3.22	8.60	2.28	5.22	2.41	5.79

As seen in Figure 4.15-16 and Table 5.8, the bandgap values of the ZnO films have decreased from 3.19 to 3.03 eV with increasing solution molarity [108]. The refractive index values of the ZnO films have increased with increasing solution molarity. Since n is strongly connected with bandgap energy, it can be concluded that the smaller band gap energy material has a larger value of the n [109]. Also, optical static dielectric constant and optical high frequency dielectric constant values have increased with increasing solution molarity.

As seen in Figure 4.17-18 and Table 5.9, the bandgap values of the ZnO films have increased from 3.14 to 3.34 eV with increasing solution molarity. The refractive index, optical static dielectric constant and optical high frequency dielectric constant values decreased with increasing solution molarity.

Figure 4.15, Figure 4.19 and Table 5.10 have showed that the bandgap values of the ZnO films have decreased from 3.22 eV to 3.19 eV with increasing growth time from 6 h to 12 h. At the same time, the refractive index values haven't changed absolutely with increasing growth time.

5.3.2 AZO Films

Figure 4.20-28 show the optical absorption spectras and the curves of $(\alpha h\nu)^2$ versus $(h\nu)$ of AZO films grown on glass substrate by hydrothermal method at different synthesis temperature (90 ^oC and 100 ^oC), different doping concentration (1%, 3%, 5%) and solution molarity (0.03 M and 0.05 M). The synthesis temperature, solution molarity and doping concentration effects on the optical absorption measurements have been investigated.

The refractive index values of the AZO films have been calculated using equation (3.6) and (3.7) .The changing of refractive index (n) with synthesis temperature, solution molarity and doping concentration has been shown in Table 5.11-14 for these two models.

Table 5.11 The bandgap (Eg), refractive index (n), optical static dielectric constant (ε_0) and optical high frequency dielectric constant (ε_∞) values at 90 ^oC, 12 h, 0.03 M AZO films and different doping concentration.

			Herve and Vandamme		Moss relation	
90 °C-0.03 M	**Eg (eV)**	**ε_0**	**n**	**ε_∞**	**n**	**ε_∞**
1%	3.14	8.85	2.31	5.32	2.42	5.86
3%	3.16	8.79	2.30	5.30	2.42	5.85
5%	3.17	8.76	2.30	5.28	2.42	5.84

Table 5.12 The bandgap (Eg), refractive index (n), optical static dielectric constant (ε_0) and optical high frequency dielectric constant (ε_∞) values at 100 ^oC, 12 h, 0.03 M AZO films and different doping concentration.

			Herve and Vandamme		Moss relation	
100 °C-0.03 M	**Eg (eV)**	**ε_0**	**n**	**ε_∞**	**n**	**ε_∞**
1%	3.16	8.79	2.30	5.30	2.42	5.85
5%	3.16	8.79	2.30	5.30	2.42	5.85

Table 5.13 The bandgap (Eg), refractive index (n), optical static dielectric constant (ε_0) and optical high frequency dielectric constant (ε_∞) values at 90 ^oC, 12 h, 0.05 M AZO films and different doping concentration.

			Herve and Vandamme		Moss relation	
90 °C-0.05 M	**Eg (eV)**	**ε_0**	**n**	**ε_∞**	**n**	**ε_∞**
1%	3.23	8.57	2.28	5.21	2.40	5.78
3%	2.90	9.59	2.38	5.66	2.47	6.10
5%	2.83	9.80	2.40	5.77	2.49	6.18

Table 5.14 The bandgap (Eg), refractive index (n), optical static dielectric constant (ε_0) and optical high frequency dielectric constant (ε_∞) values at 100 °C, 12 h, 0.05 M 5% doped AZO films

			Herve and Vandamme		Moss relation	
100 °C-0.05 M	**Eg (eV)**	**ε_0**	**n**	**ε_∞**	**n**	**ε_∞**
5%	2.89	9.62	2.38	5.67	2.47	6.11

As seen in Figure 4.20-12 and Table 5.11, the bandgap values of the AZO films have increased from 3.14 to 3.17 eV with increasing Al concentration. These results are in agreement with the literature [38, 39, 105, 110]. The increasing in the optical bandgap with increasing Al concentration may be due to the decrease in lattice constant because of the smaller ionic radio of Al^{+3} ions compared to Zn^{+2} ions [38, 111]. The refractive index, optical static dielectric constant and optical high frequency dielectric constant values of the AZO films have decreased with increasing doping concentration. The decrease of the refractive index with increasing Al concentration has been attributed to the decrease in the nanostructure size.[38, 112].

As seen in Figure 4.23-24 and Table 5.12, the energy bandgap, refractive index and dielectric constants values of the AZO films haven't changed with increasing Al concentrations.

As seen in Figure 4.25-27 and Table 5.13, the energy bandgap values of the AZO films have decreased from 3.23 to 2.83 eV with the increasing Al concentration. The decrease in bandgap may be specified as a increase in defect levels [113]. The refractive index, optical static dielectric constant and optical high frequency dielectric constant values of the films have increased with increasing Al concentration.

For 100 °C synthesis temperature and 0.05 M solution molarity, AZO films have been grown for only 5% doping concentration (Fig. 4.28 and Table 5.14). The AZO films are grown at different Al concentrations for 0.05 M at 100 °C, but it has not given better results for 0.05 M and %1, %3 Al concentration.

5.4 EDAX Results

The quantitative analysis of the films has been carried out by using the EDAX technique for the grown films at different compositions. Figure 4.29-43 show the

compositional analysis of ZnO and AZO films. EDAX analysis shows the presence of Zn, O and Al elements in the films (Fig. 4.29-33). The atomic percent values of these elements in the films have been given in the inset of EDAX spectras (Fig. 4.29-33). The presence of Si and Ca elements in the spectras may originated from substrate. The atomic ratios (at.%) of Zn, O and Al in films are approximately as same as the initial ratio.

CHAPTER 6

CONCLUSION

ZnO is a promising semiconducting material for manufacturing optoelectronic devices. Its most important properties are its wide and direct bandgap and its high electron-hole binding energy. Synthesis of ZnO in bulk and thin film form have been investigated intensively over recent decades. Similarly, nanomaterials have been in the point of focus for their different properties compared to their bulk form. The vastly increased ratio of surface area to volume and change in electronic properties with great reduction in particle size enable improved performance in conventional applications where their bulk counterparts have been used for decades. As a result of this trend, research on ZnO nanostructure synthesis and their incorporation in prototype optoelectronic devices has been intensive in recent years. So, synthesis of ZnO nanostructure in a cost effective way and understanding the factors influencing the ZnO nanostructure growth is essential for contribution to ongoing research.

It has been decided to use hydrothermal method to grow the ZnO and AZO films because of simple equipment, no catalyst growth, low cost, wide area uniform production, environment friendly, less dangerous. Different Al concentrations (1%, 3% and 5%) have been doped into the ZnO for getting the AZO film. ZnO and AZO films have been grown on glass substrates via hydrothermal method using Zinc Zitrate Tetrahydrate, Hexamethylenetetramine and Aluminum Chloride solutions. The synthesis temperature (90 ^{o}C-100 ^{o}C), solution molarity (0.03 M-0.05 M), growth time (6 h-12 h) and doping concentration (1%, 3% and 5%) effects on the structural, morphological, compositional and optical properties of the films have been investigated.

Structural analysis based on X-ray measurement has revealed that ZnO films has the polycrystal structures which belong to hexagonal wurtzite structure with a strong (101) preferred orientation. AZO films have polycrystalline structure with hexagonal wurtzite phase of ZnO. No impurity phases have been observed in all the patterns of the films and it has been believed that the impurification with Al occurs through

substitution of Zn^{2+} ions by Al^{+3} ions in the synthesis process. As the Al concentration in the ZnO films increases, the orientation changes and becomes (100) dominant peak in AZO films. The structural parameters such as grain size (D), dislocation density (δ), FWHM (β), strain (ε) for all films were calculated using XRD results. The film thickness values are calculated in micrometer size by using gravimetric method.

The surface morphology of the films has been studied using SEM and SEM images show that the ZnO and AZO films consist of nanorod structures. As the Al concentartion in the ZnO films increases, surface quality of the nanorods increases. With increasing Al concentration, the shape of nanoroad become more prominent. This study shows the presence of well grown nanorods and the films are homogeneous and dense. The compositions of the films have been measured by EDAX. These results have shown that ZnO and AZO films have been successfully grown on the glass substrate.

Absorption measurements have been carried out at room temperature. The energy bandgaps values of ZnO and AZO films have been calculated by using the optical absorption spectra. The refractive index (n), optical static and high frequency dielectric constants (ε_o, ε_∞) values have been calculated by using the energy bandgap values as a function of the synthesis temperature, solution molarity, growth time and doping concentration. According to our result the bandgap values and refractive index can be tunning by changing the growth parameters.

As a result of XRD, SEM and absorption measurements; it has been observed that ZnO and AZO films could be grown by hydrothermal method. According to the these results (XRD, SEM and optical absoprtion), it can be said that the optimal growth parameters are defined as 0.03 M, 90 ^oC and 12 h for ZnO films. It has been determined that the structural, morphological and optical properties of the films have changed with the Al concentration. According to the these results (XRD, SEM and optical absoprtion) it can be said that the optimal growth parameters are defined as 0.03 M, 90 ^oC, 12 h and 5% doping concentration for AZO films.

REFERENCES

[1] Thounthong P., Chunkag V., Sethakul P., Sikkabut S., Pierfederici S. and Davat B., "Energy Management of Fuel Cell/Solar Cell/Supercapacitor Hybrid Power Source", Journal of Power Sources, 196, 313-324, 2011.

[2] Santbergen R., Goud J.M., Zeman M., Roosmalen J.A.M. and Zolingen R.J.C., "The Am 1.5 Absorption Factor of Thin-Film Solar Cells", Solar Energy Materials & Solar Cells, 94, 715–723, 2010.

[3] Sharan, M. A., "Efficiency Enhancement of Stationary Solar Energy Based Power Conversion Systems in Canada, Applied Energy", 86, 1405-1409, 2009.

[4] Kim, Y., Tai, W., "Electrical and Optical Properties of Al-Doped ZnO Thin Films by Sol-Gel Process, Applied Surface Science", 253, 4911-4916, 2007.

[5] Chawla, A. K., Kaur, D. and Chandra, R. " Structural and Optical Characterization of ZnO Nanocrystalline Films Deposited By Sputtering", Optical Materials, 29, 995-998, 2007.

[6] Gu, Y., Kuskovsky, I. L., Yin, M., O´Brien, S. and Neumark, G. F., "Quantum Confinement in ZnO Nanorods", Appl. Phys. Lett., Vol. 85, No. 17. 2004.

[7] Li, M., Wang, D., Sheng, D., Ding, Y., Liu, J., and Liu, Z., " Synthesis and Properties of Aligned ZnO Microtube Arrays", Appl.Surf. Sci., 253, 4161-4165, 2007.

[8] Shen, W. J., Wang, J., Wang, Q. Y., Duan, Y., and Zeng, Y. P., "Structural and Optical Properties of ZnO Films on Si Substrates Using a γ-Al2O3 Buffer Layer," J. Phys. D: Appl. Phys., 39, 269-273, 2006.

[9] Yi, G., Wang, C. and Park, W., “ZnO Nanorods: Synthesis, Characterization and Applications”, Semicond. Sci. Technol. 20, S22–S34, 2005.

[10] Félix-Quintero, H., Angulo-Rocha, J., Murrieta S. H., Hernández A. J., Camarillo G. E., Flores J. M. C., Alejo-Armenta C., García-Hipolito M., Ramos-Brito F., "Study on Grow Process and Optical Properties of Zno Microrods Synthesized by Hydrothermal Method.", Journal of Luminescence, 2016.

[11] Yıldırım, M.A., "The Characterızatıon of ZnO And CdO Thin Films Grown SILAR Technique and Using In Sandwich Structures", Atatürk University Graduate School of Naturel and Applied Sciences Department of Physics, Ph. D. Thesis, 2010.

[12] Andersson M., Sterlund L., Ljungstrm S., Palmqvist A., "Preparation Nanosize Anatase and Rutile TiO2 by Hydrothermal Treatment of Microemulsions and Their Activity for Photocatalytic Wet Oxidation of Phenol", The Journal of Physical Chemistry B, 10674-10679, 2002.

[13] Ueno, N., Maruo, T., Nishiyama, N., Egashira, Y., and Ueyama, K., "Low-Temperature Synthesis of ZnO Nanorods Using a Seed Layer of Zinc Acetate/Sodium Dodecyle Sulfate Nanocomposite," Materials Letters, vol. 64, no. 4, pp. 513–515, 2010.

[14] Polsongkram, D., Chamninok, P., Pukird, S., Chow, L., Lupan, O., Chai, G., Khallaf, H., Park, S., Schulte, A., Physica B, 403, 3713– 3717, 2008

[15] Yilmaz, M., Cirak, B. B., Cirak, C. and Aydogan, S., "Hydrothermal Growth of ZnO Nanoparticles Under Different Conditions", Philosophical Magazine Letters, VOL . 96, NO . 2, 45–51, 2016.

[16] Promnimit, S., Baruah, S., Lamdub, U. and Dutta, J., "Hydrothermal Growth of ZnO Hexagonal Nanocrystals: Effect of Growth Conditions", Journal of Nano Research Vol. 21, pp 57-63, 2013.

[17] Søndergaard, M., Bøjesen, E. D., Christensen, M.,* and Iversen, B. B., "Size and Morphology Dependence of ZnO Nanoparticles Synthesized by a Fast

Continuous Flow Hydrothermal Method", Cryst. Growth Des., 11, 4027–4033, 2011.

[18] Aneesh, P. M., Vanaja, K. A., Jayaraj, M. K., "Synthesis of ZnO nanoparticles by hydrothermal method", Proc. of SPIE Vol. 6639, 2007.

[19] Tsai J., Meen T., Wu T., Lai Y., He Y., "Morphology and optical properties of ZnO microrods grown by high-temperature hydrothermal method", Microelectronic Engineering, 148, 55–58, 2015.

[20] Baruah S. and Dutta J., "Hydrothermal Growth of ZnO Nanostructures.", Sci. Technol. Adv. Mater. 10, 013001 18pp, 2009.

[21] Dangol, L., and Joshi, L. P., "Structural and Optical Characterization Of Zinc Oxide Films Prepared by Two Stage; Spin Coating And Hydrothermal Process.", Journal of Institute of Science and Technology, Vol. 21(1) : 61-64, 2016.

[22] Alkahlout, A., Dahoudi, N. A., Grobelsek, I., Jilavi, M., and Oliveira, P.W., "Synthesis and Characterization of Aluminum Doped Zinc Oxide Nanostructures via Hydrothermal Route", Hindawi Publishing Corporation Journal of Materials, Vol. 2014, 2014.

[23] Jiao, M., Chien, N. V., Duy, N. V., Hoa, N. D., Hieu, N. V., Hjort K., Nguyen H., "On-Chip Hydrothermal Growth of ZnO Nanorods at Low Temperature for Highly Selective NO2 Gas Sensor", Materials Letters, Vol. 169, 231–235, 2016.

[24] Reddy, A. R., Mallika, A. N., Babu K. S., and Reddy K. V., “Hydrothermal Synthesis and Characterization of Zno Nano Crystals”, International Journal of Mining, Metallurgy & Mechanical Engineering (IJMMME) Volume 3, Issue 2 ISSN 2320–4060 (Online), 2015.

[25] Raluca Savu, Rodrigo Parra, Bostjan Jan ˇ car, Maria Aparecida Zaghete, and Ednan Joanni “Influence of Hydrothermal Synthesis Conditions and Device

Configuration on the Photoresponse of UV Sensors Based on ZnO Nanorods" 2011

[26] Xu, X., Wu, M., Asoro M., Ferreira, P. J., and Fan, D. L., "One-Step Hydrothermal Synthesis of Comb-Like ZnO Nanostructures", Cryst. Growth Des., 2 (10), pp 4829–4833, 2012.

[27] Chitanu, E., Ionita, Gh., "Hydrothermal Growth Of ZnO Nanowires.", The Scientific Bulletin of Valahia University- Materials and Mechanics – Nr. 7 (year 10), 2012.

[28] Akhiruddin, Sugianto, Irmansyah, "The Influence of Hydrothermal Duration on Structures and Optical Properties of ZnO Nanoparticles", Journal of Materials Physics and Chemistry, Vol. 2, No. 2, 34-37, 2014.

[29] Félix-Quintero, H., Angulo-Rocha, J., Murrieta, S.H., Hernández, A.J., Camarillo, G.E., Flores, J.M.C., Alejo-Armenta, C., García-Hipolito, M., Ramos-Brito, F., "Study on Grow Process and Optical Properties of ZnO Microrods Synthesized by Hydrothermal Method", Journal of Luminescence, 2017.

[30] Gautama, K., Singh, I., Bhatnagar , P.K., Peta, K. R., "The Effect of Growth Temperature of Seed Layer on The Structural and Optical Properties of ZnO Nanorods", Superlattices and Microstructures, Vol. 93, 101–108, 2016.

[31] Kiomarsipourn N., Razavi R. S., "Hydrothermal synthesis and optical property of scale and spindle-like ZnO", Ceramics International, 39, 813–818, 2013.

[32] P. M. Aneesh, K. A.Vanaja, M. K. Jayaraj "Synthesis of ZnO nanoparticles by hydrothermal method", Kochi-682 022, India, 2007.

[33] Bai, S.N., Tsai, H.H., Tseng, T.Y., "Structural and optical properties of Al-doped ZnO nanowires synthesized by hydrothermal method", Thin Solid Films, 516, 155–158, 2007.

[34] Yun S., Lee J., Yang J., Lim S., "Hydrothermal synthesis of Al-doped ZnO nanorod arrays on Si substrate", Physica B, 405, 413–419, 2010.

[35] Burunkaya, E., Kiraz, N., Kesmez, Ö., Çamurlu, H. E., Asiltürk, M., Arpaç, E., "Preparation of Aluminum-Doped Zinc Oxide (Azo) Nano Particles by Hydrothermal Synthesis", Journal of Sol-Gel Science And Technology, Vol.55, pp.171-176, 2010.

[36] Chen, J.T., Wang, J., Zhuo, R.F., Yan, D., Feng, J.J., Zhang, F., Yan, P.X., "The effect of Al doping on the morphology and optical property of ZnO nanostructures prepared by hydrothermal process", Applied Surface Science, 255, 3959–3964, 2009.

[37] Hsieh, T., Wang J., Yang P., Hwang C.and Shye D., "Field-Emission Stability of Hydrothermally Synthesized Aluminum-Doped Zinc Oxide Nanostructures", Journal of Nanoscience and Nanotechnology, Vol. 12, 5453–5458, 2012.

[38] Shrisha, B.V., Bhat, S., Kushavah, D., Gopalakrishna Naik, K., "Hydrothermal growth and characterization of Al-doped ZnO nanorods.", Materials Today: Proceedings 3, 1693–1701, 2016.

[39] Mazilu, M., Tigau, N., Musat, V., "Optical properties of undoped and Al-doped ZnO nanostructures grown from aqueous solution on glass substrate.", Optical Materials, 34 1833-1838, 2012.

[40] Huang, S., Xiao, Q., Zhou, H., Wang, D., Jiang, W., "Hydrothermal synthesis and conductive properties of Al-doped ZnO rod-like whiskers.", Journal of Alloys and Compounds, 486, L24–L26, 2009.

[41] Chen Z., Zhan G., Wu Y., He X., Lu Z., "Sol–gel-hydrothermal synthesis and conductive properties of Al-doped ZnO nanopowders with controllable morphology", Journal of Alloys and Compounds, 587, 692–697, 2014.

[42] Sze, S. M., "Semiconductor Devices: Physics and Technology.", John Wiley and Sons, Inc., New York, 2002.

[43] Łukasiak L., Jakubowski A., "History of Semiconductors", Journal of Telecommunications and Information Technology, 2010.

[44] Zeghbroeck B. V., "Principles of Semiconductor Devices", 2011, http://ece-www.colorado.edu/~bart/book/, Visited date: 14.10.2015.

[45] Singh, Y., "Semiconductor Devices.", I. K. International Pvt Ltd Press, 2009.

[46] Mahajan, S., Sree Harsha, K. S., "Principles of Growth and Processing of Semiconductors", WCB/McGraw-Hill, 1999.

[47] http://hyperphysics.phy-astr.gsu.edu/hbase/solids/sili.html, Visited date: 14.10.2015.

[48] Lee, J., Park, B., "Transparent Conducting ZnO:Al, In and Sn Thin Films Deposited by the Sol-Gel Method, Thin Solid Films." 426, 94-99, 2003.

[49] Nunes, P., Fortunato, E., Tonello, P., Braz Fernandes, F., Vilarinhob, P. and Martins, R., "Effect of Different Dopant Elements on The Properties of ZnO Thin Films, Vacuum." 64, 281–285, 2002.

[50] Sahay, P. P., Nath, R. K., "Al Doped ZnO Thin Films as Methanol Sensors.", Sensors and Actuators B, 134, 654-659, 2008.

[51] Sahal, M., Hartiti, B., Ridah, A., Mollar, M., Marı, B., "Structural, Electrical and Optical Properties of ZnO Thin Films Deposited by Sol-Gel Method.", Microelectronics Journal, 39, 1425–1428, 2008.

[52] Xu, Z.Q., Deng, H., Li, Y., Guo, Q.H., Li, Y.R., "Characteristics of Al-doped C-Axis Orientation ZnO Thin Films Prepared by The Sol-Gel Method.", Materials Research Bulletin, 41, 354–358, 2006.

[53] Gümüş, C., Özkendir, O.M., Kavak, H., Ufuktepe, Y., "Structural and Optical Properties of Zinc Oxide Thin Films Prepared by Sprey Pyrolysis Method.", Journal of Optoelectronics and Advenced Materials, 8, 299-303, 2006.

[54] Wang, M. S., Lee, K. E., Hahn, H. S., Kim, E. J., Kim, S., Chung J., S., Shin, E. W., and Park C., "Optical and Photoluminescent Properties of Sol-Gel Al-Doped ZnO Thin Films.", Materials Letters, 61, 1118-1121., 2007.

[55] Kluth, O., Schöpe, G., Hüpkes, J., Agashe, C., Müller, J. and Rech, B., "Modified Thornton Model for Magnetron Sputtered Zinc Oxide Film Structure and Etching Behavior.", Thin Solid Films, 442, 80–85, 2003.

[56] Shishiyanu, S.T., Shishiyanu, T.S. and Lupan, O.I., "Sensing Characteristics of Tin-Doped Zno Thin Films as No2 Gas Sensor.", Sensors and Actuators B, 107, 379–386, 2005.

[57] Suvaci, E. and Özer, G.Ö., J. "Processing of Textured Zincoxide Varistors via Templated Grain Growth.", Journal of the European Ceramic Society, 25, 1663–1673, 2005.

[58] Saito, N., Haneda, H., Sekiguchi, T., Ohashi, N., Sakaguchi, I. and Koumoto, K., "Low-Temperature Fabrication of Light-Emitting Zinc Oxide Micropatterns Using Self-Assembled Monolayers.", Advanced Materials, 14, 418–421, 2002.

[59] Huang, M.H., Mao, S., Feick, H., Yan, H., Wu, Y., Kind, H., Weber, E., Russo, R. and Yang, P., "Room-Temperature Ultraviolet Nanowire Nanolasers.", 292, 1897 – 1899, 2001.

[60] Bao D., Gu H., Kuang A., "Sol-Gel-Derived C-Axis Oriented Zno Thin Films.", Thin Solid Films, 312, 37-39, 1998.

[61] Das, S., Chakrabarti, S. and Chaudhuri, S., "Optical Transmission and Photoluminescence Studies of ZnO-MgO Nanocomposite Thin Films.", Journal of Physics D: Applied Physics, 38, 4021-4026, 2005.

[62] Vafaee, M., Ghamsari, M.S., "Preparation and Chracterization of ZnO Nanoparticles by a Novel Sol-Gel Route.", Materials Letters, 61, 3265-326, 2007.

[63] Fortunato, Martins, Nunes, "Influence of the Annealing Conditions on the Properties of ZnO Thin Films.", International Journal of Inorganic Materials, 3, 1125–1128, 2001.

[64] Kuo, S., Chen, W., Lai, F., Cheng, C., Kuo, H., Wang, S. and Hsieh, W., "Effects of Doping Concentration and Annealing Temperature on Properties of Highly-Oriented Al-Doped ZnO Films.", Journal of Crystal Growth, 287, 78-84, 2006.

[65] Bouderbala, M., Hamzaoui, S., Amrani, B., Reshak, A. H., Adnane, M., Sahraoui, T. and Zerdali, M., "Thickness Dependence of Structural, Electrical and Optical Behaviour of Undoped ZnO Thin Films.", Physica B, 403, 3326–3330, 2008.

[66] Rossler, U. (ed.) Landolt-Bornstein, New Series, Group III. 17B (22) 41B Springer, Heidelberg., 1999.

[67] Baruah, S. and Dutta, J., “Hydrothermal Growth of ZnO Nanostructures”, Sci. Technol. Adv. Mater. 10, 013001, 2009.

[68] Banerjee, S. K., and Streetman, B. G.. "Solid State Electronic Devices." New Delhi: Phi Learning, 82-101, 2009.

[69] Jagadish, C., Pearton, S., “Zinc Oxide Bulk, Thin Films and Nanostructures: Processing, Properties, and Applications” Elsevier Science, 5, 2011.

[70] Singh, G., Shrivastava, S. B., Jain, D., Pandya, S., Shripathi, T., Ganesan, V., "Effect of Indium Doping on Zinc Oxide Films Prepared by Chemical Spray Pyrolysis Technique." Bulletin of Materials Science, Volume 33, Issue 5, pp 581–587, 2010.

[71] Mamat, M. H., Sahdan, M.Z., Khusaimi, Z., Zain, Ahmed, A., Abdullah, S., Rusop, M., "Influence of Doping Concentrations on The Aluminum Doped Zinc Oxide Thin Films Properties for Ultraviolet Photoconductive Sensor Applications." Optical Materials, Volume 32, Issue 6, Pages 696–699, 2010.

[72] Litton, C. W., Collins, T. C., Reynolds, D. C., Capper, P., Kasap, S., Willoughby, A., “Zinc Oxide Materials for Electronic and Optoelectronic Device Applications”, ISBN: 978-0-470-51971-4, 2011.

[73] Chen, H. X., Ding, J. J., Zhao, X. G., Ma, S. Y., "Microstructure and Optical Properties of ZnO: Al Films Prepared by Radio Frequency Reactive Magnetron Sputtering." Physica B: Condensed Matter Volume 405, Issue 5, Pages 1339–1344, 2010.

[74] Byrappa, K. and Yoshimura, M., "Handbook of Hydrothermal Technology, A Technology for Crystal Growth and Material Processing.", Noyes, New Jersey, 2001.

[75] Rabenau, A., "The Role of Hydrothermal Synthesis in Preparative Chemistry.", Angew. Chem., (English Ed.), 24:1026–1040, 1985.

[76] Lobachev, A. N., “Crystallization Processes Under HydrothermalConditions”, pp. 1-255, Consultants Bureau, New York, 1973.

[77] Roy, R., "Acceleration the Kinetics of Low-Temperature Inorganic Syntheses.", J. Solid State Chem., 111, 11–17, 1994.

[78] Byrappa, K., "Hydrothermal Growth of Crystals", pp. 1–365, Pergamon Press, Oxford, UK, 1992.

[79] Yoshimura, M. and Suda, H., "Hydrothermal Processing of Hydroxyapatite: Past, Present, and Future, in: Hydroxyapatite and Related Materials (P. W. Brown and B. Constanz, eds.).", pp. 45–72, CRC Press, Inc,1994.

[80] Suchanek, W. L., Lencka, M.M., McCandlish, L. E., Pfeffer, R. L., Oledzka, M., Mikulka-Bolen, K., Rossetti, G. A., Jr. and Riman, R. E., "Crystal Growth & Design", Vol. 5, p. 1715. , 2005.

[81] Guohong, C., "Nanostructures and Nanomaterials.", Singapore: World Scientific Publishing Company, 2004.

[82] Cullity, B.D., "Elements of X-ray Diffraction.", Massachusetts: Addison-Wesley Publishing Company, 1978.

[83] Barrett, C.S., "T.B. Massalski, Structure of Metals.", Pergamon, Oxford, p.204, 1980.

[84] Yıldırım, M. A., Ates A., "Influence of Films Thickness and Structure on The Photo-Response of ZnO Films.", Optics Communications, 283, 1370-1377, 2010.

[85] Callister, W.D., "Materials Science and Engineering -an Introduction.", John Wiley and Sons, New York, 1997.

[86] Ashraf, M., Akhtar, S.M.J., Khan, A.F., Ali, Z., Qayyum, A., J. Alloys Compd. 509, 2414–2419, 2011.

[87] "Electron beam interacts with the sample" http://www.purdue.edu/ehps/rem/rs/sem.htm, Visited date: 14.05.2015.

[88] "EDX Detector", www.lpdlabservices.co.uk/analytical_techniques/sem/sem_instrument.php, Visited date: 14.05.2015.

[89] "Schematic view of Illustrated SEM", http://www.purdue.edu/ehps/rem/rs/sem.htm, Visited date: 14.05.2015.

[90] Kurt, İ., "Influence of Al Concentration and Annealing Temperature on Structural, Optıcal and Electrical Properties of Al Codoped ZnO Thin Films.", Master of Science in Physics, 2015.

[91] Akaltun, Y., Yıldırım, M. A., Ates, A., Yıldırım, M., " The Relationship Between Refractive Index-Energy Gap and The Film Thickness Effect on The Characteristic Parameters of CdSe Thin Films" Opt. Commun. 284, 2307-2311, 2011.

[92] Hannachi, L., Bouarissa, N., " Band Parameters for Cadmium and Zinc Chalcogenide Compounds.", Physica B: Condensed Matter, 404, 3650-3654, 2009.

[93] Mezrag, F., Mohamed, W.K., Bouarissa, N., "The Effect of Zinc Concentration Upon Optical and Dielectric Properties of Cd1-xZnxSe.", Physica B, vol. 405, pp. 2272–2276, 2010.

[94] Herve, P., Vandamme, L.K.J., " General Relation Between Refractive Index and Energy Gap in Semiconductors.", Infrared Phys. Technol., 35, 609-615, 1994.

[95] Hannachi, L., Bouarissa, N., "Band Parameters for Cadmium and Zinc Chalcogenide Compounds", Physica B 404, Pages 3650-3654, 2010.

[96] Mezrag, F., Mohamed, W.K., Bouarissa, N., "The Effect of zinc Concentration Upon Optical and Dielectric Properties Of Cd, Zn, Se," Physica B, vol. 405, pp. 2272-2276, 2010

[97] Adachi, S., "Properties of Group IV, III-V and II-VI Semiconductors", John Wiley & Sons, Ltd, Chishester, 2005.

[98] Akaltun, Y., Yıldırım, M. A., Ateş, A., Yıldırım, M., "The Relationship Between Refractive Index-Energy Gap and the film thickness effect on the characteristic parameters of CdSe thin films", Optics Communications, 284 (9), 2307-2311, 2011.

[99] Yıldırım, M. A., "The Effect of Copper Concentration on Structural, Optical and Dielectric Properties of CuxZn1 − xS Thin Films", Optics Communications, Volume 285, Issue 6, Pages 1215–1220, 2012.

[100] Rosencher, E. and Vinter, B., "Optoelectronics", Cambridge University Press, page 304, 2002.

[101] Caglar, Y., Gorgun, K., Aksoy, S., "Effect of deposition parameters on the structural properties of ZnO nanopowders prepared by microwave-assisted hydrothermal synthesis", 2014.

[102] Li, S., Liu, T., Zhang, Y., Zeng, W., Pan, F., Peng, X., "Hydrothermal Synthesis of the Sealed ZnO Nanotube and Its Growth Mechanism", 2014.

[103] Muzaffar, S. M., Khan, S., Riaz, S. and Naseem, S., "Effect on Structural Orientation of ZnO Nanorods by Changing the Molarity and Reaction Time", Centre of Excellence in Solid State Physics, University of the Punjab, Lahore-54590, Pakistan, 2016.

[104] Ridhuan, N. S., Razak, K. A., Lockman, Z., Aziz, A. A., "Structural and Morphology of ZnO Nanorods Synthesized Using ZnO Seeded Growth Hydrothermal Method and Its Properties as UV Sensing", Plos One 7 (11), 2012.

[105] Akhtar, M. J., Alhadlaq, H. A., Alshamsan, A., Khan, M. A. M. and Ahamed, M., "Aluminum doping tunes band gap energy level as well as oxidative stress-mediated cytotoxicity of ZnO nanoparticles in MCF-7 cells", Scientific Reports 5, Article number: 13876, 2015.

[106] Callister, W. D., "Materials Science and Engineering-an Introduction.", New York:John Wiley and Sons, 1997.

[107] Habubi, N. F., Abood, Z. M., Algamel, A. N., "Effect of Molarity on The Structural and Optical Properties of ZnO Thin Films Deposit by CSP" World Sicientific News, 22, EISSN 2392-2192, 2015.

[108] Yamlahi Alami, Z., Salem, M., Gaidi, M., Elkhamkhami, J., "Effect Of Zn Concentration On Structural And Optical Properties Of ZnO Thin Films Deposited By Spray Pyrolysis", 2015.

[109] Yıldırım, M. A., Akaltun, Y., Ates, A., "Characteristics of SnO2 Thin Films Prepared by SILAR", Solid State Sciences, Volume 14, Issue 9, Pages 1282-1288, 2012.

[110] Karacasu, Ö., "Nanocrystalline ZnO:Al Thin Films Prepared By Sol-Gel Dip Coating Technique And ZnO:Al/P-Si Heterojunctions", M.Sc. Thesis, İstanbul Technical University, 2010

[111] Al-Ghamdi, A. A., Al-Hartomy, O. A., El Okr, M., Nawar, A.M., El-Gazzar, S., El-Tantawy, F., Yakuphanoglu, F., "Semiconducting properties of Al doped ZnO thin films", Spectrochimica Acta Part A: Molecular and Biomolecular Spectroscopy, Pages 512-517, 2014.

[112] Ferro, R. and Rodriguez, J. A., "Some Physical Properties of F-doped CdO thin Films Deposited by Spray Pyrolysis". Thin Solid Films, ISSN: 0040-6090, Volume 347, Pages 295-298, 1999.

[113] Santos-Cruz, J., Torres-Delgado, G., Castanedo-Perez, R., Jımenez-Sandoval, S.,Jimenez-Sandoval, O., Zunigaromero, C. I., Marquez Marin, J., Zelaya-Angel, O., "Dependence of Electrical and Optical Properties of Sol-Gel Prepared Undoped Cadmium Oxide Thin Films on Annealing Temperature" Thin Solid Films, Volume 493, Pages 83-87, 2005.

CURRICULUM VITAE

PERSONAL INFORMATION

Name Surname : Ümmügülsüm VAROL

Date of Birth : 1988

Phone : (0312) 324 15 55

E-mail : uotgun@ybu.edu.tr

EDUCATION

High School : Akşehir Selçuklu Super High School

Bachelor : Süleyman Demirel University, Isparta, Physics Department

Master Degree : Ankara Yıldırım Beyazıt University

WORK EXPERIENCE

Research Assist. : Ankara Yıldırım Beyazıt University

PUBLICATIONS

- Ümmügülsüm Varol, Irmak Karaduman, Tuğba Çorlu, Sümeyra Tuna Yıldırım, Memet Ali Yıldırım, Aytunç Ateş, Selim Acar, "Mn Doped ZnO Nanostructure For Low Temperature Gas Sensor", 2nd International Congress on The World of Technology and Advanced Materials-WITAM-2016, 2016.